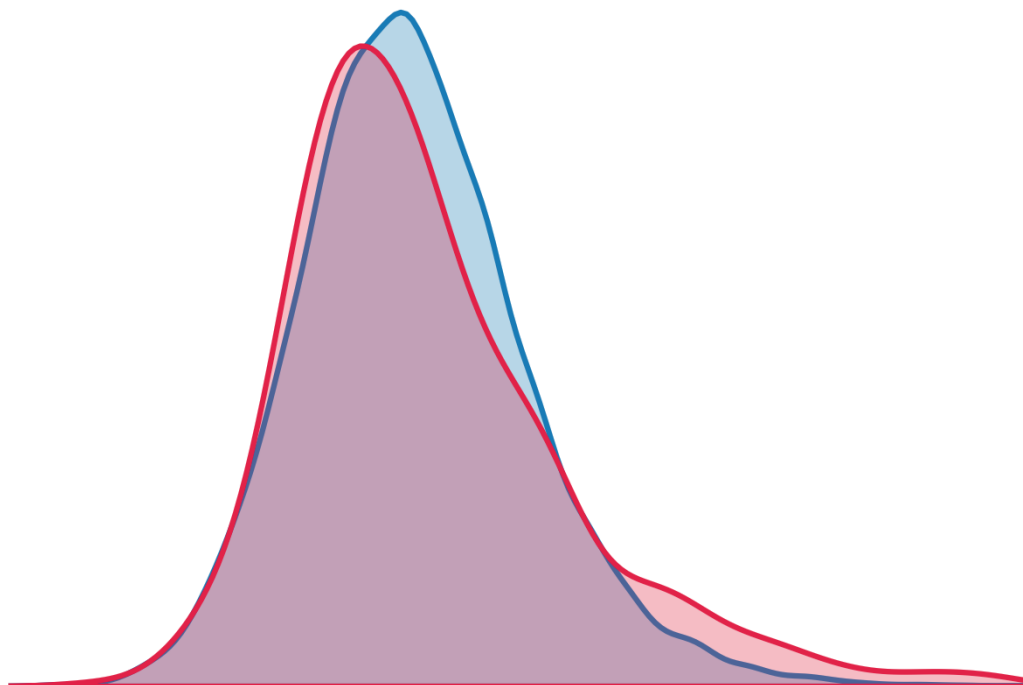




Signatures of Eurasian heat waves in the  
global Rossby wave spectra in reanalyses  
and CMIP models



Iana Strigunova

Hamburg 2023

## Hinweis

Die Berichte zur Erdsystemforschung werden vom Max-Planck-Institut für Meteorologie in Hamburg in unregelmäßiger Abfolge herausgegeben.

Sie enthalten wissenschaftliche und technische Beiträge, inklusive Dissertationen.

Die Beiträge geben nicht notwendigerweise die Auffassung des Instituts wieder.

Die "Berichte zur Erdsystemforschung" führen die vorherigen Reihen "Reports" und "Examensarbeiten" weiter.

## Anschrift / Address

Max-Planck-Institut für Meteorologie  
Bundesstrasse 53  
20146 Hamburg  
Deutschland

Tel./Phone: +49 (0)40 4 11 73 - 0  
Fax: +49 (0)40 4 11 73 - 298

name.surname@mpimet.mpg.de  
www.mpimet.mpg.de

## Notice

*The Reports on Earth System Science are published by the Max Planck Institute for Meteorology in Hamburg. They appear in irregular intervals.*

*They contain scientific and technical contributions, including PhD theses.*

*The Reports do not necessarily reflect the opinion of the Institute.*

*The "Reports on Earth System Science" continue the former "Reports" and "Examensarbeiten" of the Max Planck Institute.*

## Layout

*Bettina Diallo and Norbert P. Noreiks  
Communication*

## Copyright

*Photos below: ©MPI-M  
Photos on the back from left to right:  
Christian Klepp, Jochem Marotzke,  
Christian Klepp, Clotilde Dubois,  
Christian Klepp, Katsumasa Tanaka*



# Iana Strigunova

aus Glasow, Russland

Max-Planck-Institut für Meteorologie  
The International Max Planck Research School on Earth System Modelling  
(IMPRS-ESM)  
Bundesstrasse 53  
20146 Hamburg

Universität Hamburg  
Erdsystemwissenschaften  
Bundesstr. 55  
20146 Hamburg

Tag der Disputation: 31. März 2023

Folgende Gutachter empfehlen die Annahme der Dissertation:

Prof. Dr. Nedjeljka Žagar  
Dr. Richard Blender

Vorsitzender des Promotionsausschusses:

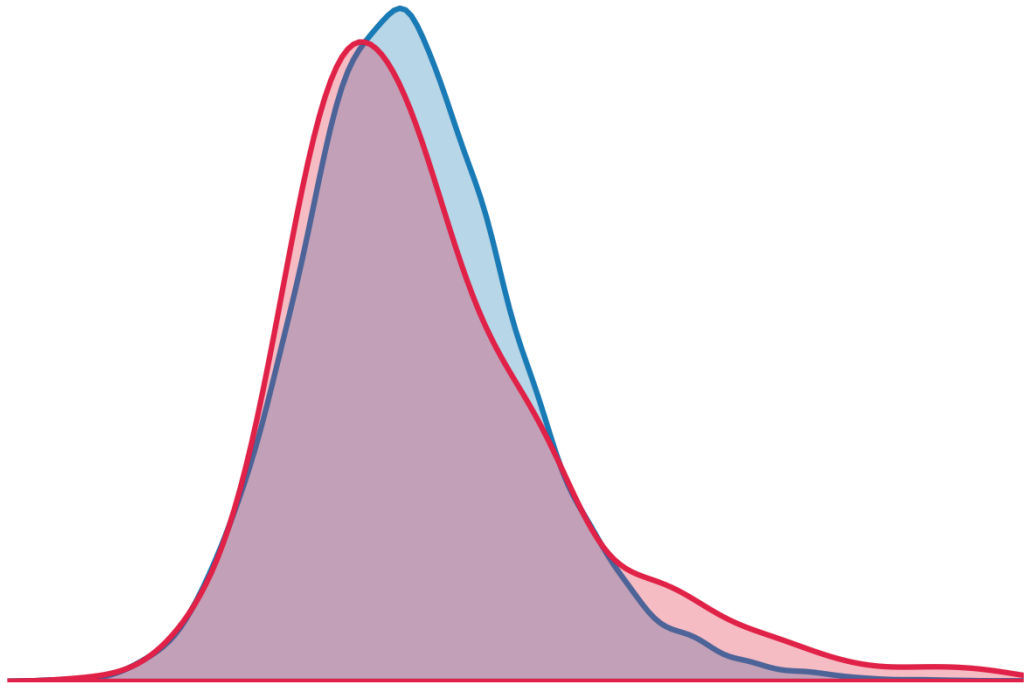
Prof. Dr. Hermann Held

Dekan der MIN-Fakultät:

Prof. Dr.-Ing. Norbert Ritter

Titelgrafik von Iana Strigunova:  
*Change in planetary-scale Rossby waves during Eurasian heat waves*

Signatures of Eurasian heat waves in the  
global Rossby wave spectra in reanalyses  
and CMIP models



Iana Strigunova

Hamburg 2023

**Iana Strigunova**

Signatures of Eurasian heat waves in the global  
Rossby wave spectra in reanalyses and CMIP models



"Nothing in life is to be feared, it is only to be understood.  
Now is the time to *understand more*, so that we may *fear less*."

— Marie Curie

*Memento mori*

Dedicated to beloved grandfather, Nicolai

1939–2020

and to dear friend, Andrey

1995–2021





## ABSTRACT

---

Atmospheric heat waves lead to substantial economic damage and fatalities. The formation, maintenance mechanisms and long-term prediction of heat waves remain a challenge. Given their increasing number and strength due to climate change, the importance of understanding processes involved with heat waves can hardly be overstated.

Previous studies focused on regional processes associated with heat waves. This thesis diagnoses heat waves from a global framework employing a novel method for the regime- and scale-dependent decomposition. The thesis focuses on Eurasian heat waves defined by the 2-meter temperature exceeding the 95th percentile over three consecutive days, and the associated global circulation. Daily circulation fields are decomposed into scales and Rossby and non-Rossby components using the normal-mode function framework. Energy anomalies associated with heat waves are analysed separately for the zonal-mean state (zonal wavenumber  $k=0$ ), planetary-scale ( $k=1-3$ ) and synoptic-scale ( $k=4-10$ ) Rossby waves. The key question asked is how the scale-dependent, spatio-temporal variance distribution of troposphere-barotropic Rossby waves changes during Eurasian heat waves in reanalysis datasets and how these changes are simulated by the models involved in the Coupled Model Intercomparison Project Phase 5 (CMIP5). The four modern reanalyses are combined to analyse the present climate. Several CMIP5 models are analysed, including their atmospheric simulations forced by the observed sea-surface temperature (AMIP) and coupled atmosphere-ocean simulations of the present climate, and the results are compared with the reanalyses. The probability density functions (PDFs) of the Rossby wave energy anomalies are found to be skewed. The skewness parameter is used to describe the change in the PDFs during Eurasian heat waves with respect to the climatological PDFs. The results reveal that during Eurasian heat waves, the PDFs of the Rossby waves change differently at different scales. At planetary scales, the skewness increases due to an increase in probabilities of large energy anomalies. For the synoptic-scale Rossby waves, a shift in the PDF towards larger positive energy anomalies is found, which coincides with an increase in intramonthly variability. The skewness remains almost unchanged for the zonal-mean state, which can be related to the opposite changes in the intramonthly variability at different latitude belts.

The AMIP simulations by the CMIP5 models are able to represent the main aspects of the Eurasian heat waves and the associated planetary-scale Rossby circulation found in the reanalysis data, but discrepancies are noticed in the simulated temporal variability of global energy. In contrast, the coupled CMIP5 simulations struggle to represent the main features of the Rossby-wave circulation during Eurasian heat waves. The discrepancy may be related to a poor representation of

air-sea interactions in coupled models and the interaction between the surface and troposphere above it. Future efforts should be spent on understanding the coupling between thermodynamic processes near the surface and large-scale tropospheric circulations contributing to the development of heat waves.

## ZUSAMMENFASSUNG

---

Atmosphärische Hitzewellen können zu Todesfällen und erheblichen wirtschaftlichen Schäden führen. Die Entstehung, die Mechanismen zur Aufrechterhaltung und die langfristige Vorhersage von Hitzewellen bleiben eine Herausforderung. Angesichts ihrer zunehmenden Anzahl und Stärke aufgrund des Klimawandels kann die Bedeutung des Verständnisses von Prozessen im Zusammenhang mit Hitzewellen kaum genug betont werden.

Frühere Studien konzentrierten sich auf regionale Prozesse im Zusammenhang mit Hitzewellen. Diese Dissertation diagnostiziert Hitzewellen aus globaler Perspektive unter Verwendung einer neuen Methode zur regime- und skalenabhängigen Darstellung. Die Arbeit konzentriert sich auf eurasische Hitzewellen, definiert durch die Überschreitung des 95%-Perzentil der 2-Meter-Temperatur an drei aufeinanderfolgenden Tagen, und die damit verbundene globale Zirkulation. Tägliche Zirkulationsfelder werden unter Verwendung von Normal-Modelfunktionen in verschiedene Skalen und Rossby- und Nicht-Rossby-Komponenten zerlegt. Energieanomalien im Zusammenhang mit Hitzewellen werden getrennt für Rossby-Wellen im zonalen Mittel (zonale Wellenzahl  $k=0$ ), auf planetarer Skala ( $k=1-3$ ) und auf synoptischer Skala ( $k=4-10$ ) analysiert. Die Hauptfrage ist, wie sich die skalenabhängige, räumlich-zeitliche Verteilung der Varianz von troposphärisch-barotrope Rossby-Wellen während eurasischer Hitzewellen in Reanalyse-Datensätzen ändert und wie diese Änderungen von am Coupled Model Intercomparison Project Phase 5 (CMIP5) beteiligten Modellen simuliert werden. Die vier modernen Reanalysen werden verwendet, um das gegenwärtige Klima zu analysieren. Mehrere atmosphärische Simulationen von CMIP5-Modelle, die durch die beobachtete Meeresoberflächentemperatur (AMIP) und gekoppelte Atmosphäre-Ozean-Simulationen des gegenwärtigen Klimas angetrieben werden, werden analysiert und mit den Reanalysen verglichen. Die Wahrscheinlichkeitsdichten (PDFs) der Rossby-Wellenenergieanomalien sind schief. Die Schiefe der PDFs wird verwendet, um die Änderung der PDFs während eurasischer Hitzewellen in Bezug auf die klimatologischen PDFs zu beschreiben. Die Ergebnisse zeigen, dass sich die PDFs der Rossby-Wellen während eurasischer Hitzewellen skalenabhängig ändern. Auf planetaren Skalen nimmt die Schiefe aufgrund einer Zunahme der Wahrscheinlichkeiten großer Energieanomalien zu. Für die Rossby-Wellen auf synoptischer Skala wird eine Verschiebung der PDF hin zu größeren Anomalien positiver Energie gefunden, die mit einer Zunahme der Variabilität innerhalb eines Monats zusammenhängt. Die Schiefe bleibt für das zonale Mittel nahezu unverändert, was mit den gegenläufigen Änderungen der intramonatlichen Variabilität in verschiedenen Breitengraden zusammenhängen kann.

Die AMIP-Simulationen der CMIP5-Modelle sind in der Lage, die Hauptaspekte der eurasischen Hitzewellen und der damit verbundenen Rossby-Zirkulation auf planetarer Skala darzustellen, die in den Reanalysedaten gefunden wurden; es werden jedoch Unterschiede in der simulierten zeitlichen Variabilität der globalen Energie festgestellt. Im Gegensatz dazu werden in den gekoppelten CMIP5-Simulationen Hauptmerkmale der Rossby-Wellen-Zirkulation während eurasischer Hitzewellen unzureichend wiedergegeben. Die Diskrepanz kann mit der Parametrisierung der Ozean-Atmosphäre- und der Land-Atmosphäre-Wechselwirkungen in gekoppelten Modellen zusammenhängen. Zukünftige Anstrengungen sollten unternommen werden, die Kopplung zwischen thermodynamischen Prozessen nahe der Oberfläche und der großräumigen troposphärischen Zirkulationen zu verstehen, die zur Entwicklung von Hitzewellen beitragen.

## PUBLICATIONS

---

### FIRST AUTHOR

#### Appendix A

Strigunova, I., R. Blender, F. Lunkeit, and N. Žagar (2022). “Signatures of Eurasian heat waves in global Rossby wave spectra.” In: *Weather Clim. Dynam.* 3.4, pp. 1399–1414. DOI: [10.5194/wcd-3-1399-2022](https://doi.org/10.5194/wcd-3-1399-2022).

#### Appendix B

Strigunova, I., R. Blender, F. Lunkeit, and N. Žagar (n.d.). “CMIP5 models (in?)ability to simulate signatures of Eurasian heat waves in troposphere-barotropic planetary-scale Rossby circulation.” - *to be submitted*.

### MINOR CONTRIBUTIONS

I was involved in developing data processing and visualisation scripts while participating in the discussion of the meteorological part of the analysis.

Custódio, D., K. A. Pfaffhuber, T. G. Spain, F. F. Pankratov, I. Strigunova, K. Molepo, H. Skov, J. Bieser, and R. Ebinghaus (2022). “Odds and ends of atmospheric mercury in Europe and over the North Atlantic Ocean: temporal trends of 25 years of measurements.” In: *Atmospheric Chem. Phys.* 22.6, pp. 3827–3840. DOI: [10.5194/acp-22-3827-2022](https://doi.org/10.5194/acp-22-3827-2022).



*If he hadn't done it,  
if he hadn't been so convinced  
that he had right visions,  
then he would never have succeeded.*

— (Gleick, 1997)

## ACKNOWLEDGEMENTS

---

My PhD is a time of great lessons I could not imagine 3 years ago. The first lesson I learnt was to stay calm. PhD requires wisdom, patience and compassion, especially for yourself. The second lesson was to defend your opinion, be open to others and always be kind. The third lesson was to stay strong. We are fragile mortals, even our beloved ones. The fourth lesson was to let people help you and being not afraid to ask and be honest. This is why I would like to say "thank you" to all of you.

The first I want to acknowledge is my remarkable supervisor, Nedjeljka Žagar. Thank you for giving me an opportunity to work with you and supporting me in many different ways, especially numerous efforts to review my work. I am thankful to my co-supervisors, Richard Blender and Frank Lunkeit, for your support, knowledge, and experience. It was a great pleasure to have an opportunity to discuss science with you. I would like to thank all of you for your great ideas and staying patient. I would like to express immense gratitude to my panel chair Johanna Baehr. For your support, not only for taking care that I was still on track but also for being responsive in moments when I needed the most. Even within your busy schedule, you always find the time.

I am grateful to the IMPRS-ESM for providing extremely useful courses, an opportunity to be among fantastic IMPRS students and a chance to be a member of MPI-M. I am especially grateful to the IMPRS Office (Antje Weitz, Cornelia Kampmann, Michaela Born) for being available, helping with different stages of the PhD and advising in difficult situations.

I am much obliged to Vera Melinda Galfi. From the beginning to the end, you stayed with me. You helped me to be where I am, and you are part of this success. My special thanks go to Elliot Mckinnon-Gray for correcting all my first writing in English, Clara Henry for correcting my English in the first manuscript, Mateo Duque Villegas for helping improve one of the thesis chapters, Valentino Neduhal for giving feedback on chapters about the MODES. I am indebted to Leam Mykel Martes for helping improve the essay, reading the thesis several times, and being so supportive. I am particularly appreciative to George Datsaris for the valuable lessons and for helping me in a hard moment. I am especially grateful to Lya Lugon Cornejo von Marttens, Julianna Carvalho Oliveira and Jairo Segura for always being positive.

I am sincerely grateful to my present and former colleagues (Sándor, Chen, Alexia, Yuan-Bing, Katharina, Sergiy and Heena, Gözde, Denny, Weinlin, Valerio, Qiyun, Verena, Paolo) for a friendly and creative environment. My big thanks go to Frank Sielmann for handling all technical issues, Leonard Borchert for valuable discussion on complicated matters of biases in CMIP models, also to Goratz Beobide Arsuaga for many discussions about heat waves.

Next, I am thankful to my friends Darya, Tatiana, Evgeniy, Bahram, Ksenia, Anastasia (x2), Vladimir and others for adding colours to my life. I am also thankful to my Mom for being a great mother.

Finally, I would not be here without my former supervisor Kirill Bulgakov and my friend Danilo Custodio. Thank you for giving me a chance and helping me take the first steps in stormy life and the exciting profession of being a scientist.



# CONTENTS

---

<b>Unifying text</b>	<b>1</b>
<b>1 MOTIVATION AND THE RESEARCH QUESTIONS</b>	<b>3</b>
<b>2 INTRODUCTION</b>	<b>7</b>
2.1 Connection between the surface heat waves and atmospheric circulation . . . . .	7
2.1.1 From large- to small-scale drivers of the Eurasian heat waves	7
2.1.2 Statistics of atmospheric circulation associated with heat wave	11
2.2 Global three-dimensional modal decomposition . . . . .	14
2.3 Heat waves and related atmospheric circulation in the CMIP models	15
2.3.1 How well are they simulated? . . . . .	16
2.3.2 Possible sources of the biases . . . . .	17
<b>3 CONTRIBUTIONS OF THIS DISSERTATION</b>	<b>19</b>
3.1 Modal statistics and associated processes in Rossby circulation across scales . . . . .	19
3.2 Model evaluation in the present climate . . . . .	24
<b>4 DISCUSSION</b>	<b>27</b>
<b>5 CONCLUSIONS</b>	<b>29</b>
5.1 Paths forward . . . . .	31
<b>Appendices</b>	<b>33</b>
<b>A SIGNATURES OF EURASIAN HEAT WAVES IN GLOBAL ROSSBY WAVE SPECTRA</b>	<b>35</b>
A.1 Introduction . . . . .	37
A.2 Method and data . . . . .	39
A.2.1 Normal-mode function decomposition of global circulation .	40
A.2.2 Heat waves . . . . .	42
A.2.3 Time series of Rossby wave energy anomalies . . . . .	43
A.3 Results . . . . .	45
A.3.1 Northern Hemisphere midlatitude circulation during heat waves . . . . .	45
A.3.2 Global statistics in Rossby-wave space: climatology . . . . .	46
A.3.2.1 Changes in the Rossby-wave energy statistics during heat waves . . . . .	49
A.3.3 Changes in planetary-scale circulation during heat waves . .	52
A.3.4 Changes in intramonthly variance during the surface heat waves . . . . .	52
A.4 Conclusions . . . . .	55

B	CMIP5 MODELS (IN?)ABILITY TO SIMULATE SIGNATURES OF EURASIAN HEAT WAVES IN TROPOSPHERE–BAROTROPIC PLANETARY-SCALE ROSSBY CIRCULATION	59
B.1	Introduction	60
B.2	Data and Methods	63
B.2.1	Heat Waves	63
B.2.2	CMIP5: climatology of Rossby-wave circulation	63
B.3	Results	64
B.3.1	Metrics of HWs in CMIP5 models	64
B.3.2	Present-day climatology of the troposphere–barotropic planetary-scale Rossby waves in CMIP5 models	67
B.3.3	Do HWs in reanalyses and CMIP5 models have the same signatures on planetary scales?	70
B.4	Conclusions	72
B.5	Discussion	73
	BIBLIOGRAPHY	75

## LIST OF FIGURES

---

Figure 1	Schematic representation of processes contributing to mid-latitude summer heatwaves. From Domeisen et al. (2022). . . . .	8
Figure 2	Schematic representation of the MODES decomposition only for the wind field at 300 hPa averaged throughout the 2010 Russian heat wave. . . . .	14
Figure 3	PDFs of the normalised energy anomalies in the global balanced (Rossby mode) circulation for (a) all wavenumbers, (b) the zonal-mean state, (c) planetary-scale waves and (d) synoptic-scale waves. The empirical PDFs are depicted as green bars. The dark green curve is the kernel density estimator (KDE). The red bars and curves illustrate the same but for the Eurasian heat waves (HWs) listed in Table 1. . . . .	21
Figure 4	Zonal-mean zonal wind in the northern hemisphere troposphere in 1980-2019, May-Sep ERA5 data. (a) Climatology, (b) Eurasian HWs and (c) HWs - climatology. . . . .	23
Figure A.1	Vertical structure functions (VSFs) for the first seven vertical modes. VSFs are derived for 43 $\sigma$ levels using the stability profile of ERA-Interim data. VSFs that do not change the sign below the tropopause (defined as 250 hPa level) are troposphere–barotropic modes. . . . .	41
Figure A.2	Atmospheric energy distribution for the Rossby wave with the zonal wavenumber $k = 7$ , meridional mode $n = 3$ and vertical mode index $m = 1$ in ERA5 for 1980–2014. The dashed black lines correspond to the theoretical $\chi^2$ distribution (df represents the degrees of freedom). . . . .	46
Figure A.3	(a),(b) Climatological Rossby wave circulation for extended boreal summer (MJJAS) at the $\sigma$ level close to 500 hPa in the midlatitudes. (a) All zonal wavenumbers $k > 0$ , all meridional modes $n$ and all vertical modes $m$ are included. (b) As in (a), but only troposphere–barotropic vertical modes, $m = 1 - 5$ . (c) As in (b) but for the Russian heat wave (HW) in 2010. (d) Difference between the (c) and (b). (e) As in panel (b), and panel (f) is as in (d) but for the European HW in 2019. Coloured contours are geopotential height anomalies (in gpm). The wind speed is shown by the length of the wind vectors (with $15 \text{ ms}^{-1}$ as a reference vector). . . . .	47

Figure A.4	PDFs of the normalised energy anomalies in the global balanced (Rossby mode) circulation for (a) all wavenumbers $k$ , (b) the zonal-mean state ( $k = 0$ ), (c) planetary-scale waves ( $k = 1 - 3$ ) and (d) synoptic-scale waves ( $k = 4 - 10$ ). The empirical PDFs are depicted as green bars. The dark green curve is the kernel density estimator (KDE). . . . .	48
Figure A.5	Box plots for the (a) skewness and (b) excess kurtosis of the PDFs of normalised energy anomalies for four circulation components: all Rossby modes (all $k$ ), the zonal-mean flow ( $k = 0$ ), planetary-scale Rossby waves ( $k = 1 - 3$ ), and synoptic-scale Rossby waves ( $k = 4 - 10$ ). Vertical lines mark 95% confidence intervals. Green and red shades denote the climatology and HWs, respectively. . . . .	49
Figure A.6	As in Fig. A.4, but for the Eurasian heat waves listed in Table 1.	50
Figure A.7	Planetary-scale, troposphere–barotropic Rossby waves ( $k = 1 - 3$ , $m = 1 - 5$ , all $n$ ) at the $\sigma$ level close to 500 hPa in ERA5. (a) Mean circulation in May–September in 1980–2019, (b) composite of 28 Eurasian heat waves (HWs) presented in Table 1 and (c) difference between (b) and (a). Coloured contours are geopotential height anomalies, every 20 gpm. The wind speed is shown by the arrow length. (d)–(f) Longitude–pressure cross sections of planetary-scale geopotential height (colours) and meridional wind (isolines) perturbations along $54^\circ\text{N}$ . (d) Climatology, (e) HWs, and (f) difference between (d) and (e). Solid and dashed contours in (d)–(f) correspond to the northward and southward meridional wind speed, respectively, every $2 \text{ ms}^{-1}$ . . . . .	53
Figure A.8	(a) Intramonthly variance spectra of the Rossby waves for the climatology (blue) and Eurasian heat waves (magenta). The embedded panel shows the relative change in percentages of the climatology. The blue shading denotes the 95%-confidence intervals. (b) Changes in the intramonthly variance with respect to climatology as a function of the zonal wavenumber and meridional mode including the zonal-mean state. . . . .	55
Figure A.9	Zonal-mean zonal wind in the Northern Hemisphere troposphere in 1980–2019, May–Sep ERA5 data. (a) Climatology, (b) Eurasian heat waves (HWs) and (c) climatology - HWs. .	56

Figure B.1	Box plots of daily 2 m temperature (T2m) averaged over Eurasia. ERA5 is shown as a green boxplot. CMIP5 coupled simulations are displayed as blue box plots, the uncoupled as red box plots. MPI-ESM-LR temperature time series is displayed as a purple boxplot. Interquartile ranges (IQRs) are displayed as whiskers with boxes framed with vertical lines (25th and 75th percentiles). . . . .	65
Figure B.2	The same as in Fig. B.1 but only positive deviations from 95th percentile identified for every dataset separately. . . .	65
Figure B.3	Climatological Rossby wave circulation for extended boreal summer (MJJAS) at the $\sigma$ level close to 500 hPa in the mid-latitudes in ERA5 (a) and difference in CMIP5 models (c), (e), (g) in coupled and (b), (d), (f), (g) in uncoupled. Only zonal wavenumbers $k = 1 - 3$ , all meridional modes $n$ and vertical modes $m = 1 - 5$ ( $m = 1 - 2$ for CNRM-CM5 and MIROC5) are included. . . . .	68
Figure B.4	Quantile-quantile (Q-Q) plots of the normalised energy anomalies in the global balanced (Rossby mode) planetary circulation ( $k = 1 - 3$ ). (a) all reanalyses (x-axis) compared with all CMIP5 models (y-axis). CMIP5 HIST (coupled) are displayed as green dots and AMIP (uncoupled) as blue dots. (b) the same as (a), but only one reanalysis (ERA5) and one model (CNRM-CM3) are displayed. The same is for GFDL-CM3 in (c), MIROC5 in (d) and MPI-ESM-LR in (e). Note that the last model is presented only with an AMIP run. Dashed lines are a "perfect" fit for each comparison. . .	69
Figure B.5	Box plots for the skewness of the PDFs of normalised energy anomalies for planetary-scale Rossby waves ( $k = 1 - 3$ ) from ERA5 and each CMIP5 model. . . . .	69
Figure B.6	PDFs of the normalised energy anomalies in the global balanced (Rossby mode) planetary circulation ( $k = 1 - 3$ ). (a) the same as Fig. 6c in Strigunova et al. (2022). Model ensembles with coupled and uncoupled simulations are shown in (b) and (c), respectively. Red curves with shading are energy anomalies only during Eurasian HWs. Note that the identification algorithm is applied for each model and simulation separately. . . . .	70

Figure B.7	Planetary-scale, troposphere–barotropic Rossby waves ( $k = 1 - 3$ , $m = 1 - 5$ , all $n$ ) at the $\sigma$ level close to 500 hPa in ERA5. (a) Mean circulation in May–September in 1980–2019, (b) composite of 28 Eurasian Heat Waves (HWs), (c) difference between (b) and (a). Coloured contours are geopotential height anomalies, every 20 gpm. The wind speed is shown by the arrow length. (d) The same as (a), but GFDL-CM3 (coupled) is displayed (only 1979–2005). (e) the same as (b) but a composite of 23 Eurasian Heat Waves (HWs), (f) the same as (c). Similarly, GFDL-CM3 AMIP is shown in (g)–(I). . . . .	71
Figure B.8	The same as in Fig. B.7 but ERA5 fields are subtracted from GFDL-CM3’s accordingly. . . . .	72

## LIST OF TABLES

---

Table 1	Heat waves in Eurasia during May–September 1980–2019 . .	22
Table A.1	Heat waves in Eurasia during May–September 1980–2019 . .	43
Table B.1	CMIP5 model parameters and their truncations in MODES (HIST is short for historical simulation, and AMIP stands for "atmosphere-only" simulations) . . . . .	64
Table B.2	HW metrics (Perkins-Kirkpatrick and Gibson, 2017). Uncoupled simulations are shown in parentheses. . . . .	66

## UNIFYING TEXT





## MOTIVATION AND THE RESEARCH QUESTIONS

---

Heat waves are extreme events in the climate system with scales starting from 1000 km or more and a lifetime ranging from days and months. Physical processes associated with heat waves vary in space and time, with larger scales influencing the scales below them and vice versa. An example of small-scale processes are surface fluxes, these occur locally with a lifetime of a few minutes to hours. On an intermediate scale, one can find synoptic systems, in particular, blocking (persistent high-pressure systems), that is on a regional scale and with a lifetime ranging from days to weeks. Furthermore, there are large-scale (planetary) structures, known as Rossby waves, lasting for multiple weeks. These act on continental-sized areas, and sometimes even larger, as was exemplified in the Northern Hemisphere heat waves in 2010 (e.g. Schubert et al., 2014) and 2018 (e.g. Kueh and Lin, 2020). On larger temporal scales, one can find remote sea surface temperature (SST) anomalies that may influence heat wave formation months in advance (e.g. Della-Marta et al., 2007). There is a rising concern that anthropogenic activity also influences heat wave dynamics (Eyring et al., 2021), with scales varying from annual to centennial. Hence, heat waves can be described as the product of a complex interaction between different components, which is reflected in a wide variety of heat wave definitions (Horton et al., 2016). A common way to define heat waves is by their intensity and persistence, such as Heat Wave Magnitude Index (Russo et al., 2015) or warm spell duration, one of the indices proposed by the Expert Team on Climate Change Detection (ETCCDI, <https://www.wcrp-climate.org/etccdi>). Another type of common definition: heat exposure, is based on impacts. The primary impact is the influence on human health, in particular the cardiovascular system (e.g. Kenney et al., 2014). Heat waves also have impacts on ecosystems (e.g. Stillman, 2019), agricultural and energy sectors (e.g. Amazirh et al., 2017), and on infrastructure (e.g. Zuo et al., 2015), which when sufficiently deteriorated by heat waves can lead to additional, indirect, fatalities. Moreover, future impacts may be more severe as heat waves are expected to increase in frequencies and magnitudes (Seneviratne et al., 2021). Hence, it is necessary to understand heat waves and their drivers to improve predictions of future extreme events which, in turn, contribute to improvements in climate adaptation and mitigation.

Underlying processes leading to and occurring during heat waves are the outgoing scientific challenges which can be described by a quote from Domeisen et al., 2022: "A better understanding of the relevant drivers and their model representation, including atmospheric dynamics, atmospheric and soil moisture, and surface cover should be prioritized to improve heatwave prediction and projection". Every mentioned driver has been studied in different frameworks. Atmospheric and

soil moisture together with surface cover are associated with "thermodynamics". Atmospheric dynamics are defined as atmospheric processes contributing to heat waves. These are typically associated with persistent high-pressure patterns, blocking, and large-scale Rossby waves. Rossby-wave propagation and amplification are suggested to be determining factors in heat wave formation (e.g. Screen and Simmonds, 2014; Teng and Branstator, 2019). However, no study has yet attempted to explore whether Rossby waves can be affected by heat waves or, in other words, whether heat waves have signatures in the Rossby wave spectrum<sup>1</sup>. To fill this gap, I pose the following research question:

*How do heat waves, by definition regional phenomena, affect the global troposphere-barotropic Rossby wave spectrum?*

To answer this question, in the first step, I perform a statistical analysis on the circulation associated with the Rossby waves at different zonal scales, i.e. the zonal wavenumbers with the troposphere-barotropic structure. The analysis employs reanalysis datasets and focuses on Eurasia.

In the next step, the results of the statistical analysis are interpreted in the context of dynamics, i.e. processes in atmospheric circulation, within these ranges to understand the following:

*What large-scale processes are associated with signatures of heat waves in the global variance spectra<sup>2</sup>?*

Answers to these questions allow for 1) the development of a new, spatially three-dimensional diagnostic tool and 2) an intercomparison of obtained results with previous studies, mainly two-dimensional in space domain, thus connecting processes occurring in spectral space with those in physical space. For spectral analysis and transformation back to physical space, I project reanalysis datasets into the normal-mode functions, a concept described in Section 2.2.

Finally, the new methodology is applied to the Coupled Model Intercomparison Project Phase 5 (CMIP5) models to evaluate their performance. The evaluation is done by answering the third research question:

*Do heat waves have the same signatures in CMIP5 models on planetary scales as in reanalyses?*

The answers to the research questions are given in Section 3 and Appendices. This essay aims to present their research context. A secondary aim is to interpret and evaluate these findings by explaining how they contribute to existing scientific knowledge. In Section 2.1, I give an overview of drivers of heat waves from a multi-scale point of view and what statistical tools can be applied to study associated physical processes. In Section 2.2, the global three-dimensional modal

---

<sup>1</sup> Here, the Rossby wave spectrum is defined as a continuous range of wave frequencies associated with a wide range of spatio-temporal scales.

<sup>2</sup> Here, "variance spectra" are defined as intramonthly variance distributions on different spatial scales.

decomposition used in this study is briefly introduced. Section 2.3 describes how heat waves and their associated atmospheric circulation are simulated in CMIP5 models, further elaborating on what systematic errors (biases) are detected in the existing literature. Section 3 consists of the results of modal statistics accompanied by a discussion of associated processes across scales and its evaluation in models. In Section 4, the discussion of the strengths and limitations of a statistical analysis in modal space is shown. In Section 5, I give a summary of the answers to the research questions and conclude with an outlook at the end of the thesis.



## INTRODUCTION

---

In this section, I explore drivers of heat waves, including Rossby waves, give an overview of applied statistical methods, introduce the MODES software for the decomposition of atmospheric circulation and discuss how CMIP models simulate the heat waves and associated high-pressure systems, so-called blockings which are parts of Rossby waves.

### 2.1 CONNECTION BETWEEN THE SURFACE HEAT WAVES AND ATMOSPHERIC CIRCULATION

This section provides an overview of existing literature on drivers of heat waves at different scales and how they can be analysed in a statistical sense.

#### 2.1.1 *From large- to small-scale drivers of the Eurasian heat waves*

Heat waves are the product of complex interactions occurring in the Earth system. In particular, the large-scale atmospheric circulation (dynamic factor) and land processes (thermodynamic factor) are key drivers discussed in exhaustive studies. Nevertheless, a complete understanding is still challenging due to processes acting on different spatiotemporal scales. A recent study by Domeisen et al. (2022) demonstrated that the heat wave phenomenon is multi-scale (see Fig. 1), not only in driving processes but also in impacts. In this dissertation, I follow a similar approach and discuss factors of heat waves occurring over Eurasia according to their scales. I start the discussion with large-scale remote structures, such as quasi-stationary Rossby waves (e.g. Stefanon et al., 2012) and sea surface temperature (SST) anomalies (e.g. Ding and Wang, 2005) and then I move to local land processes. Soil moisture content, in particular, also plays a role in heat wave formation (e.g. Miralles et al., 2014) and can amplify already existing extreme hot conditions (e.g. Fischer et al., 2007; Seneviratne et al., 2010). The latter highlights the complexity of interaction with non-linear dynamics involved (e.g. Horton et al., 2016; Ma and Franzke, 2021). This dissertation is not intended to formulate an overarching theory; however, it demonstrates that even within a linear dynamics framework, heat waves appear in global atmospheric circulation.

In the atmosphere, large-scale quasi-stationary wave patterns are associated with persistent high-pressure systems (blockings) that circumvent the westerly flow to the north and south, thus increasing the meridional component. Blocking, a main dynamical driver of heat waves, is a multi-scale process with a lifetime ranging

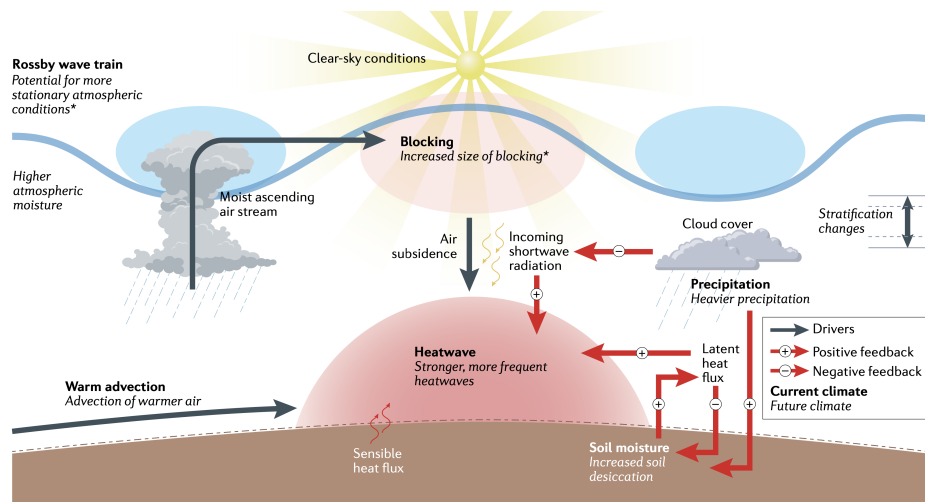


Figure 1: Schematic representation of processes contributing to midlatitude summer heatwaves. From Domeisen et al. (2022).

from days to weeks, or in exceptional cases, even months (e.g. Kautz et al., 2022). Therefore, various processes occur around blocks, and what prevails defines the onset and decay phases.

Several previous studies focused on the effect of large-scale atmospheric modes of variability on Eurasian heat waves. For example, the summer North Atlantic Oscillation was identified by Folland et al. (2009) and contributed to the 2018 summer heat wave (Kueh and Lin, 2020). Another large-scale mode of variability, the summer Northern Hemisphere annular mode, may play a role in heat wave formation and maintenance, as it was illustrated by Feudale and Shukla (2011) and Ogi et al. (2005) for the 2003 European heat wave.

Blockings are considered to be a part of Rossby waves propagating away from sources and their further amplification (White et al., 2022). There is no unifying theory which could explain the entire process. One of the existing mechanisms is the global teleconnection pattern (Ding and Wang, 2005), described as a circum-global wave train within a jet stream, a narrow band of upper tropospheric winds. For instance, Drouard and Woollings (2018) showed that the formation of blocking over Western Russia is preceded by a low-frequency large-scale wave train and defined by low-frequency processes. Schubert et al. (2011) identified recurring Eurasian stationary waves as part of the variability during the 2003 European and 2010 Russian heat waves. Deng et al. (2018) found that jet weakening over the Atlantic region leads to the amplification of the Rossby-wave trains at the jets' exit, thus strengthening anticyclones over Eastern Europe and Northern China.

The Rossby waves are usually excited due to diabatic heating (heating caused by energy exchange) in the tropics (e.g. Teng and Branstator, 2019). Di Capua et al. (2020) analysed the connection between tropical convective activity and circum-global Rossby-wave trains and found the influence of the South Asian monsoon

on the circumglobal teleconnections, particularly in the Eurasian region. Trenberth and Fasullo (2012) demonstrated that the atmospheric blocking during the 2010 Russian heat wave was maintained by the anomalous Rossby wave train from the tropics. Schneidereit et al. (2012) showed that La Niña conditions favour the occurrence of the blocking observed during this heat wave by modulating stationary waves.

Another proposed forcing of Rossby waves is found in polar regions through Arctic amplification (e.g. Coumou et al., 2018), the theory of wave excitation due to rapidly warming high latitudes. The role of this process is actively debated due to model biases in these regions (e.g. Anstey et al., 2013), the way waviness is analysed (e.g. Screen and Simmonds, 2013) and the lack of a sufficient length of observations, as these mechanisms act on larger scales (e.g. Blackport and Screen, 2020). Another disputable theory is quasi-resonance amplification (Petoukhov et al., 2013), which relies on resonance between two components of Rossby waves, the stationary parts (excited due to orography and land-sea contrasts) and the travelling or free parts. The resonance occurs in the presence of waveguides, in other words, two jet streams on two latitudes, and thus travelling Rossby waves are trapped. The trapped Rossby waves resonate with stationary Rossby waves, which results in increased wave amplitudes observed during several heat waves in recent studies (e.g. Kornhuber et al., 2019). However, the lack of sufficient data length, and the necessity of idealised experiments, means that this theory remains disputable.

Instead of circumglobal Rossby-wave trains, it is suggested that upper-tropospheric Rossby-wave packets (RWPs) are dominant in heat wave formation (Chang, 2001). RWPs are defined as localised large-amplitude waves. Fragkoulidis et al. (2018) demonstrated that the surface extremes are better confined with RWPs rather than circumglobal patterns. Ali et al. (2021) revealed recurrent synoptic-scale RWPs as being important in modulating the persistence of heat waves. It has been shown in some studies (e.g. Chang et al., 2016) that synoptic variability is expected to decrease along with the weakening of the jet stream (Coumou et al., 2015). However, according to theory (Coumou et al., 2014), the weakening of zonal flow leads to meandering, which leads to wave amplification and, consequently, to more extremes on the surface. Therefore, it is unclear what is leading what, which in turn affects future projections.

Another cause for future projections' uncertainties is systematic errors (biases) in general circulation models (GCMs). For example, biases in North Atlantic SSTs affect the representation of several processes, including blocking and heat waves, over Europe. Nabizadeh et al. (2021) demonstrated that the cold North Atlantic SSTs, observed in early summer, favour jet stream meandering and the ridge over Europe and, thus, triggering heat waves in 2015 and 2018. Extratropical SSTs are connected with tropical SSTs (e.g. Wu et al., 2007). Tropical SSTs, being Rossby wave sources, also influence monsoon onset, which is shown to affect heat wave occurrences, as very hot and dry long periods (e.g. Teng et al., 2013). Indian Ocean

SSTs are found to have an influence on heat waves over Europe (e.g. Bader and Latif, 2005; Behera et al., 2012), whereas Pacific SSTs have more relevance to hot extremes over northern America (e.g. McKinnon et al., 2016).

On shorter spatiotemporal scales, the thermodynamic drivers can be of the same importance as the dynamic ones, which are mainly represented as the advection of tropical air masses for midlatitudes (Della-Marta et al., 2007) and warmer air masses for high latitudes. The latter is found to be a reason for the recent Antarctic heat wave of March 2022 (Turner et al., 2022). Nevertheless, the advection is of second-order importance for European heat wave formation. The primary factor is air subsidence (downward motion) from upper levels. For the British Isles, as an example, along with subsidence, adiabatic heating (heating caused by air mass compression without heat transfer) is primary in heat wave formation. In contrast, the thermodynamic factor is becoming more important for western Russia through diabatic heating and influence from remote energy fluxes (Zschen-derlein et al., 2019). The energy transfer between the atmosphere and surface is provided through energy fluxes (sensible and latent heat fluxes). The sensible heat flux represents the direct heat transfer, whereas the latent heat flux depends on the moisture content and energy release through evaporation. Therefore, the lesser the moisture, the smaller the latent heat fluxes and the larger the sensible heat fluxes. The larger sensible heat fluxes mean more surface warming and drier soil, thus, generating positive soil-moisture-temperature feedback, inevitably resulting in prolonged heat waves and droughts. For instance, Whan et al. (2015) showed that this feedback also plays a role in spring dry soil anomalies, which are considered to be precursors to summer heat waves over Europe. Similarly, Schumacher et al. (2019) pointed out the importance of considering remote heat fluxes as their advection favours the occurrence of intensive heat waves.

The coupling between land and atmosphere can also explain different types of heat waves. Thomas et al. (2020) demonstrated that daytime and nighttime heat waves have different mechanisms. For daytime, clear-sky conditions increase incoming shortwave radiation, which enhances sensible heat fluxes of dry soil, and leads to a rise in surface temperature. Nighttime heat waves occur mainly due to scattered radiation, moist air and temperature advection. Similar processes have been outlined for another type of heat wave - the wet heat wave, a phenomenon recently separated due to the vital role of humidity (Yu et al., 2021). The high humidity limits water vapour release from the soil, which is important for cloud formation and surface cooling. Other factors like vegetation and land use can accentuate or mitigate land-atmosphere feedback. In the case of vegetation, the effects can be described via mechanisms of evapotranspiration, the process involving plant transpiration and moisture evaporation from the soil. If transpiration is weak and moisture content is low, the atmosphere is less humid, and vice versa. Even the type of vegetation is important: broad-leaved or needle-leaved forests are more likely to reduce heat (e.g. Schwaab et al., 2020; Eyster and Beckage, 2022). As for land use, it is known that irrigation decreases surface temperature, meaning



that agricultural activities are non-negligible in areas where heat waves are more likely to occur (Lobell et al., 2008).

To conclude, heat waves are multi-scale processes. It involves planetary scales with Rossby waves and remote SST anomalies, along with local effects where the vegetation and moisture content defines its further evolution. To better understand the processes leading to extremes, several studies (e.g. Terray, 2021; Wehrli et al., 2019) used different approaches to disentangle dynamic and thermodynamic factors. According to Suarez-Gutierrez et al. (2020), the dynamic factor is the dominant driver of variability in extreme European summer temperatures in the present and future. However, it has been found that, in the future, local thermodynamic mechanisms will prevail in extreme occurrences. However, related future dynamics (atmospheric circulation) projections are largely uncertain (Shepherd, 2014), and current models contain numerous biases, which are discussed in Section 2.3.

### 2.1.2 *Statistics of atmospheric circulation associated with heat wave*

The climate and its variability are characterised by a broad spectrum of spatiotemporal scales. In each window of this spectrum, there is an infinite number of modes and their interactions. When extreme events, such as heat waves, occur, some interactions might be enhanced or weakened. To identify robust features, the statistical analysis offers a variety of methods. Inferential statistics, or the analysis of distributions of the variables of interest, is traditionally applied in order to draw conclusions about the processes behind the data. This thesis aims to understand the distributions of the global balanced circulation and how they change during heat waves by ascribing them to certain theoretical distributions. According to the central limit theorem, in high-dimensional systems, such as atmospheric circulation, sums of independent distributions with equal mean and variance will be Gaussian. Moreover, variables averaged or summed over long enough periods would also exhibit Gaussian or "normal" behaviour.

Nonetheless, in general, atmospheric fields are found to be non-Gaussian (e.g. Sura et al., 2005). Probability distributions of near-surface temperatures from different locations are shown to be skewed. With the help of Monte-Carlo simulations, Perron and Sura (2013) computed the skewness of several atmospheric variables from every grid. For instance, the temperature at 925 hPa is characterised by non-Gaussian distribution dependent on climatological highs and lows that define the sign of skewness. The skewness of low-level zonal wind is positive in the tropics, but changes sign in mid and high latitudes. Zonally averaged fields have almost no skewness. Positive skewness is found in the Northern Hemisphere in the meridional wind but positive in the Southern Hemisphere with some small regional differences, probably associated with impacts from the surface. For the horizontal wind speed, the skewness is mainly positive globally, except for localised negative skewness in tropical regions. The distribution of low-level horizontal wind is likely described by Weibull distribution or a special case of Rayleigh distribution. At

higher vertical levels (300 hPa), the skewness of the relative velocity field depends on latitude but with maximum values near the jet streams. Barnes and Polvani (2013) discussed jet stream latitude anomaly distributions in GCMs and identified that those models, which tend to simulate jets closer to the equator, are usually more positively skewed. The skewness is zero or even negative in models where the jet stream is closer to the poles. Geopotential height at 500 hPa has positive skewness in equatorial and polar regions, but it is negative in the midlatitudes.

Therefore, the above-mentioned scientific literature highlights the importance of considering skewness, as most distributions are asymmetric with respect to the mean. Furthermore, changes in skewness, along with excess kurtosis, a measure relative to the normal distribution, reflect changes in the probabilities of tails and hence, probabilities of extremes in the data. Statistical modelling studies of extremes often apply extreme value theory. This theory allows for gaining return levels which would not be present in observational data but are essential in infrastructural engineering, insurance and other sectors with long-term planning. However, the major challenge in applications to climate data is the small length of such data sets because the statistics are performed on tails of distributions which often contain a small number of occurrences.

Still, skewness and excess kurtosis are useful parameters to describe non-Gaussian distributions. For instance,  $\chi^2$  distribution is used to define the number of degrees of freedom as a criterion for modelling heat waves in Australia (Wong, 2015). The concept of the number of degrees of freedom often appears in physical and mathematical studies. In dynamical systems theory, it is exploited to evaluate different regimes. On the example of the blocking regime over the Atlantic, Lucarini and Gritsun (2020a) showed that the number of degrees of freedom is increased during the onset and decay of blocking; therefore, these states are of low predictability. In contrast, during the mature phase, the number of degrees of freedom decreases; therefore, these states are highly predictable. Another advanced statistical method - the large deviation theory - applied by Galfi and Lucarini (2021). The results showed that the dynamic of persistent weather patterns observed during heat waves is part of the natural variability of the climate. However, it is also rather atypical in terms of the intensity of the considered anomalies.

Moreover, the application of dynamical systems theory and large deviation theory to climate and weather problems is relatively new. More traditional and intuitive methods are based on correlating atmospheric fields representing atmospheric motions (geopotential height at 500 and 300 hPa or streamfunctions on similar levels) corresponding blocking indices with surface variables, mainly 2 m temperature (T2m) (e.g. Sousa et al., 2018). For example, Pfahl and Wernli (2012) found that the evolution of blocking is strongly connected to heat wave formation by correlating events of intensive blocking with extreme T2m values.

The Fourier transform is a widely used approach for analysing atmospheric fields, where data are projected into a set of trigonometric functions. It allows

analysing the wavenumber spectra, including dominant frequencies identified as peaks in the spectrum within a specified domain. For the midlatitudes and on monthly scales, Screen and Simmonds (2014) found the change in the mean and variance of the distribution of large-scale waves (zonal wavenumbers 3-8) during temperature extremes compared to near-averaged weather. In a similar way, several studies (e.g. Coumou et al., 2014; Kornhuber et al., 2017) revealed that the Fourier amplitudes of zonal wavenumbers 5-8 of meridional wind at different levels are amplified during recent heat waves. Not only the Fourier amplitudes but also phase speeds are investigated in relation to temperature extremes. Riboldi et al. (2020) used composites of high and low phase speeds of Fourier harmonics obtained from meridional wind at 250 hPa. They confirmed findings from previous studies (e.g. Kornhuber et al., 2019) showing that low phase speeds are typical during surface temperature extremes.

Empirical orthogonal functions are useful in identifying dominant patterns primarily associated with modes of variability. These modes of variability are typically analysed in teleconnection studies and, in particular, to diagnose Rossby-wave train propagation (e.g. Tachibana et al., 2010; Schubert et al., 2014). These studies demonstrated that anomalies in Rossby waves are part of the dynamics preceding heat waves.

Similarly, self-organising maps (SOMs), which identify patterns based on artificial neural networks, are becoming more widely used. This approach does not require approximations, making it more flexible than other methods. Lee et al. (2017) applied SOMs and found that enhanced teleconnections are highly correlated with temperature extremes over the Northern Hemisphere. Other advanced methods, such as Peter and Clark - Momentary Conditional Information algorithm or Maximum Covariance Analysis, are used to detect co-variability between tropical regions as sources of Rossby waves and extremes in the midlatitudes (e.g. Di Capua et al., 2020; Vijverberg and Coumou, 2022).

In summary, the described methods are used to study particular aspects of heat waves, including the influence of remote regions. In contrast, I apply a simple statistical analysis on the distributions of global Rossby circulation to examine its climatology and how it changes during Eurasian heat waves. The analysis is performed in modal space after reanalysis datasets are projected into the normal-mode functions, a concept described in Section 2.2.

*Our picture of the atmosphere is that of a vibrating system with many modes of oscillations, like a musical instrument.*

— (Žagar et al., 2015)

## 2.2 GLOBAL THREE-DIMENSIONAL MODAL DECOMPOSITION

Atmospheric circulation is typically described as wind and temperature fields. In this thesis, I employ a modal view of global circulation, where these fields are decomposed into a series of two-dimensional oscillations associated with various vertical structures. This subsection describes a concept, whereas the complete theory and other applications can be found in Žagar and Tribbia (2020) and the references therein.

Within linear theory, atmospheric circulation is represented as a set of normal modes with small amplitudes around the basic state of rest. These motions can be further separated into low- and high-frequency parts, which I refer to as balanced (Rossby) and unbalanced (inertia–gravity) dynamics with different horizontal and vertical scales. To separate into different horizontal scales, the input data are projected into the complete set of the Hough functions, examples of which are presented in Fig. 2. In order to decompose input data into different vertical scales, the vertical structure functions are applied. These structures are coupled by a parameter, the so-called equivalent depth. These procedures are incorporated in the MODES software (Žagar et al., 2015) with the output of the time series of the Hough expansion coefficients. Every coefficient represents a single normal mode, a function of the zonal wavenumber,  $k$ , meridional mode,  $n$  and vertical-mode index,  $m$ .

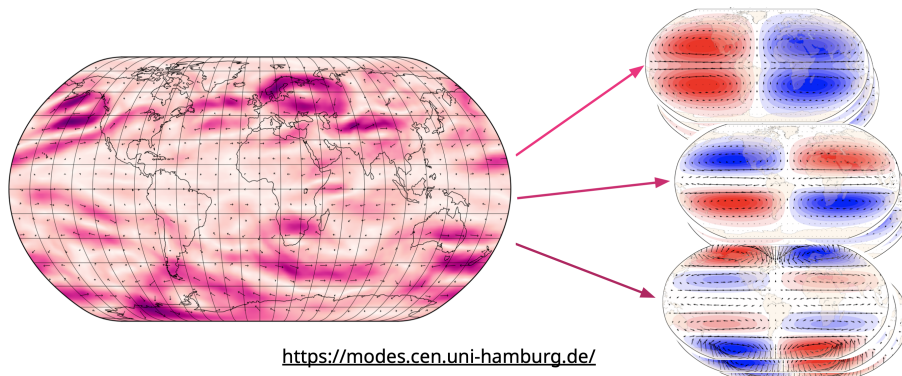


Figure 2: Schematic representation of the MODES decomposition only for the wind field at 300 hPa averaged throughout the 2010 Russian heat wave.

The variations in the global circulation can be described by the changes in modes with different spatio-temporal scales. Spatial variability is represented by the global total (kinetic plus available potential) energy spectra (e.g. Žagar et al.,

2017). Temporal variability can also be analysed in terms of the spectra of temporal variance as for example by (Žagar et al., 2020). The temporal variability is computed as deviations from their respective climatological means over different time scales (annual, monthly, daily). For heat waves, as multi-scale events, it is relevant to consider all scales. However, in this study, I discuss only intramonthly variability, where I identify significant changes. The results are presented in Section 3 and Appendix A.

### 2.3 HEAT WAVES AND RELATED ATMOSPHERIC CIRCULATION IN THE CMIP MODELS

Numerical models in weather and climate are mathematical formulations of processes governed by natural laws. There is a wide range of model applicability: the verification of specific hypotheses, the prediction of system evolution, and the treatment of missing data. Before models can be applied to any of the tasks, they have to be validated with observational datasets, reanalyses or other models.

The largest project, where models are validated and re-applied, is the Coupled Model Intercomparison Project (CMIP). It consists of several phases, with Phase 6 (CMIP6) being the most recent one with the largest number of models, better vertical and horizontal resolution, improved physics, and inclusion of more Earth system components (Eyring et al., 2019).

One of the major aims of CMIP is to perform and evaluate future projections of climate extremes. In the case of extremes, such as heat waves, this is challenging due to different definitions of the events and the sensitivity of these definitions to the input data (Perkins, 2015). Moreover, due to climate change, the time series of climate variables, including their extremes, are non-stationary, meaning that what statistical relations identified for the present might not hold in the future (Seneviratne et al., 2021). Because of these uncertainties, their future drivers and interconnections still need to be fully understood. Nevertheless, future heat wave projections are considered to be robust and display a severe global increase in magnitude and frequency by the end of the century (Seneviratne et al., 2021).

It is important to keep in mind that models are biased. In other words, there is a discrepancy between actual Earth system processes and our simulations of them. To reduce this discrepancy, process-based estimation studies are performed. In the case of extreme surface temperatures, for example, several studies (e.g. Wehrli et al., 2019) reported that biases in thermodynamics lead to higher surface temperatures in models. In contrast, blocking tends to be underrepresented (e.g. Davini and d'Andrea, 2020). Both affect the representation of heat wave metrics. In this spirit, I first give an overview of CMIP models' performance of heat waves, blocking and associated Rossby waves with their biases origins discussed in the second part of this subsection.

### 2.3.1 *How well are they simulated?*

In order to numerically simulate the climate system, one has to know the governing dynamical and thermodynamical equations. The thermodynamic energy equation describes the evolution of temperature. The quasi-geostrophic theory is a good description of the large-scale atmospheric circulation in the midlatitudes. However, the mathematical description of heat waves and blocking remains a challenge partially due to the involved sub-grid-scale processes unresolved in climate models. Therefore, model biases are inevitable. To evaluate the impact, the model performance is usually assessed.

The heat wave performance is analysed throughout CMIP model generations and related metrics. CMIP Phase 3 (CMIP3) performs well at capturing monthly hot extremes (Yao et al., 2013). Daily extreme indices (the number of warm days, maximum temperature, the number of tropical nights) in CMIP5/6 are comparably well simulated with a decreased inter-model spread from CMIP3 to CMIP5 (Sillmann et al., 2013) and from CMIP5 to CMIP6 (Kim et al., 2020).

However, global warm spell duration remains overestimated (Fan et al., 2020), whereas global heat wave frequency is still underestimated (Hirsch et al., 2021). Di Luca et al. (2020) demonstrated that warm biases in temperature anomalies on the global scale are the result of biases in regional estimations, such as mean and maximum temperatures (e.g. Park et al., 2016) and their percentiles (Kim et al., 2020). These variables significantly differ from observations in CMIP5/6 models over Europe (Cattiaux et al., 2013; Carvalho et al., 2021). Marginal improvements from CMIP5 to CMIP6 are also found in the representation of heat wave duration and magnitude (Hirsch et al., 2021).

Plavcova and Kysely (2016) demonstrated that a mismatch in heat wave duration is connected to the misrepresentation in blocking persistence. Schiemann et al. (2020) showed that the model's median spread had not been changed for blocking persistence, but it decreased twice for blocking frequency from CMIP5 to CMIP6. However, Davini and d'Andrea (2020) identified that blocking frequency is still underrepresented in models. Therefore, blocking and heat waves representation still suffer from biases identified in previous generations (Schiemann et al., 2020).

The representation of blocking is affected by the zonal-mean flow and Rossby wave propagation. While several biases in the zonal-mean flow are identified (Berckmans et al., 2013), the midlatitude Rossby wave climatology is well reproduced in CMIP5 and CMIP6 models (Luo et al., 2022). Nevertheless, biases in Rossby waves might originate from their sources, such as orography, land-sea contrast and tropical diabatic heating. Nie et al. (2019) discussed the climatology of the Rossby wave sources (RWS) during the summer season. It is found that RWS are reproduced in the ensemble mean of the CMIP5 models over the globe but overestimated in the subtropics and underestimated in the midlatitudes.

To conclude, despite an overall improvement in CMIP models, biases are identified in global and regional metrics of heat waves and the related atmospheric circulation. The second part of the subsection explores their possible sources.

### 2.3.2 Possible sources of the biases

Biases in numerical models have different origins: numerical scheme, i.e. how future states are connected with previous ones; resolution, i.e. how fine the grid (the size of cells) is constructed to capture physical processes; parameterisations, i.e. representation of sub-grid-scale processes and complex processes that cannot be described by the model equations based on numerical schemes and equations derived empirically. The above sources of biases affect the representation of heat-waves and the associated atmospheric circulation as well. Problems with numerical schemes lead to blocking and heat waves simulations straying from observational data. A resolution that is too coarse does not allow for the capture of physical processes affecting the blocking and heat wave lifecycles. The issue with parameterisation influences all those mentioned above because many processes essential for heat wave evolution are parameterised. Thus, by improving all of these aspects, the representations of heat waves and blocking have to be improved as well.

The most common way, or "cure for biases", is the increase in temporal and spatial resolution. More time steps mean that the evolution is captured more accurately, while more processes can be resolved with finer horizontal and vertical grids. Moreno-Chamarro et al. (2022) demonstrated that an increase in horizontal model resolution improves the overall performance of climate models by reducing biases in the midlatitude SST and zonal winds along with precipitation and cloud cover in the tropics. Moreover, according to Di Luca et al. (2020), the errors in temperature extremes are reduced in models with higher resolution. However, in the example of blocking frequency, Davini and d'Andrea (2020) illustrated that biases are not entirely alleviated simply by improving resolution.

Over the Euro-Atlantic region, for instance, the biases in blocking representation can be associated with smoothed topography and overall parameterisations of convection and microphysics. Sandu et al. (2019) showed that the representation of the atmospheric circulation might be affected by how parameterisations deal with topographic processes. This also affects the representation of large-scale quasi-stationary Rossby waves because they originate from orography, which is poorly represented in models (Pithan et al., 2016).

According to Zelinka et al. (2020), the biases in the parameterisation of low-level clouds can explain with higher 95th percentiles for warm extremes in CMIP6 models. Fewer clouds and, therefore, a drier atmosphere leads to higher surface temperatures in the model simulations. Higher surface temperatures lead to larger sensible fluxes which, in turn, affect blocking maintenance (Pfahl et al., 2015). Remote fluxes can lead to biases as well. Lee et al. (2019) illustrated that biases in Arctic moisture flux are connected to tropical temperatures in the upper troposphere.

Thus, due to the effect of remote biases, the improvement of local processes is not sufficient.

Another strategy to diagnose and alleviate biases is to perform simulations where some parts of the Earth system (ocean, for instance) are uncoupled from other parts (atmosphere, for instance). Uncoupling the ocean from the atmosphere means that the air-sea interaction, the connection between atmosphere and ocean, is missing. These simulations are called "atmosphere-only" and, in the CMIP framework, they are known as Atmospheric Model Intercomparison Project (AMIP) experiments. These experiments allow diagnosing only the atmospheric model, where SST and sea ice are observed. By comparing it with coupled simulations, reveals whether errors remain when SST and sea ice are prescribed. One of the numerous studies using this diagnostic tool, Scaife et al. (2011) illustrated that blocking climatology is presented better in "atmosphere-only" runs. On the contrary, Davini and D'Andrea (2016) showed that both simulations perform similarly. Therefore, the effect of biases associated with SST errors is an ongoing challenge.

Overall, several studies show a marginal improvement in heat waves and blocking simulations between different CMIP generations, suggesting that significant improvements in spatial resolution, cloud parameterisations and many resolved processes do not guarantee that models will be free of biases. This holds especially for the Euro-Atlantic region: numerous studies focus on this region using high-resolution models and improved parameterisation, but still, the blocking persistence is not well-captured (e.g. Kautz et al., 2022) and surface temperatures still deviate from observations (e.g. Carvalho et al., 2021).



## CONTRIBUTIONS OF THIS DISSERTATION

---

Sections 2.1 and 2.3 demonstrated how much has been accomplished to understand and simulate heat waves and associated atmospheric circulation. Still, questions of what processes lead to heat waves, how they are maintained, and how atmospheric circulation responds remain open. Furthermore, to understand the whole picture, not only local or regional processes should be considered, but also global-scale processes. As an initial step in better understanding the connection between heat waves and global Rossby wave circulation, I formulated the following research questions outlined in Section 1:

- *How do heat waves, by definition regional phenomena, affect the global troposphere-barotropic Rossby wave spectrum?*
- *What large-scale processes are associated with signatures of heat waves in the global variance spectra?*
- *Do heat waves have the same signatures in CMIP5 models on planetary scales as in reanalyses?*

To answer the first question, I analysed anomalies in global total energy (the kinetic energy plus the available potential energy) in modal space. The interpretation of energy anomaly results allows answering the second question with the help of computed intramonthly variances, i.e. global variance spectra. The third question is answered by comparing results based on reanalysis datasets with CMIP5 models.

### 3.1 MODAL STATISTICS AND ASSOCIATED PROCESSES IN ROSSBY CIRCULATION ACROSS SCALES

It is evident that the processes in the atmosphere are connected with processes at the surface. In this thesis, Rossby waves are associated with blockings which are weather regimes observed during heat waves. Most of the previous studies focused only on the midlatitudes. Some other studies discussed the effect of extratropical and tropical dynamics on heat waves (e.g. Trenberth and Fasullo, 2012; Di Capua et al., 2020) or polar regions (e.g. Coumou et al., 2018). Therefore, the dynamics of heat waves are connected with dynamics that occur on a global scale. Particularly, this connection can be considered as heat wave effects on the global circulation.

While no current study addresses this aspect, I aimed to explore this gap by asking the following question:

*How do heat waves, by definition regional phenomena, affect the global troposphere-barotropic Rossby wave spectrum?*

To answer this question, I performed statistical analysis on global total energy anomalies, which can be described in several steps.

- (i) Reanalysis datasets are projected into the normal-mode functions. Their outputs are used to compute energy.
- (ii) By subtracting the annual cycle, its anomaly is computed. These time series are referred to as the climatological Probability Density Functions (PDFs).
- (iii) Energy anomalies for days with heat waves are sampled and compared with climatological PDFs.

In the first step, the four reanalysis datasets: European ERA5 (Hersbach et al., 2020), ERA-Interim (Dee et al., 2011), the Japanese 55-year Reanalysis (Kobayashi et al., 2015), and the Modern-Era Retrospective analysis for Research and Applications (Rienecker et al., 2011), which were projected into the normal-mode functions over May-September 1980-2014 (for ERA5, 1980-2019). The output of this procedure was daily Hough expansion coefficients, where every coefficient represents every circulation mode in three dimensions. These three-dimensional coefficients were used to compute daily energy time series, which, as I found, follow the  $\chi^2$  distribution in a single normal mode. As examples with wind speed and geopotential height distributions showed, non-zero skewness is expected. Because the atmosphere is the superposition of different waves on a defined background, the exact distribution is undetectable.

In the second step, I computed energy anomalies to remove the annual cycle and then normalised them by standard deviation. Normalised time series were combined into three ranges: the zonal-mean state, planetary-scale, and synoptic-scale Rossby waves with the troposphere-barotropic part, a structure observed during heat waves (e.g. Feudale and Shukla, 2011). Figure 3 depicts PDFs consisting of all time steps and all reanalyses as green bars and curves. I refer to these PDFs as climatological. Note that Fig. 3a shows normalised energy anomalies for the zonal-mean state and Rossby waves together. Figure 3 demonstrates that all distributions are skewed; therefore, the approximation of the  $\chi^2$  distribution is still valid. The highest asymmetry is found in the PDFs of the zonal-mean circulation (Fig. 3b) and planetary Rossby waves (Fig. 3c). The asymmetry is described by skewness, a parameter used further in the analysis.

In the third step, I proceeded with analysis during heat waves. I employed 2 m temperature (T2m) in the Eurasian region limited by the Ural mountains (exact latitude-longitude domain [35°N-65°N, 10°W-60°E]) and then spatially averaged to obtain T2m time series. Heat waves were defined via the 95th percentile of

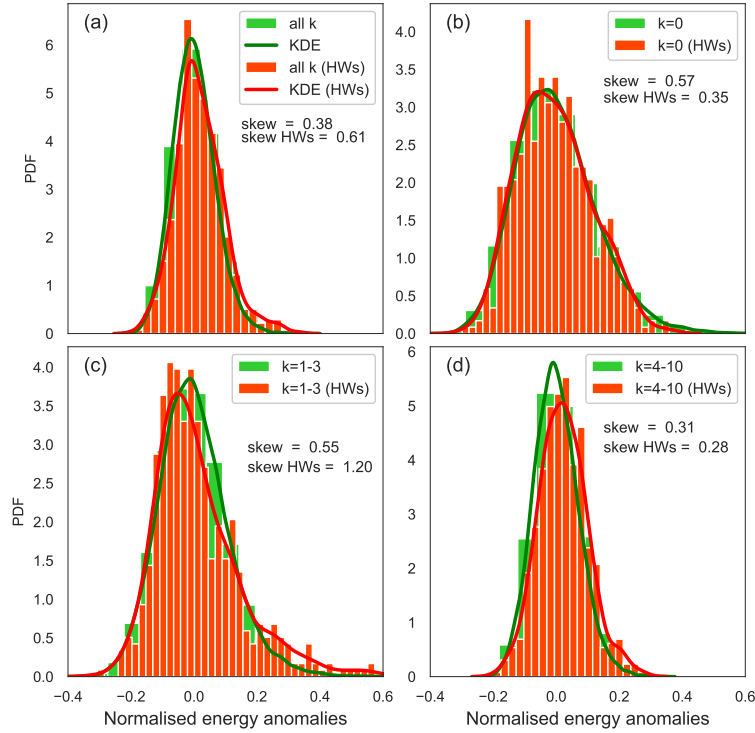


Figure 3: PDFs of the normalised energy anomalies in the global balanced (Rossby mode) circulation for (a) all wavenumbers, (b) the zonal-mean state, (c) planetary-scale waves and (d) synoptic-scale waves. The empirical PDFs are depicted as green bars. The dark green curve is the kernel density estimator (KDE). The red bars and curves illustrate the same but for the Eurasian heat waves (HWs) listed in Table 1.

temperature time series with exceedances of more than three days. This procedure was done separately for every reanalysis. Based on the results, 13 heat wave events were present in all datasets, with 15 more events only for ERA5 (Table 1). Identified time steps with heat waves were used to sample energy anomalies. By comparing the climatological PDFs and the PDFs during Eurasian heat waves (red bars and curves in Fig. 3), I identified changes in circulation across scales, such as skewness decrease in the zonal-mean state, its increase in planetary-scale Rossby waves and an overall shift of the PDF in synoptic waves. To understand the processes that associated to these changes, I proceeded further and asked:

*What large-scale processes are associated with signatures of heat waves in the global variance spectra?*

Presented above statistical analysis revealed changes in the PDFs, one of which is the increase in skewness in planetary scale-Rossby waves. I found the relation between relative change in the skewness and the number of degrees of freedom. According to the analysis, the decrease in the number of degrees of freedom is

Table 1: Heat waves in Eurasia during May-September 1980-2019

		ERA5	ERA-Interim	JRA-55	MERRA
	Start date	Number of detected days			
1	1994-09-23	3	3	2	3
2	2006-06-18	12	10	12	10
3	2006-09-20	3	5	6	2
4	2007-05-20	12	12	12	12
5	2007-08-21	6	6	6	6
6	2008-09-05	4	3	4	3
7	2010-06-28	26	27	27	26
8	2010-07-27	21	21	19	21
9	2012-05-09	4	4	4	4
10	2012-06-14	4	3	4	3
11	2013-05-02	7	7	6	5
12	2014-05-17	5	3	3	3
13	2014-06-05	5	6	5	6
14	2015-06-02	3	-	-	-
15	2015-08-11	3	-	-	-
16	2015-09-17	11	-	-	-
17	2016-06-21	4	-	-	-
18	2016-08-20	9	-	-	-
19	2018-05-02	8	-	-	-
20	2018-06-27	4	-	-	-
21	2018-07-13	22	-	-	-
22	2018-08-29	7	-	-	-
23	2018-09-11	12	-	-	-
24	2019-06-01	3	-	-	-
25	2019-06-08	5	-	-	-
26	2019-06-18	3	-	-	-
27	2019-06-23	4	-	-	-
28	2019-07-24	3	-	-	-
$\Sigma$ days		213	110	110	104

25% which is likely associated with the coarse structure and the persistent nature of blocking.

By performing additional analysis on intramonthly variance describing temporal variability, I identified a reduction in zonal wavenumber 3 and an increase in zonal wavenumber 8, which is likely associated with increased synoptic activity during heat waves (Shutts, 1983; Yamazaki and Itoh, 2013). With this approach, I detected the largest change in meridional components for the zonal-mean state, implying that the zonal wind field is also modified. To assess it, I transformed the data back to physical space. The result is shown in Fig. 4, where the zonally averaged zonal wind is depicted. Figure 4b resembles the double-jet structure, where the second jet stream occurs in high latitudes during heat waves (Ogi et al., 2005; Rousi et al., 2022a). Figure 4c shows the difference between the climatological zonal wind and zonal wind during heat waves. According to this figure, there is a weakening and a slight northward shift of the maximum zonal-mean zonal wind at 45°N, whereas, in high latitudes (60°N-90°N), the winds are twice as strong as with the largest difference at 75°N.

The processes associated with identified signatures are scale-dependent: the amplitudes of planetary waves are increased with intramonthly variability being reduced. In contrast, the variability of synoptic-scale Rossby waves is increased with the probabilities of larger energy anomalies compared to climatology. In the zonal-mean flow, an increase in variability of meridional modes may be related to eddy-zonal mean interaction and associated with the weakening of the main jet and enhancement of the secondary one detected in high latitudes, a structure similar to the double-jet phenomenon.

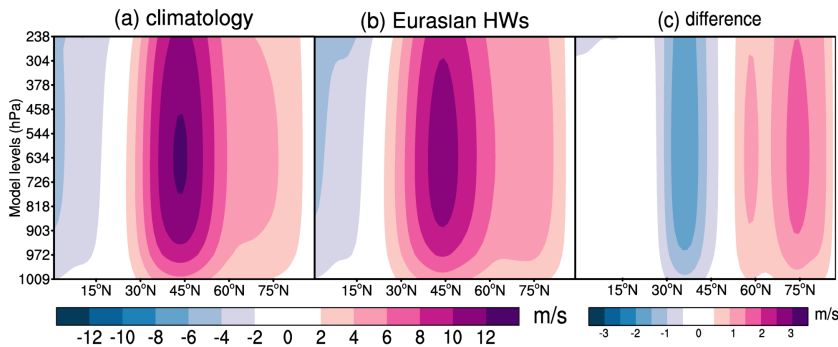


Figure 4: Zonal-mean zonal wind in the northern hemisphere troposphere in 1980-2019, May-Sep ERA5 data. (a) Climatology, (b) Eurasian HWs and (c) HWs - climatology.

The analysis demonstrated that Eurasian heat waves have signatures in the troposphere-barotropic Rossby-wave circulation across scales. According to the most recent IPCC report (2021), heat waves are expected to become more intensive and frequent. However, no clear trend is found for atmospheric circulation. Thus, the projections remain uncertain. In this thesis, I was focused on evaluating how models used for climate projection (CMIP5, Taylor et al. (2012)) simulate sig-

natures by applying the methodology outlined above. The details are explained in the following subsection.

### 3.2 MODEL EVALUATION IN THE PRESENT CLIMATE

The model evaluation is often obtained by comparing observational datasets with models of different generations. According to numerous studies, heat wave and blocking metrics are long-lasting challenges for GCMs. Schaller et al. (2018) demonstrated that the link between blocking and heat waves is well-presented in models; however, Van Oldenborgh et al. (2022) pointed out that heat wave variability remains to be improved. To identify directions of improvement, one can make use of several metrics. Signatures discussed in the previous section could also be considered as metrics. In this thesis, I explored this opportunity by asking the following:

*Do heat waves have the same signatures in CMIP5 models on planetary scales as in reanalyses?*

To answer this question, single members of four CMIP5 models (CNRM-CM5, GFDL-CM3, MIROC5, MPI-ESM-LR) with historical (coupled) and "atmosphere-only" (AMIP, uncoupled) runs were projected into the normal-mode functions in the same way as reanalysis datasets. Due to different vertical and horizontal resolutions, the truncation is different; therefore, the number of troposphere-barotropic modes is also different. For GFDL-CM3 and MPI-ESM-LR, the first five vertical modes are troposphere-barotropic, whereas for CNRM-CM5 and MIROC5, only the first two.

Before discussing circulation during heat waves, I discussed how CMIP5 heat wave representation and the climatology of Rossby waves are similar to ERA5 and other reanalyses. The climatology is obtained for the 27-year period (1979-2005) for May-September.

In the first step, I evaluated how heat wave metrics are presented. For each model and simulation, the set of heat waves was identified. To compare results among models and ERA5, I employed T2m distributions and metrics introduced by Perkins-Kirkpatrick and Gibson (2017).

In the next step, I evaluated the similarity of the climatology of Rossby waves between CMIP5 and reanalyses by discussing their mean circulation with a focus on how their Rossby-wave patterns resemble each other in physical space. The comparison was also made in modal space by comparing quantiles of normalised energy anomaly distributions for the model ensemble and each model separately. In the first case, I compared the distribution of the model ensemble with the reanalysis ensemble. In the second case, each model's distribution was compared with ERA5's distribution separately. This two-step analysis was performed to understand whether 1) models robustly simulate the climatology and 2) a single model is capable of simulating the same climatology as ERA5. Similarly, AMIP simulations were evaluated.

Lastly, I discussed how mean circulation and normalised energy anomaly PDFs during heat waves are simulated in models with coupled and uncoupled simulations. Mean circulation was analysed for each model separately, while model PDFs are compared with reanalysis PDFs. The findings are presented in three steps.

In the first step, statistics of heat waves were assessed in CMIP5 models and ERA5. Models showed similar results in all metrics and were comparable to ERA5 results, including T2m distributions and their anomalies with respect to the mean, 50th and 95th percentiles. No systematic differences between coupled and uncoupled simulations were identified.

In the second step, I compared the climatology of planetary Rossby-wave circulation in CMIP5 and reanalyses, along with individual models and ERA5. Most models showed small differences with ERA5 planetary Rossby-wave climatology, except MIROC5, where anomalies in the geopotential height field were larger than in ERA5. Quantile-quantile (Q-Q) plots of normalised energy anomalies demonstrated a good agreement between models and reanalyses. Nevertheless, higher quantiles in models were found to be overestimated. A similar pattern was observed when I compared individual models (GFDL-CM3 and MPI-ESM-LR) with ERA5.

I also compared the confidence intervals (CIs) of skewness and excess kurtosis by applying bootstrapping procedure on these two parameters for ERA5 and each model to estimate whether their inter-quantile ranges match each other. For skewness (for excess kurtosis, results were similar) showed that only CNRM-CM5 and MIROC5 were within CIs identified from the ERA5 distribution, whereas GFDL-CM3 and MPI-ESM-LR were outside due to larger positive energy anomalies.

Therefore, only CNRM-CM5 demonstrated similar climatology of planetary Rossby waves, whereas MIROC5 had the largest discrepancies in the time-averaged (mean) circulation at 500 hPa. In contrast, GFDL-CM3 and MPI-ESM-LR demonstrated a good agreement in the mean circulation with ERA5, but their energy anomaly distributions were statistically different from ERA5 distributions.

In the third step, I noted that the mean circulation during heat waves resembled the same patterns in coupled and uncoupled simulations, whereas the intensity was reproduced only in uncoupled simulations. Thus, coupled runs struggle to simulate planetary Rossby circulation during the Eurasian heat waves. I did not find statistically significant changes in the PDFs of planetary-scale Rossby waves. It suggests that the temporal variability of energy anomalies in models differs from those found in reanalyses.

In summary, some signatures are similar to those in reanalyses, but not all. Coupled and AMIP runs struggle to simulate the temporal variability of energy anomalies, but at least AMIP can simulate the time-averaged circulation during the Eurasian heat waves. Further work may shed light on the reasons behind this result. The explanation might be related to the models' poor representation of air-sea coupling. The discussion on possible causes is presented in Section 5 and Appendix B.





## DISCUSSION

---

This thesis introduces a new methodology of scale-dependent filtering of global Rossby-wave circulation associated with regional surface extremes, i.e. heat waves. Although I focused on the Eurasian heat waves, the method can be applied for any region of interest and other types of extreme events. It is therefore pertinent to discuss the strengths and limitations of the approach.

### *Multi-variate diagnostic tool and selection of different horizontal and vertical scales*

The applied decomposition is multi-variate, i.e. analysed quantities represent mass and velocity fields simultaneously. Moreover, by this decomposition, one can separate three-dimensional atmospheric circulation into a set of modes corresponding to the two prevalent flows (Rossby and inertia-gravity waves).

### *Global statistics in modal space*

The global total energy and its anomalies can be computed for each mode. By analysing energy anomaly distributions of selected modes, I obtained information on the temporal variability of energy. The analysis of distributions allows for the identification of skewness as one of the key parameters to describe changes during heat waves, which I analysed as a set of events rather than as individual events.

### *Scale-selective filtering*

Selected modes of atmospheric circulation can be projected back to physical space. It allows for diagnosing spatial patterns and their changes during events of interest.

Based on this, I propose this global multi-variate approach as complementary to the regional-based single-level Fourier analysis with the following limitations:

### *Linear solutions*

The MODES software applied in this thesis is based on the linearised equation system, where every normal mode is orthogonal to each other. Thus, no interactions are considered. According to Ma and Franzke (2021), non-linear processes and their interactions can also play a crucial role in heat wave evolution.

### *Assumption about dry atmosphere*

The linearised system is also adiabatic, meaning that moisture effects are not directly included. Thus, some effects like latent heat release in clouds and its role in blocking formation and maintenance (Pfahl et al., 2015) are not represented.

*Composites of circulation and inability to track atmospheric dynamics during heat wave evolution*

In this thesis, I discussed only the composites, i.e. time-averaged circulation over time steps with heat waves. Thus, I could not estimate how circulation changes within the heat wave lifecycle. However, the modal regression technique introduced in Žagar and Franzke (2015) might be an addition to the presented methodology.

## CONCLUSIONS

---

Heat waves involve many different scales. Most studies analysed regional circulation within the midlatitudes. Previous studies also identified that heat waves have remote drivers. Thus, I formulated the research question in the following way:

*How do heat waves, by definition regional phenomena, affect the global troposphere-barotropic Rossby wave spectrum?*

- Several signatures were identified in the PDFs and their skewnesses of normalised energy anomalies. In the zonal-mean state, the skewness is decreased, which is likely associated with the weakening mechanism proposed by Coumou et al. (2015).
- At planetary scales, I found a statistically significant increase in the skewness of PDFs with an increase of geopotential height anomalies at 500 hPa over the region where heat waves were observed.
- At synoptic scales, I detected the statistically significant shift of the entire distribution, which is likely associated with larger amplitudes observed during heat waves.

The next step is to relate PDF changes with changes observed in physical space and intramonthly variance spectra by answering the next question:

*What large-scale processes are associated with signatures of heat waves in the global variance spectra?*

- The persistence of blocking is likely associated with a decreased number of degrees of freedom and reduced intramonthly variability.
- In contrast, the variability of synoptic-scale Rossby waves is increased with the probabilities of larger energy anomalies compared to climatology. It could be associated with intense precipitation observed around the blocking.
- In the zonal-mean flow, an increase in variability of meridional modes may be related to eddy-zonal mean interaction and associated with weakening of the main jet and enhancement of the secondary one detected in high latitudes, a structure similar to the double-jet phenomenon.

CMIP models used for climate projections contain biases in the representation of heat waves and associated atmospheric circulation. Thus, it is helpful to evaluate how these models simulate the signatures discussed above. For this, I asked:

*Do HWs have the same signatures in reanalyses and CMIP5 models on planetary scales as in reanalyses?*

- All heat wave metrics in models are similar to those in ERA5. I found the same results in T2m and its anomalies with respect to the mean, 50th and 95th percentiles. Analysis of their box plots revealed the similarity between models and ERA5.
- The composites of mean planetary Rossby circulation at 500 hPa showed similar patterns as ERA5, but a difference in intensity was found. In particular, MIROC5 tended to overestimate geopotential height anomalies in the midlatitudes.
- Comparison between different simulations revealed no significant biases in SST; however, I noted that anomalies of different sign could cancel each other out when averaging over time steps.
- The model ensemble with energy anomalies had a good agreement with the ensemble of reanalysis. No significant difference was identified between historical and AMIP simulations.
- Model-to-model comparison revealed significantly different skewness in energy anomaly distributions of GFDL-CM3 and MPI-ESM-LR.
- During heat waves, the composites of geopotential height anomalies at 500 hPa among models showed an increase in anomalies over northern Europe, similar to ERA5. Marginal differences were found among historical and AMIP runs.
- Analysis of models PDFs, nevertheless, did not exhibit the same shift as in ERA5, with skewness estimation being largely uncertain. The same applies to comparisons between simulations along with model and reanalysis ensembles.

To conclude, historical runs of CMIP5 models reproduce patterns but not intensity in the mean circulation of planetary-scale Rossby waves during the Eurasian heat waves. In contrast, AMIP runs simulate patterns and intensity of Rossby waves. Thus, this signature is the same in reanalyses and CMIP5 models. However, another signature, a statistically significant increase in skewness, is not present in models in both simulations.

On a final note, the key finding of this dissertation is the evidence of the Eurasian heat wave signatures in the Rossby-wave circulation. These signatures were evaluated in CMIP5 models in coupled and AMIP simulations. The results conclude

that AMIP simulations can simulate the planetary-scale Rossby circulation but with discrepancies in the PDFs of the global total energy anomalies. Contrary to uncoupled runs, coupled simulations have difficulty simulating the signatures in the planetary-scale Rossby waves. The possible causes are likely associated with the poor representation of air-sea interactions and the land-atmosphere feedback. Therefore, further studies should focus on understanding the coupling between thermodynamic processes near the surface and dynamic processes in the troposphere, factors both contributing to heat wave development.

## 5.1 PATHS FORWARD

The next step would be to investigate the scale-dependent dynamics behind these signatures. For example, one could compute wave activity fluxes and E vectors for stationary and transient Rossby waves, respectively. This methodology has already been applied in Schneidereit et al. (2012), where it has been shown that both contributed to blocking maintenance in the 2010 Russian heat wave.

Other types of waves might be diagnosed as well. For example, inertia-gravity waves are prevalent in the tropics, regions known as Rossby wave sources. Other special types of waves (Kelvin and Mixed-Rossby-gravity waves) could also be examined as they are shown to be related to Madden-Julian Oscillation, which is part of dynamics associated with heat waves in the western United States (Lee and Grotjahn, 2019) and northeastern Asia (Hsu et al., 2020).

The findings of the second paper suggest that coupled simulations cannot simulate planetary Rossby circulation during the Eurasian heat waves. In contrast, atmosphere-only (AMIP) simulations are capable of it. Considering the large importance of parameterisations and known issues, one might study how well they represent certain processes and how well the connection with the dynamical core of models is presented. For example, the air-sea interactions and the land-atmosphere feedbacks are the first processes which should be evaluated in models. The possible reasons for the discrepancy are problems with the schemes parameterising surface fluxes. These schemes are influenced by the evolution of SSTs and sea ice together with soil temperatures and soil moisture. Involved temperature and specific humidity are core variables also used in other schemes parameterising convection, clouds, and turbulence in the planetary boundary layer. The parameterisation of convection and clouds affect moisture fluxes which are essential in simulating soil moisture-temperature feedbacks (Stéfanon et al., 2014). The parameterisation of the planetary boundary layer and turbulence define the level of entrainment (or the top level of the planetary boundary layer) and the strength of vertical mixing, which are crucial for blocking and heat wave evolution (Wei et al., 2017). This list is not complete. Other possible sources of biases, such as biases in the zonal-mean state, parameterisation of orography and the effect of the horizontal and vertical resolution, were discussed in Section 2.3.

The results obtained for only single members in CMIP5 could also be further validated by applying the same methodology to CMIP6 models or the entire ensemble of one model as it has been applied in Suarez-Gutierrez et al. (2020) to diagnose the simulations of the 2003 European heat wave.

Finally, it is possible to study three-dimensional atmospheric circulation in climate projections within different scenarios by applying the same methodology. However, the biases and their sources in the present climate have to be examined first.

## APPENDICES







## SIGNATURES OF EURASIAN HEAT WAVES IN GLOBAL ROSSBY WAVE SPECTRA

---

The Appendix consists of a paper that have been published in *Weather and Climate Dynamics* as Strigunova et al. (2022):

Strigunova, I., R. Blender, F. Lunkeit, and N. Žagar (2022). “Signatures of Eurasian heat waves in global Rossby wave spectra.” In: *Weather Clim. Dynam.* 3.4, pp. 1399–1414. DOI: [10.5194/wcd-3-1399-2022](https://doi.org/10.5194/wcd-3-1399-2022).

IS developed the algorithm, performed the data analysis and wrote a first draft of the article. All authors contributed to the study conception and design. All authors participated in data interpretation and revised previous versions of the article. All authors read and approved the final article.

# Signatures of Eurasian heat waves in global Rossby wave spectra

Iana Strigunova<sup>1</sup>, Richard Blender<sup>1</sup>, Frank Lunkeit<sup>1</sup>, Nedjeljka Žagar<sup>1</sup>

<sup>1</sup>*Meteorological Institute, Center for Earth System Research and Sustainability (CEN), Universität of Hamburg, Grindelberg 5, 20144 Hamburg, Germany*

## ABSTRACT

This paper investigates systematic changes in the global atmospheric circulation statistics during Eurasian heat waves (HWs). The investigation of Rossby wave energy anomalies during HWs is based on the time series of Hough expansion coefficients representing Rossby waves with the troposphere–barotropic structures through the extended boreal summer in the European ERA5, ERA-Interim, Japanese 55-year Reanalysis (JRA-55) and Modern-Era Retrospective analysis for Research and Applications (MERRA) reanalyses. The climatological Rossby wave energy distribution is shown to follow a  $\chi^2$  distribution with skewness dependent on the zonal scale.

The applied multivariate decomposition reveals signatures of the Eurasian HWs in the probability density functions (PDFs) of the Rossby wave energy across scales. Changes in the PDFs are consistent with changes in the intramonthly variance during HWs. For the zonal-mean state (the zonal wavenumber  $k = 0$ ), a decrease in skewness is found, although it is not statistically significant. A reduction in skewness hints to an increase in the number of active degrees of freedom, indicating more independent modes involved in the circulation. A shift in the spectral distribution of the  $k = 0$  intramonthly variance is shown to describe a weakening of the mean westerlies near their core at  $45^\circ\text{N}$  and their strengthening at high latitudes. At planetary scales ( $k = 1 - 3$ ), the skewness in the troposphere–barotropic Rossby wave energy significantly increases during HWs. This coincides with a reduction of intramonthly variance, in particular at  $k = 3$ , and persistent large-scale circulation anomalies. Based on the  $\chi^2$  skewness, we estimate a reduction of the active degrees of freedom for the planetary-scale Rossby waves of about 25% compared to climatology. At synoptic scales ( $k = 4 - 10$ ), no change in skewness is detected for the Eurasian HWs. However, synoptic waves  $k = 7 - 8$  are characterised by a statistically significant increase in intramonthly variance of about 5% with respect to the climatology. In addition, a shift of the entire Rossby wave energy distribution at synoptic scales, along with amplification, is observed during HWs.

## A.1 INTRODUCTION

Heat waves, periods with the daily maximum temperatures exceeding the climatological conditions by certain thresholds, have been increasing in number and magnitude, especially over Eurasia (e.g. Rousi et al., 2022b). While the current operational numerical weather and ensemble prediction systems forecast such extremes several weeks ahead (e.g. Emerton et al., 2022), understanding the mechanism and dynamics of heat waves poses a challenge. Heat waves (HWs) are connected with persistent high-pressure systems (blockings). Numerous studies focus on the onset and drivers of blocking; however, no consensus exists due to the complexity of the dynamical and thermodynamical processes involved (e.g. Kautz et al., 2022). Blockings are often parts of large-scale quasi-stationary wave patterns (e.g. Stefanon et al., 2012). On one side, persistent weather patterns are part of internal variability. On the other side, the effect of climate change on the frequency and persistence of these patterns is still under debate (Woollings et al., 2018). For example, Park and Lee (2019) showed that these persistent weather patterns can be forced or triggered by remote anomalous tropical heating. While the physical mechanisms leading to blockings are under discussion (Petoukhov et al., 2013; Nakamura and Huang, 2018; Teng and Branstator, 2019; Wirth and Polster, 2021), the quasi-stationary behaviour of these wave patterns is shown to lead to concurrent extreme events (Kornhuber et al., 2020; Fuentes-Franco et al., 2022).

In contrast to previous studies investigating particular aspects of HWs, our research aims to identify changes in the global Rossby wave energy statistics during Eurasian HWs and to couple them with the observed circulation. While a number of studies addressed particular aspects of HWs over Eurasia (e.g. Feudale and Shukla, 2011; Schneidereit et al., 2012; Trenberth and Fasullo, 2012; Drouard and Woollings, 2018), their effects on the global spatio-temporal variance spectra have not been studied. We analyse the global three-dimensional (3D) circulation in terms of horizontal and vertical scales of the Rossby waves and compare the HWs with the climatology. As we show, the probability density function (PDF) of the Rossby wave energy, which is described by the  $\chi^2$  distribution, changes during the Eurasian HWs. The changes are quantified by skewness of the PDFs for different zonal wavenumbers. The associated reduction of the number of active degrees of freedom compared to climatology can be used to explain the coarse structure of blocking events in the midlatitude troposphere.

The distributions of atmospheric fields are in general known to be non-Gaussian (Sura et al., 2005; Perron and Sura, 2013). However, the central limit theorem may still be applicable when the sums of components in high-dimensional systems are involved, with assumptions of independent and identical distributions of summing components<sup>1</sup>. As we demonstrate, the distributions of anomalies in atmospheric

---

<sup>1</sup> Under the independence of components or variables in a high-dimensional system, one can consider that their time series are uncorrelated. The identity of distributions of summing components can be regarded in terms of their mean and variances being equal.

energy can appear visually close to the normal distribution due to the central limit theorem. However, the energy anomaly distributions are still skewed, which can be considered an inherited property from energy ( $\chi^2$  distributions). The skewness,  $\gamma$ , of the  $\chi^2$  distribution is given by  $\sqrt{8/df}$ , and the excess kurtosis,  $\kappa$ , is given by  $12/df$  with the number of independent degrees of freedom denoted by  $df$  (Wilks, 2011). In the  $\chi^2$  distribution, the term “degrees of freedom” is defined by the number of sum of squares of independent (uncorrelated) normally distributed variables. In our analysis, the number of degrees of freedom is the number of all possible modes used in the projection, while the number of active degrees of freedom is a measure of the concentration of energy in large wavenumbers during a heat wave. It is important that localised structures like blocking do not consist of a finite set of low wavenumber modes but can also include contributions from higher wavenumbers (as is the case for Fourier series). Therefore, the number of active degrees of freedom is not a sharp condition but can be used to measure the system’s complexity. Note that because the atmospheric circulation is the composite of the zonal-mean state and the superposition of waves which might be dependent, the statistical properties might deviate from the ideal situation.

Advanced statistical methods are common tools in the research of extreme weather events. For example, Galfi and Lucarini (2021) analysed surface HWs using the large deviation theory and found that the associated persistent atmospheric patterns are not typical (in the statistical sense) when compared to the climatology, but follow a dynamic which is already encoded in the natural climate variability. Lucarini and Gritsun (2020b) considered blockings to be manifestations of unstable periodic orbits and their stability to be an indicator of predictability and the involved number of degrees of freedom. They find low predictability at the onset and the decay and increased predictability in the mature phase of blocking events in the Atlantic.

A more common tool for the examination of midlatitude circulation during heat waves is the Fourier series analysis of single-variable data along the latitude circles. This approach identifies anomalies in the planetary- and synoptic-scale Rossby waves during extreme events in terms of the Fourier amplitudes and phases of temperature, geopotential or wind variables at different levels. For example, Screen and Simmonds (2014) found a significant increase in the monthly variance and mean of anomalies of the Fourier amplitudes of 500 hPa geopotential heights for zonal wavenumbers 3-8 and suggested that amplified planetary waves are connected to temperature and precipitation extremes. Coumou et al. (2014) analysed wind fields at 300 and 500 hPa and found that zonal wavenumbers 6 – 8 are the most probable candidates for quasi-resonance (amplified quasi-stationary Rossby waves due to the resonance with free waves trapped within the waveguide) according to Petoukhov et al. (2013). More recently, Kornhuber et al. (2019) showed the coupling between the zonal wavenumber 7 in daily wind and temperature data at several standard pressure levels and surface extremes, such as HWs and floods which occurred during the boreal summer 2018.

Our heuristic approach to spectral analysis of HWs considers the horizontal and vertical scales simultaneously by using the normal-mode function (NMF) decomposition to project daily circulation fields onto Rossby and non-Rossby components (Žagar and Tribbia, 2020). The NMF decomposition is multivariate meaning that the wind and geopotential variables are represented by the same spectral expansion coefficient thereby separating the circulation into the balanced (or Rossby) and unbalanced (non-Rossby) components<sup>2</sup>.

Previous applications of the NMF decomposition showed that modal analysis complements other methods of analysing global circulation by providing scale- and dynamical-regime-dependent information on the variability and by quantifying it in wavenumber space (Žagar et al., 2017; Žagar et al., 2020; Žagar et al., 2019). Žagar et al. (2020) quantified amplitudes and trends in midlatitude travelling and quasi-stationary Rossby waves and in the equatorial wave activity in the reanalysis data. They found a statistically significant reduction of subseasonal variance in Rossby waves with zonal wavenumber  $k = 6$ , along with an increase in variance in wavenumbers  $k = 3 - 5$  in the summer seasons of both hemispheres. However, they did not attempt to relate these changes to the surface weather or extreme events. This task is carried out in the present study.

Our goal is to investigate whether and how surface heat waves during boreal summer over Eurasia affect the global atmospheric variability spectrum. While it is not evident *a priori* that regional HWs have their signatures in the global Rossby wave spectra, we show that this is, in fact, the case. First, we demonstrate statistically significant changes in the global total energy anomalies probability density functions (PDFs) during HWs. Then, we interpret the dynamics of the planetary Rossby waves through the change in active degrees of freedom and in temporal variance on intramonthly scales. At last, we provide an overall picture of the changes in atmospheric circulation across scales.

The paper is organised as follows. The 3D decomposition method, statistical analysis and the heat wave identification algorithm are explained in Section A.2. Section A.3 contains results. First, we present examples of the NMF decomposition for two recent HWs. This is followed by the results of statistical analysis of spatial spectra (climatological and HWs energies) and its interpretation by filtering parts of balanced circulation back to physical space. Finally, we discuss how temporal variance spectra change during HWs. Conclusions are presented in Section A.4.

## A.2 METHOD AND DATA

In this section we describe our research method that makes use of the NMF decomposition and the MODES software (Žagar et al., 2015). The method is applied

---

<sup>2</sup> The real-time decomposition of the ECMWF circulation in Rossby and non-Rossby components is available on the MODES web page at <https://modes.cen.uni-hamburg.de> (last access: 27.01.2023).

to the four modern reanalysis datasets. We present the criteria for Eurasian surface HWs and associated selection method for the spectral expansion coefficients.

### A.2.1 Normal-mode function decomposition of global circulation

The NMF decomposition is carried out in the terrain-following global coordinate system  $(\lambda, \varphi, \sigma)$ , where  $\sigma = p/p_s$  is the ratio of the vertical level pressure  $p$  and the surface pressure  $p_s$ ,  $\lambda$  denotes longitude and  $\varphi$  is latitude. At every time step  $t$ , the horizontal winds  $(u, v)$  and geopotential height  $(h)$  on  $\sigma$  levels are projected to precomputed vertical and horizontal structure functions (VSFs and HSFs, respectively). The VSFs are the numerical solutions of the vertical structure equation whereas the HSFs are eigensolutions of the Laplace equation without forcing and are given in terms of the Hough harmonics. The Hough harmonics are defined as a product of the latitude-dependent Hough functions and harmonic waves in the longitudinal direction (e.g. Žagar and Tribbia, 2020). The horizontal and vertical structures are coupled by the eigenvalues of the vertical structure equation, the so-called "equivalent depth". The reader is referred to Žagar et al. (2015) and Žagar and Tribbia (2020) and the references therein for details of the theory.

The projection of discrete data consists of two steps. In the first step, the data vector  $\mathbf{X}(\lambda, \varphi, \sigma) = (u, v, h)^T$  is expanded into a series of orthogonal VSFs denoted  $G_m$  according to

$$\mathbf{X}(\lambda, \varphi, \sigma) = \sum_{m=1}^M G_m(\sigma) \mathbf{S}_m \mathbf{X}_m(\lambda, \varphi). \quad (1)$$

The vertical-mode index  $m$  ranges from 1 to  $M$ , the total number of vertical modes, that can be equal or less than the number of vertical levels. For every  $m$ , the nondimensional data vector  $\mathbf{X}_m(\lambda, \varphi) = (\tilde{u}, \tilde{v}, \tilde{h})^T$  is obtained by the normalisation by the  $3 \times 3$  diagonal matrix  $\mathbf{S}_m$  with elements  $\sqrt{gD_m}$ ,  $\sqrt{gD_m}$  and  $D_m$ , where  $D_m$  denotes the equivalent depth of the vertical mode  $m$ . The nondimensional variables are denoted with  $(\tilde{\cdot})$ .

In the second step, the horizontal nondimensional motions are projected onto a series of Hough harmonics  $\mathbf{H}_n^k$  for every  $m$  as

$$\mathbf{X}_m(\lambda, \varphi) = \sum_{n=1}^R \sum_{k=-K}^K \chi_n^k(m) \mathbf{H}_n^k(\lambda, \varphi; m), \quad (2)$$

where  $K$  denotes the total number of zonal waves and  $R$  is the total number of meridional modes. The complex Hough expansion coefficients  $\chi_n^k(m)$  depend on three indices:  $m$ , meridional mode index  $n$  and zonal wavenumber  $k$ . For every  $n$ , the projection includes two types of motions: Rossby modes<sup>3</sup> (quasi-geostrophic or balanced dynamics) and inertia-gravity modes that represent divergence-dominated unbalanced dynamics. The inertia-gravity modes consist of eastward-

and westward-propagating solutions and together with the equatorial Kelvin and mixed Rossby–gravity waves constitute the non-Rossby modes that are not used in this study.

It is the inverse of Eq. (1) and Eq. (2) that is solved in the forward projection. The second step gives the complex Hough expansion coefficients  $\chi_n^k(m)$  as

$$\chi_n^k(m) = \frac{1}{2\pi} \int_0^{2\pi} \int_{-1}^1 \mathbf{X}_m [\mathbf{H}_n^k]^* d\mu d\lambda, \quad (3)$$

where  $\mu = \sin(\varphi)$  and the asterisk (\*) denotes the complex conjugate. The integrations in the zonal and meridional directions are calculated by the fast Fourier transform and the Gaussian quadrature, respectively.

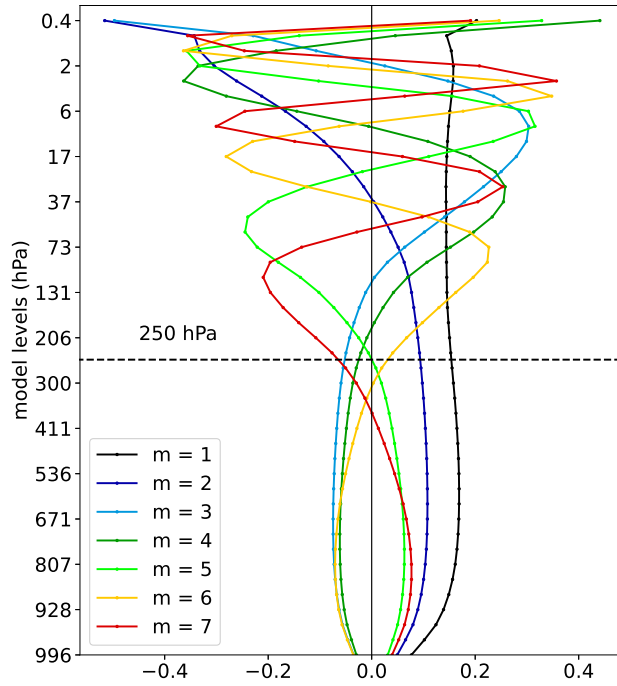


Figure A.1: Vertical structure functions (VSFs) for the first seven vertical modes. VSFs are derived for 43  $\sigma$  levels using the stability profile of ERA-Interim data. VSFs that do not change the sign below the tropopause (defined as 250 hPa level) are troposphere–barotropic modes.

MODES is applied to the four modern reanalyses: European ERA5 (Hersbach et al., 2020), ERA-Interim (Dee et al., 2011), the Japanese 55-year Reanalysis (JRA-55) (Kobayashi et al., 2015), and the Modern-Era Retrospective analysis for Research and Applications (MERRA) (Rienecker et al., 2011). We use daily data at 12 UTC from 1980–2014 (1980–2019 for ERA5) on the regular Gaussian grid that consists of  $256 \times 128$  grid points in the zonal and meridional directions, respectively. Vertically

<sup>3</sup> We use both ‘modes’ and ‘waves’ interchangeably but the latter refers to the case without the zonal-mean state ( $k = 0$ ).

the data are interpolated on the predefined 43  $\sigma$  levels. The same datasets and setup were used in Žagar et al. (2020) except that ERA5 has been extended for the period 2015-2019. The projection is carried out using the following truncations:  $K = 100$ ,  $M = 27$ , and  $R = 150$  which combines 50 meridional modes for the Rossby modes, for the eastward inertia-gravity and for westward inertia-gravity waves modes. Since the mixed Rossby-gravity mode is counted as the first balanced mode, the present study makes use of 49 Rossby modes for every  $m$  and  $k$ , with the meridional mode index going from  $n = 1$  to  $n = 49$ .

We are interested in the balanced circulation with the troposphere–barotropic vertical structure that characterises the midlatitude weather during HWs. This is taken into account by selecting a subset of the VSFs that do not change their signs within the tropopause. In the NMF decomposition, the rigid lid is at zero pressure, just like in the models used for reanalyses. The 43-level datasets extend vertically up to about 0.5 hPa so that a number of VSFs are characterised by a barotropic structure within the troposphere meaning no zero crossing below the tropopause. The first seven VSFs are shown in Fig. A.1. With the middle-latitude tropopause taken at 250 hPa, the VSFs with  $m = 1 - 5$  can be regarded as troposphere–barotropic modes.

#### A.2.2 Heat waves

The study area is the Eurasian region limited by the Ural mountains ( $[35^{\circ}\text{N}-65^{\circ}\text{N}, 10^{\circ}\text{W}-60^{\circ}\text{E}]$ ). The study area is frequently affected by HWs (e.g. Zhou and Wu, 2016), in particular, eastern Europe and western Russia, a location of one of the strongest HWs observed in recent decades (e.g. Barriopedro et al., 2011). For heat wave identification, we analyse daily 2 m temperature fields for the extended boreal summer (months May to September, denoted MJJAS) from 1980-2014 (until 2019 for ERA5). The identification algorithm of Ma and Franzke (2021) applies the following two criteria: (i) the temperature exceeds the 95th percentile threshold and (ii) the duration of the exceedance is longer than three consecutive time steps (three days). Table 1 presents the list of days with HWs in the four reanalysis datasets, which is based on the algorithm. As the identification algorithm is performed independently for each reanalysis, it is expected to have discrepancies among them as seen in Table 1. A total of 13 HWs are identified in ERA-Interim, JRA-55 and MERRA, but the duration of HWs in individual datasets differs. Note that there are two cases with a shorter duration (2 days instead of 3 days) that were included to recognise that the four reanalyses reproduce the same HW events. All together, there are 537 days with HWs; this is about 1.5% of the total number of days, which is a percentage expected for extreme events.



Table A.1: Heat waves in Eurasia during May-September 1980-2019

		ERA5	ERA-Interim	JRA-55	MERRA
	Start date	Number of detected days			
1	23 September 1994	3	3	2	3
2	18 June 2006	12	10	12	10
3	20 September 2006	3	5	6	2
4	20 May 2007	12	12	12	12
5	21 August 2007	6	6	6	6
6	5 September 2008	4	3	4	3
7	28 June 2010	26	27	27	26
8	27 July 2010	21	21	19	21
9	9 May 2012	4	4	4	4
10	14 June 2012	4	3	4	3
11	2 May 2013	7	7	6	5
12	17 May 2014	5	3	3	3
13	5 June 2014	5	6	5	6
14	2 June 2015	3	-	-	-
15	11 August 2015	3	-	-	-
16	17 September 2015	11	-	-	-
17	21 June 2016	4	-	-	-
18	20 August 2016	9	-	-	-
19	2 May 2018	8	-	-	-
20	27 June 2018	4	-	-	-
21	13 July 2013	22	-	-	-
22	29 August 2018	7	-	-	-
23	11 September 2018	12	-	-	-
24	1 June 2019	3	-	-	-
25	8 June 2019	5	-	-	-
26	18 June 2019	3	-	-	-
27	23 June 2019	4	-	-	-
28	24 July 2019	3	-	-	-
$\Sigma$ days		213	110	110	104

### A.2.3 Time series of Rossby wave energy anomalies

Our statistics make use of Rossby wave energy anomalies during HWs in comparison to the climatology. We compute the energy time series, their anomalies and

standard deviations used for normalisation, followed by combining normalised time series for all troposphere–barotropic modes and statistical analysis. In the first step, the total energy (the kinetic energy plus the available potential energy) is computed for every circulation mode  $\nu$ ,  $\nu = (k, n, m)$ , as the square of the absolute value of the complex Hough expansion coefficient  $\chi_\nu$ :

$$I_\nu = I_n^k(m) = \frac{1}{2}gD_m \left| \chi_n^k(m) \right|^2, \quad (4)$$

where  $g$  is the gravity. For the derivation of Eq. (4), see Žagar and Tribbia (2020) or Kasahara and Puri (1981).

The time series of the daily total energy,  $I_\nu(t)$ , span over the MJJAS period within 35 years (1980–2014) for ERA-Interim, JRA-55 and MERRA ( $N_y = 35$ ) as well as 40 years (1980–2019) for ERA5 ( $N_y = 40$ ). The climatological annual cycle is defined as an average over all years ( $N_y$ ) for each day in MJJAS as

$$\langle I_\nu \rangle = \frac{1}{N_y} \sum_{y=1}^{N_y} I_{\nu,y}, \quad (5)$$

and subtracted from daily energies to compute the energy deviations (or anomalies) as

$$I'_\nu = I_\nu - \langle I_\nu \rangle. \quad (6)$$

In the further analysis, the time series of the anomalous daily energies,  $I'_\nu$ , is considered to be the climatological state (climatology) as a reference state for the comparison with the time series of anomalous energies during heat waves. The latter is formed combining only time steps of the observed HWs according to Table 1. For every mode  $\nu$ , we divide energy anomalies by their climatological standard deviation  $\sigma_\nu$ ,

$$\tilde{I}'_\nu = \frac{I'_\nu}{\sigma_\nu}. \quad (7)$$

The mode-wise normalisation by the standard deviation is crucial since the energy spectrum is red not only in terms of the horizontal scales (Žagar et al., 2017), but also in terms of the vertical scale. Note that the entire time series of energy anomalies (climatology) and time series during HWs are normalised by different  $\sigma$ . This procedure is applied for every reanalysis independently.

The next step is to split the normalised energy anomalies of the single Rossby modes into planetary ( $k = 1 - 3$ ) and synoptic ( $k = 4 - 10$ ) scales and to average over the five troposphere–barotropic modes. The mean zonal flow defined by  $k = 0$  is analysed separately. For each  $k$ , averaging is applied also over meridional modes whenever the results are discussed in terms of the zonal wavenumber. Finally, we combine the time series of the normalised energy anomalies from the four reanalyses in the three subdomains of the global circulation: the zonal-mean

state, the planetary waves and the synoptic waves. Žagar et al. (2020) showed that the differences between climatological variance spectra for the four reanalyses are minor. Therefore, our PDFs consist of independent but similar time series. Thus, we can detect robust features of distributions of energy anomalies across different datasets.

### A.3 RESULTS

Our presentation of the results starts by showing that the selected Rossby modes from the NMF decomposition and the applied HW detection method correspond to the circulation patterns typical for the HW events. After demonstrating our methodology, we continue with the statistical analysis of the Eurasian HWs in global spectra and wrap up by coupling statistical properties with the circulation changes during HWs. But first we demonstrate in Fig. A.2 that the global energy in a single Rossby mode is  $\chi^2$ -distributed<sup>4</sup>. The presented example uses the energy  $I_\nu$  (Eq. 4) of the Rossby mode with  $\nu = (k, n, m) = (7, 3, 1)$ , which represents a part of midlatitude barotropic circulation at synoptic scales. The histogram and the fit of the  $\chi^2$  distribution with two degrees of freedom,  $df = 2$ , correspond to the real and the imaginary parts of the time series of  $I_n^k(m) = I_3^7(1)$ . The Kolmogorov-Smirnov test reveals a negligible p-value, confirming the fit. Therefore, we find that the approximation of  $\chi^2$ -distributed energy is satisfied to a high degree, as expected.

#### A.3.1 Northern Hemisphere midlatitude circulation during heat waves

Now we demonstrate that the selected subset of vertical modes is suitable for the statistical analysis of HWs by showing the climatological state and two selected events. Figure A.3a depicts the May–September balanced wave circulation (Rossby modes with  $k > 0$  and all  $m, n$ ) at  $\sigma$  level close to 500 hPa. The pattern remains almost the same when only the troposphere–barotropic vertical modes,  $m = 1 - 5$ , are retained (Fig. A.3b). This confirms our selection of the VSFs. Figure A.3 is based on the ERA5 results, but other datasets provide similar results.

The circulation during the Eurasian HWs is commonly associated with the blocking and can be in the NMF-filtered circulation during two recent HW events: the Russian heat wave in 2010 (Barriopedro et al., 2011) shown in Fig. A.3c and the European heat wave in 2019 (Xu et al., 2020) displayed in Fig. A.3e. The difference with respect to climatology in Fig. A.3b is seen in greatly enhanced amplitudes of the anticyclonic circulation over the observed surface temperature extremes (Western Russia and Europe). For the Russian heat wave (Fig. A.3c,d), anomalies over Asia have been coupled to the Pakistan flood (Lau and Kim, 2012). Similarly, the

<sup>4</sup> The Greek letter  $\chi$  used for the statistical distribution is not related to our Hough expansion coefficient  $\chi_\nu$ , the notation of which follows Žagar et al. (2015).

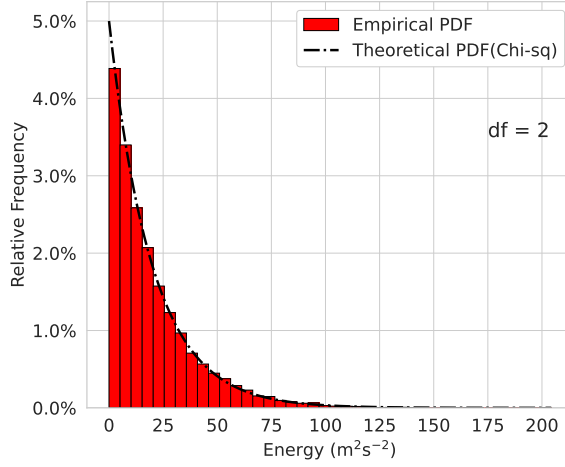


Figure A.2: Atmospheric energy distribution for the Rossby wave with the zonal wavenumber  $k = 7$ , meridional mode  $n = 3$  and vertical mode index  $m = 1$  in ERA5 for 1980–2014. The dashed black lines correspond to the theoretical  $\chi^2$  distribution ( $df$  represents the degrees of freedom).

wavy pattern along the latitudinal belt depicts teleconnections (Teng and Branstator, 2019). The difference between climatology and HWs (Fig. A.3d,f) shows the meridional extension of the circulation anomalies from the tropics to the polar regions in agreement with the suggested coupling of these regions during mid-latitude extremes (Behera et al., 2012). Overall, the patterns shown in Fig. A.3 are qualitatively known from previous studies. The novelty is that our results are produced by multivariate filtering of the global 3D circulation, allowing a scale-dependent quantification of the circulation and anomalies associated with extreme events.

### A.3.2 Global statistics in Rossby-wave space: climatology

Our next step is to investigate how the Eurasian HWs affect the global spatial variability spectrum, i.e. their impact on global circulation. Here, the term global variability spectrum refers to the PDFs of the normalised anomalies in global energy, whereas the effects (or signatures) of HWs imply significant changes in the distribution of energy anomalies. The climatological PDFs are analysed for zonal wavenumbers corresponding to three ranges as described in Section A.2: (i) the zonal-mean state,  $k = 0$ , (ii) the planetary-scale circulation  $k = 1 - 3$ , and (iii) the synoptic-scale circulation with  $k = 4 - 10$ . We focus on the skewness which is not impacted by the normalisation.

Figure A.4a shows the PDF for the case when all zonal wavenumbers are included in the analysis. With the skewness equal to 0.38, the PDF clearly deviates

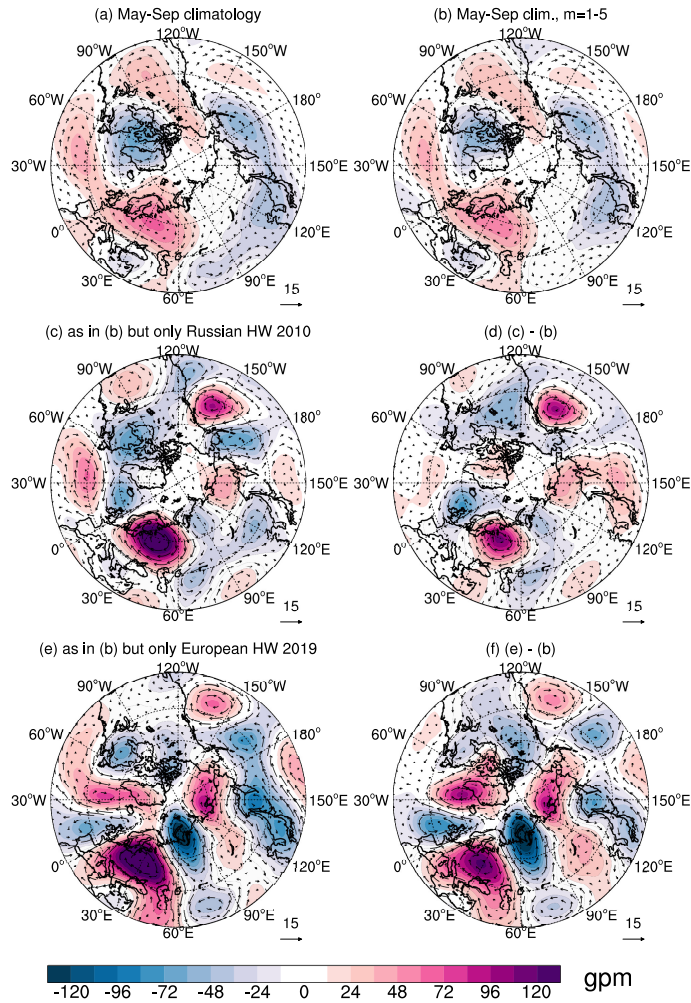


Figure A.3: (a),(b) Climatological Rossby wave circulation for extended boreal summer (MJ-JAS) at the  $\sigma$  level close to 500 hPa in the midlatitudes. (a) All zonal wavenumbers  $k > 0$ , all meridional modes  $n$  and all vertical modes  $m$  are included. (b) As in (a), but only troposphere–barotropic vertical modes,  $m = 1 - 5$ . (c) As in (b) but for the Russian heat wave (HW) in 2010. (d) Difference between the (c) and (b). (e) As in panel (b), and panel (f) is as in (d) but for the European HW in 2019. Coloured contours are geopotential height anomalies (in gpm). The wind speed is shown by the length of the wind vectors (with  $15 \text{ ms}^{-1}$  as a reference vector).

from a Gaussian distribution. A deviation from the normal distribution is found for all three ranges of wavenumbers (Fig. A.4b-d). While the all ranges exhibit noticeable asymmetry, the skewness for the zonal mean and planetary-scale wave PDFs is almost 2 times greater than that of the synoptic-scale waves. In addition, we note that the distributions for the zonal-mean state and the planetary scales are broader than for the synoptic scales. This may reflect more timescales with a larger range of magnitudes being associated with large-scale variability in comparison to the synoptic scales.

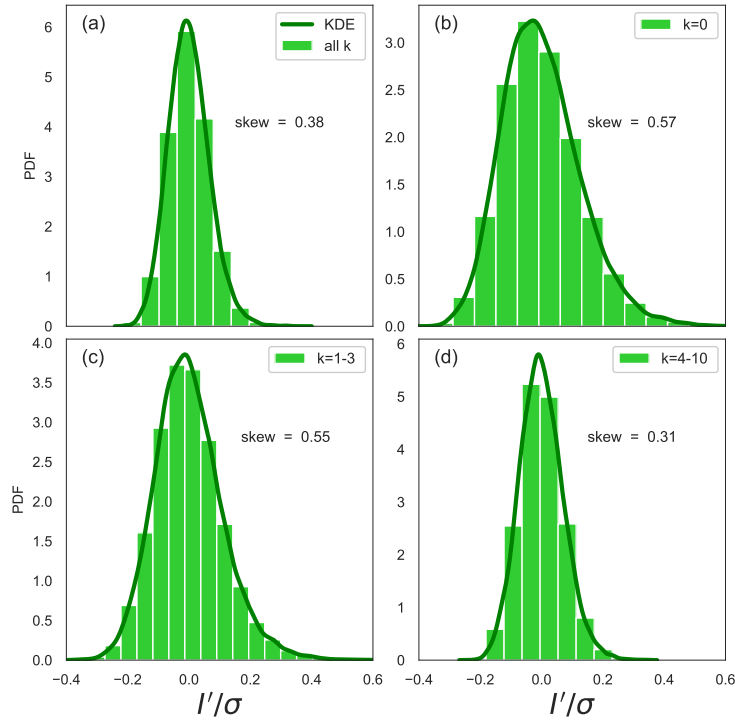


Figure A.4: PDFs of the normalised energy anomalies in the global balanced (Rossby mode) circulation for (a) all wavenumbers  $k$ , (b) the zonal-mean state ( $k = 0$ ), (c) planetary-scale waves ( $k = 1 - 3$ ) and (d) synoptic-scale waves ( $k = 4 - 10$ ). The empirical PDFs are depicted as green bars. The dark green curve is the kernel density estimator (KDE).

Focusing on the skewness and kurtosis of the PDFs, Figure A.5 shows box plots of the respective parameters for all four PDFs. Both the climatology and the HWs are presented in the figure, but the latter will be discussed in the next section together with the HW PDFs. The robustness of the statistical analysis is checked by applying bootstrapping with replacement for skewness and excess kurtosis with 1000 realisations for every presented wavenumber range. All results are found to

be within the defined 95% confidence intervals (CIs) for each wavenumber range (not shown). The skewness and kurtosis show that the normalised energy anomaly distribution has the highest asymmetry at the planetary scales and the zonal-mean circulation seen as extended right tails in the PDFs in Fig. A.4. The different numbers of contributing modes can partly explain the different skewnesses in the four wavenumber ranges. However, changes in the dynamics, such as during HWs, can modify the skewness and the active degrees of freedom, as discussed next.

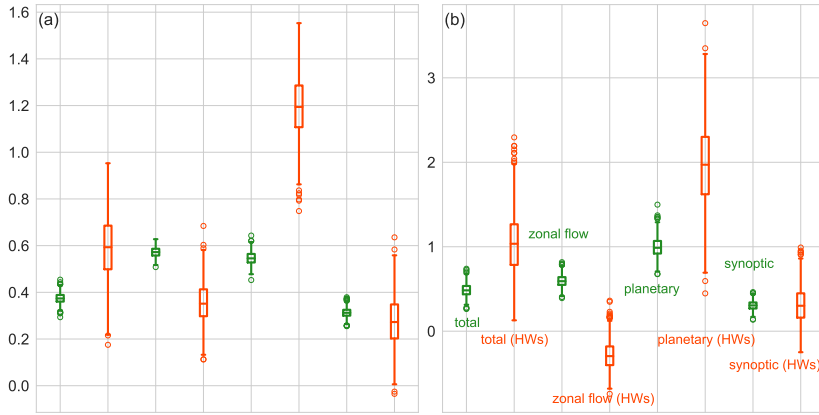


Figure A.5: Box plots for the (a) skewness and (b) excess kurtosis of the PDFs of normalised energy anomalies for four circulation components: all Rossby modes (all  $k$ ), the zonal-mean flow ( $k = 0$ ), planetary-scale Rossby waves ( $k = 1 - 3$ ), and synoptic-scale Rossby waves ( $k = 4 - 10$ ). Vertical lines mark 95% confidence intervals. Green and red shades denote the climatology and HWs, respectively.

### A.3.2.1 Changes in the Rossby-wave energy statistics during heat waves

Now we compare PDFs during the observed HWs over Eurasia with the climatology in terms of the skewness and excess kurtosis that diagnose the changes in shape, especially in the tails of distributions.

The PDFs of the normalised energy anomalies in Fig. 3 demonstrate how probabilities of the energy deviations change during HWs. For the normalised total energy anomalies (all  $k$ ; Fig. 3a) the PDF becomes broader with a longer positive tail indicating more high-energy extremes. For the zonal-mean flow ( $k = 0$ ; Fig. 3b) only small changes are visible on the first view. The PDF of the planetary waves ( $k = 1 - 3$ ; Fig. 3c) shows a shift of the maximum towards negative values and more positive values. While the aforementioned changes in the entire PDFs are not significant, we identify a statistically significant change (according to the Mann-Whitney U test with 95% confidence) in the PDFs of synoptic Rossby waves ( $k = 4 - 10$ ; Fig. 3d). Here, the complete distribution is shifted to higher values without change in its shape. The shift can be interpreted as increased positive deviations in the synoptic-scale energy during HWs. More energy in synoptic-scale circulation can be viewed as more intensive cyclones and anticyclones which are

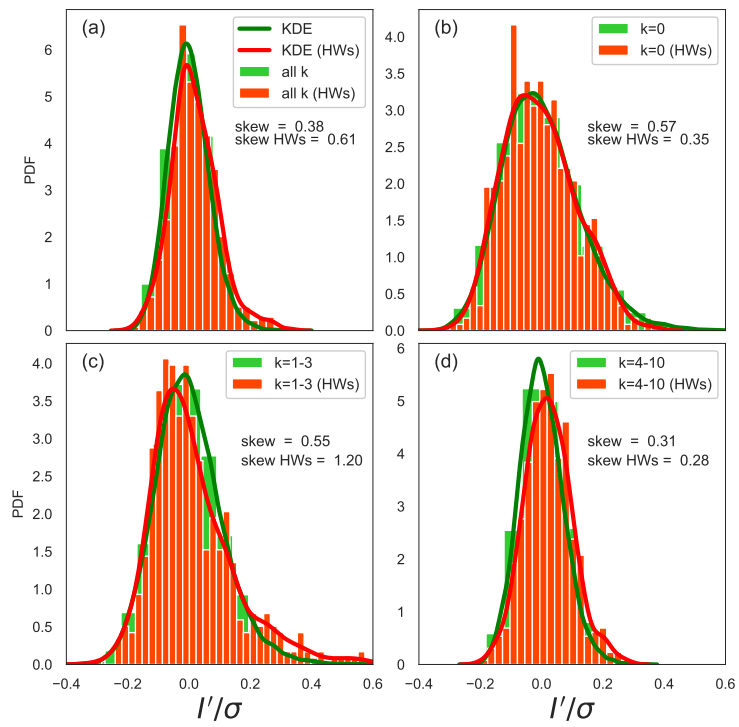


Figure A.6: As in Fig. A.4, but for the Eurasian heat waves listed in Table 1.



found to maintain blocking by eddy straining (Shutts, 1983) and selective absorption (Yamazaki and Itoh, 2013) mechanisms.

How do the skewness and the excess kurtosis change during the Eurasian HWs? An increase (decrease) in skewness hints to fewer (more) active degrees of freedom, which can be interpreted as less (more) independent modes contributing to the variability. This can be caused by both a change in the number of contributing modes and a change in temporal coherence between different modes contributing. An increase in excess kurtosis reflects a rise in the probability of extreme values.

Together with the climatology, Figure A.5 shows the skewness and the excess kurtosis for the HWs. For HW events, the two quantities change qualitatively the same way for different ranges of the wavenumbers. While we find almost no changes for the synoptic waves, changes are the largest at the planetary scales in the excess kurtosis (Fig. A.5b). In this case, the excess kurtosis for extreme events is approximately twice as large as than climatology, which reflects a rise in the probability of extreme values. The opposite change is found for the zonal-mean flow, where skewness and the excess kurtosis decrease; this implies that the distribution has fewer extreme values. We conclude that anomalies of the planetary-scale circulation show relatively less (and more coherent) variability in general and persistent anomalies are generated as shown in Fig. A.3d and f, although positive extremes are more likely. On the other hand, the zonal-mean flow anomalies become weaker in general, in agreement with Coumou et al. (2014).

The change in skewness allows for the estimation of the change in the active degrees of freedom during the HWs compared to the climatology. For the estimation, we use the exact relation for the skewness of the  $\chi^2$ -distributed variable,  $\gamma = \sqrt{8/df}$ , where  $df$  is the number of squares of the independent Gaussian variables with a unit variance which defines the  $\chi^2$ -distributed variable. We use  $df_e/df_c = \gamma_c^2/\gamma_e^2$ , which says that the ratio between the number of active degrees of freedom during HWs and climatology,  $df_e$  and  $df_c$  respectively, is equal to the ratio of their skewnesses  $\gamma_e$  and  $\gamma_c$ , respectively. For the planetary waves which show the largest change, the estimated  $\gamma_e \approx 1.2$  and  $\gamma_c \approx 0.6$  (see Fig. A.5a) yield a reduction of the active degrees of freedom of about 25% during HWs.

Finally, we make a note of the fact that the changes in PDFs during the Eurasian HWs apply to the global atmosphere. Our Rossby modes consist of symmetrical ( $n$  odd) and asymmetrical ( $n$  even) components with symmetry with respect to the Equator defined for the geopotential height and zonal wind fields. We checked that both symmetrical and asymmetrical parts contribute to the PDFs of all meridional modes. In other words, the Rossby waves in the Southern Hemisphere might have contributed to the results presented. However, taking into account the lower frequency of atmospheric blocking (Wiedenmann et al., 2002) in the Southern Hemisphere might have contributed to the results presented. However, taking into account the lower frequency of atmospheric blocking (Wiedenmann et al., 2002) in the Southern Hemisphere, we may assume that this influence is negligible.

### A.3.3 Changes in planetary-scale circulation during heat waves

The changes in the PDFs for different scales can be physically interpreted by filtering selected Rossby waves to physical space, similar to what has been done in Fig. A.3. Instead of case studies, we now present the planetary-scale circulation averaged over all days with observed extremes. As earlier, we show the horizontal circulation at ERA5  $\sigma$  level near 500 hPa as representative for the troposphere–barotropic circulation.

Figure A.7a is very similar to Fig. A.3b which included all zonal wavenumbers. Figures A.7b and c reveal that during the Eurasian HWs, a large enhancement of the positive geopotential height anomaly over northern Europe and a negative geopotential anomaly over the North Atlantic and central Asia take place. The vertical cross sections along the latitude circle  $54^\circ\text{N}$  reveal the expected troposphere–barotropic vertical structure of anomalous circulation that extends throughout the lower stratosphere (Fig. A.7d,e). The northward winds over Europe ( $0^\circ - 30^\circ\text{E}$ ) and southward winds over the Asian part of Russia ( $60^\circ - 90^\circ\text{E}$ ) are enhanced during HWs. Overall, we find an increase in wave amplitudes, and change in phases as can be noticed by westward and northward shifts in Fig. A.7b,c and Fig. A.7d,e in the Baikal lake area ( $90^\circ - 120^\circ\text{E}$ ). The results in Fig. A.7 align with Teng and Branstator (2012) and Ragone and Bouchet (2021), where the zonal wavenumber  $k = 3$  pattern was found to be dominant for HWs that occurred in the US, France and Scandinavia. Therefore, the results demonstrate that changes in atmospheric circulation during surface extremes occur not only regionally but also in remote regions, similar to the idea of teleconnection patterns noted in recent studies (e.g. Kornhuber et al., 2019).

### A.3.4 Changes in intramonthly variance during the surface heat waves

So far, we discussed signatures of HWs in spatial variance (energy). Now we investigate related changes in temporal variance on intramonthly scales. The temporal variance and its square root, variability, are usually studied at single points or using the time series of atmospheric indices such as the North Atlantic Oscillation. The global intraseasonal variance was analysed by Žagar et al. (2020) who showed statistically significant trends in both midlatitude Rossby waves and in large-scale equatorial waves. Here, we compare the climatological intramonthly variance with that for the months with the observed Eurasian HWs in all reanalyses.

The unbiased variance ( $\text{Jkg}^{-1}$ ) is computed as

$$V_v = \frac{1}{N-1} \sum_{t=1}^N gD_m |\chi_v(t) - \bar{\chi}_v|^2, \quad (8)$$

where  $\bar{\chi}_v$  is the monthly mean and  $N$  is the number of days in a single month. As the 3D NMF expansion is a complete representation of the system, the components

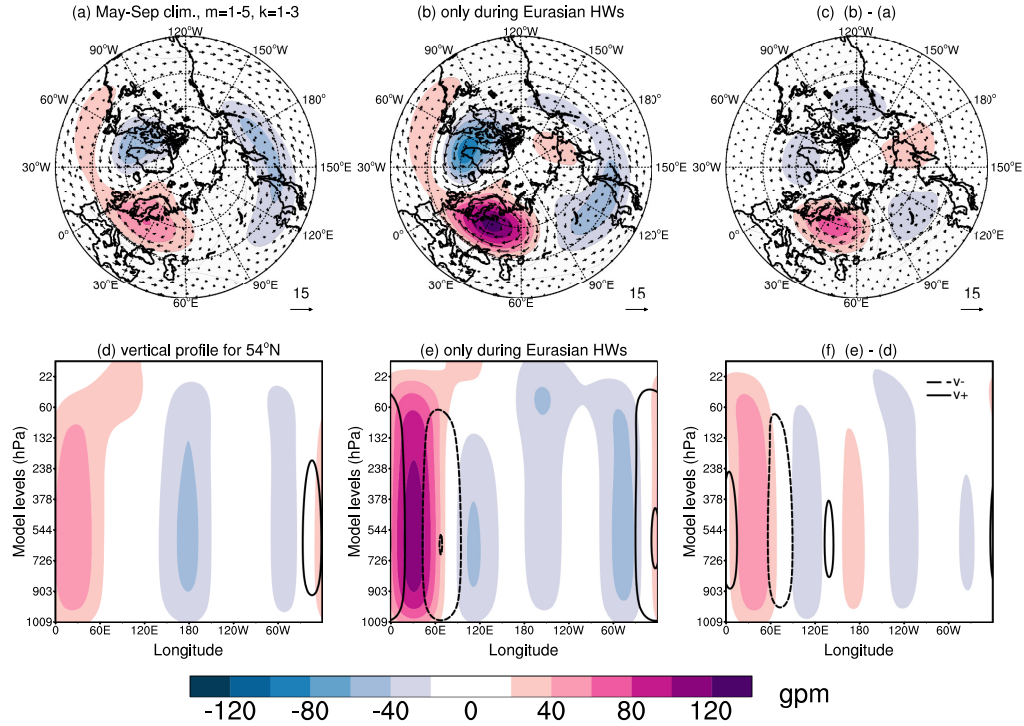


Figure A.7: Planetary-scale, troposphere–barotropic Rossby waves ( $k = 1 - 3$ ,  $m = 1 - 5$ , all  $n$ ) at the  $\sigma$  level close to 500 hPa in ERA5. (a) Mean circulation in May–September in 1980–2019, (b) composite of 28 Eurasian heat waves (HWs) presented in Table 1 and (c) difference between (b) and (a). Coloured contours are geopotential height anomalies, every 20 gpm. The wind speed is shown by the arrow length. (d)–(f) Longitude–pressure cross sections of planetary-scale geopotential height (colours) and meridional wind (isolines) perturbations along  $54^\circ\text{N}$ . (d) Climatology, (e) HWs, and (f) difference between (d) and (e). Solid and dashed contours in (d)–(f) correspond to the northward and southward meridional wind speed, respectively, every  $2 \text{ ms}^{-1}$ .

$v$  of the state vector are statistically independent and correspond to independent degrees of freedom, as discussed in Section A.2. The zonal wavenumber variance spectra are obtained by summing the variances in the five vertical and all meridional modes as previously.

Intramonthly variance is computed for all months and averaged to create the climatological variance spectrum,  $V_v$ . The averaging over all months with heat waves gives us the HW variance spectrum  $V_v^h$  (here we drop extra signs for the averaging operator). The relative change in intramonthly variance due to HWs is

$$\frac{V_v^h - V_v}{V_v} \quad \text{or} \quad \frac{V_v^h}{V_v} - 1. \quad (9)$$

The global intramonthly Rossby wave variance spectrum is shown in Fig. A.8a. It is a red spectrum, similar to the subseasonal variance spectra in Žagar et al. (2020). The redness of the spectra in Fig. A.8a makes differences between the climatology and HWs difficult to detect, but they are made clear by zooming in on the planetary and synoptic scales displayed as an inset panel. It shows a variance reduction of about 6% in the zonal wavenumber  $k = 3$  along with the 5% variance increase in  $k = 7 - 8$ . We note that the changes in intramonthly variance are consistent with the shifts of the maxima of the respective normalised energy anomaly PDFs (Fig. 3c,d). In addition, the reduction of planetary wave intramonthly variance is also consistent with the appearance of the persistent large-scale anomaly shown in Fig. A.7.

The blue shading around the variance spectra in Fig. A.8a depicts the 95%-CI obtained through bootstrapping. It suggests the largest uncertainty at planetary wavenumbers. The variance reduction at  $k = 3$  is within 95% CI and is therefore insignificant. At  $k = 7 - 8$ , the intramonthly variance during HWs is slightly outside the CI; therefore, the variance change is considered significant. We note here that our findings are based on a relatively small sample of identified HWs and that many events lasted under a week. To provide stronger evidence, general circulation model (GCM) simulations can be performed, which is the scope of future studies.

A more detailed view of the changes in the global intramonthly variance during HWs is provided in Fig. A.8b also including the zonal-mean state. The variance reduction at  $k = 3$  and an increase at  $k = 7 - 8$  are seen across multiple meridional modes  $n$  in agreement with the midlatitude character of HWs. The quantitatively largest variance change is, however, seen in the zonal-mean state  $k = 0$  with a positive and negative change in the two asymmetrical meridional modes,  $n = 4$  and  $n = 6$ , respectively. The change in  $k = 0$  can be explained using the latitudinal profile of the zonal-mean zonal wind presented in Fig. A.9. First, it shows that the maximum zonal-mean zonal wind at  $45^\circ\text{N}$  during HWs is about 10% weaker than the climatology and slightly shifted (about  $1^\circ$ ) northward. The jet near  $45^\circ\text{N}$  is more confined in the troposphere, with the  $10 \text{ ms}^{-1}$  isoline near 300 hPa compared

to 200 hPa in climatology. This means that the vertical shear of the mean zonal wind decreases during the Eurasian HWs.

Other features of the HWs seen in Fig. A.9 are twice as strong as zonal-mean zonal winds in the latitude belt between 60°N and 90°N with a peak difference of up to 3 ms<sup>-1</sup> at 75°N. The dipole shape of the difference in Fig. A.9c is in Fig. A.8b seen as a variance decrease in the meridional mode n = 4 and an increase in n = 6. Note that Fig. A.9 is obtained by filtering  $\bar{\chi}_n^0$  to physical space. Similar filtering for any horizontal or vertical scale of interest is straightforward, which makes the holistic modal-space statistics an attractive global complement to the single-variable, single-level Fourier analysis. We speculate that the enhancement of high-latitude k = 0 zonal winds is a component of more persistent double jets over Eurasia during HWs recently discussed by Rousi et al. (2022b).

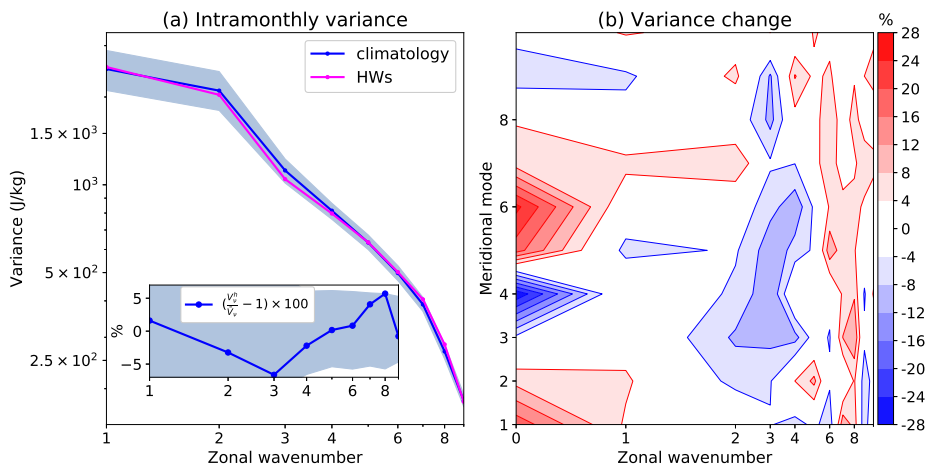


Figure A.8: (a) Intramonthly variance spectra of the Rossby waves for the climatology (blue) and Eurasian heat waves (magenta). The embedded panel shows the relative change in percentages of the climatology. The blue shading denotes the 95%-confidence intervals. (b) Changes in the intramonthly variance with respect to climatology as a function of the zonal wavenumber and meridional mode including the zonal-mean state.

#### A.4 CONCLUSIONS

Extreme events such as surface HWs are accompanied by changes in atmospheric circulation across many scales. Our study shows that Eurasian HWs have signatures in the global balanced circulation. The changes in global statistics of the Rossby-wave variance are made evident by analysing the four modern reanalyses: the ERA5, ERA-Interim, JRA-55, and MERRA datasets. The Rossby waves are identified by a multivariate projection of the global horizontal winds and geopotential height on the eigensolutions of the linearised primitive equations on the sphere with a basic state at rest (the so-called normal-mode functions). A complete pro-

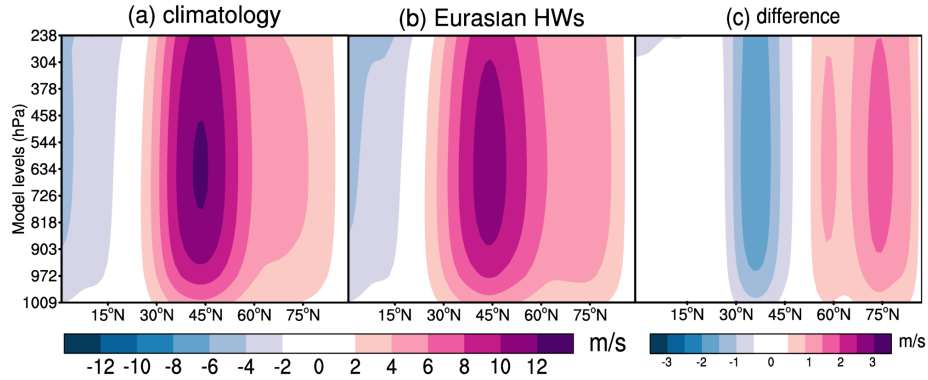


Figure A.9: Zonal-mean zonal wind in the Northern Hemisphere troposphere in 1980-2019, May-Sep ERA5 data. (a) Climatology, (b) Eurasian heat waves (HWs) and (c) climatology - HWs.

jection basis provides global statistics of Rossby waves as a function of the zonal wavenumber, the meridional mode index and the vertical modes associated with the vertical structure functions. The method includes scale-selective multivariate Rossby-wave filtering in physical space offering an attractive global complement to the single-variable, single-level Fourier analysis.

Our analysis focuses on the Rossby waves with the barotropic structure within the troposphere that is characteristic of the midlatitude circulation during HWs. The reconstructed physical space picture of the Eurasian HWs is in agreement with previous studies (Lau and Kim, 2012; Behera et al., 2012; Coumou et al., 2014; Teng and Branstator, 2019). We find largely increased amplitudes of the positive geopotential height anomaly over northern Europe, otherwise typical for the extended summer period, and a negative geopotential anomaly over the North Atlantic and central Asia. The anomalous circulation extends throughout the lower stratosphere. In addition, there are westward and northward shifts in the circulation. During HWs, the zonal mean westerlies somewhat weaken near their climatological maximum at 45°N but get twice as strong in high midlatitudes (centred at 75°N). Future work should couple these findings with the study by Wirth and Polster (2021) on the role of Rossby waves in processes leading to the double jet formation, recently discussed for Eurasian HWs by Rousi et al. (2022b).

The statistical analysis is carried out on the complex time series of the Hough expansion coefficients representing Rossby modes across many horizontal scales with the troposphere–barotropic vertical structure. We demonstrate that the energy distribution of a single mode follows a  $\chi^2$  distribution. Statistics of the normalised energy anomalies show that the zonal-mean state ( $k = 0$ ) and the planetary-scale ( $k = 1 - 3$ ) circulation are more skewed than the synoptic and smaller scales, with extended right tails. Increased skewness of the distribution hints to the reduction

in active degrees of freedom. This can be interpreted as fewer independent modes contributing to the observed variability, either because the number of total modes is smaller or because there is temporal coherence between different modes.

During the Eurasian HWs, the skewness in planetary-scale Rossby waves increases, while the opposite occurs in the zonal-mean state. The increase in skewness for planetary-scale waves reveals the decrease in the number of active degrees of freedom during HWs. This aligns with the results of Lucarini and Gritsun (2020b), which are based on the atmospheric stability during Atlantic blockings. Based on the  $\chi^2$  skewness, we estimate a reduction of the active degrees of freedom for the planetary-scale Rossby waves during Eurasian HWs of about 25% compared to climatology.

Consistent changes in wavenumber space are found in the intramonthly variance. Eurasian HWs are characterised by a statistically significant increase of about 5% in the intramonthly variance at synoptic scales  $k = 7 - 8$  with respect to climatology. This is consistent with increased synoptic activity during blocking (e.g. Shutts, 1983; Yamazaki and Itoh, 2013). In contrast, a reduction of intramonthly variance in  $k = 3$  of about 6% is found not to be statistically significant. Future studies with longer datasets, such as climate model outputs, are an opportunity for models' validation and larger datasets of extreme events.

Despite the uncertainties due to the limited sample size, our results provide the following overall picture, consistent with previous studies. During HWs, the planetary-scale Rossby waves (primarily  $k = 3$ ) exhibit reduced intramonthly variability. The involved modes are less independent from one another and a persistent large-scale anomaly is formed, typically referred to as blocking. On the other hand, the intramonthly variability of the synoptic Rossby waves increases, particularly at the zonal wavenumbers  $k = 7 - 8$ . The contributions of more active meridional modes to the zonal-mean flow during HWs, perhaps excited by eddy-mean flow interactions, show as an enhancement of the mean westerlies north of  $60^\circ\text{N}$  and their weakening near  $45^\circ\text{N}$ .

**CODE AND DATA AVAILABILITY.** The ERA-Interim datasets are available via <https://apps.ecmwf.int/datasets/data/interim-full-daily/levtype=ml/> (last access: 18 November 2022; Dee et al., 2011; <https://doi.org/10.1002/qj.828>), and ERA5 reanalysis datasets are available via <https://cds.climate.copernicus.eu/cdsapp#!/search?text=ERA5> (last access: 18 November 2022; Hersbach et al., 2020; <https://doi.org/10.1002/qj.3803>). The MERRA and JRA-55 are available at <https://disc.gsfc.nasa.gov/datasets?project=MERRA> (last access: 18 November 2022; Rienecker et al., 2015; <https://doi.org/10.1175/JCLI-D-11-00015.1>) and <https://search.diasjp.net/en/dataset/JRA55> (last access: 18 November 2022; Kobayashi et al., 2015; <https://doi.org/10.2151/jmsj.2015-001>), respectively. The MODES software can be requested via <https://modes.cen.uni-hamburg.de>. The time series of the Hough expansion coefficients for the four reanalyses are available upon the request from the authors.

**AUTHOR CONTRIBUTIONS.** All authors contributed to the study conception and design. IS developed the algorithm, performed the data analysis and wrote a first draft of the article. All authors participated in data interpretation and revised previous versions of the article. All authors read and approved the final article.

**COMPETING INTERESTS.** The contact author has declared that none of the authors has any competing interests.

**DISCLAIMER.** Publisher's note: Copernicus Publications remains neutral with regard to jurisdictional claims in published maps and institutional affiliations.

**ACKNOWLEDGEMENTS.** This work was funded by the Deutsche Forschungsgemeinschaft (DFG, German Research Foundation) under Germany's Excellence Strategy – EXC 2037 “CLICCS – Climate, Climatic Change, and Society” (CLICCS, A6) – project number 390683824, contribution to the Center for Earth System Research and Sustainability (CEN) of Universität Hamburg. We thank the former MODES group members at the University of Ljubljana, Damjan Jelić and Khalil Karami, for the MODES decomposition of the four reanalysis datasets, Žiga Zaplotnik for his advice on processing the Hough coefficients in Python, Qiyun Ma for the algorithm for the heat wave identification, and Frank Sielmann for the variance analysis and technical support. We would also like to thank Valerio Lucarini for the discussion, as well as two anonymous reviewers and the editor Gwendal Rivière for their constructive comments on the article.

**FINANCIAL SUPPORT.** This research has been supported by the Deutsche Forschungsgemeinschaft (grant no. 390683824).

**REVIEW STATEMENT.** This paper was edited by Gwendal Rivière and reviewed by two anonymous referees.



CMIP<sub>5</sub> MODELS (IN?)ABILITY TO SIMULATE SIGNATURES  
OF EURASIAN HEAT WAVES IN  
TROPOSPHERE–BAROTROPIC PLANETARY-SCALE ROSSBY  
CIRCULATION

---

The Appendix consists of a paper that is indented to be submitted:

Strigunova, I., R. Blender, F. Lunkeit, and N. Žagar (n.d.). “CMIP<sub>5</sub> models (in?)ability to simulate signatures of Eurasian heat waves in troposphere–barotropic planetary-scale Rossby circulation.” - *to be submitted*.

IS developed the algorithm, performed the data analysis and wrote a first draft of the article. All authors contributed to the study conception and design.

# CMIP5 models (in?)ability to simulate signatures of Eurasian heat waves in troposphere–barotropic planetary-scale Rossby circulation

Iana Strigunova<sup>1</sup>, Richard Blender<sup>1</sup>, Frank Lunkeit<sup>1</sup>, Nedjeljka Žagar<sup>1</sup>

<sup>1</sup>*Meteorological Institute, Center for Earth System Research and Sustainability (CEN), Universität of Hamburg, Grindelberg 5, 20144 Hamburg, Germany*

## ABSTRACT

Heat waves (HWs) identified in reanalysis datasets have signatures in the global Rossby-wave spectrum. In this study, we evaluate the ability of CMIP5 models to simulate these signatures during extended boreal summer. The evaluation is based on comparing energy anomaly distributions obtained for ERA5 and other reanalyses with CMIP5 models. Daily energy time series are computed from the time series of Hough expansion coefficients representing global circulation with the possibility of analysing only troposphere–barotropic planetary-scale Rossby waves. The procedure of how models simulate Rossby-wave circulation is formulated in three steps. In the first step, we detect HWs based on 2 m temperatures (T2m) averaged over Eurasia. The probability density functions (PDFs) of T2m from CMIP5 models have the same distributions as in ERA5, with little differences in HW metrics. In the second step, the model ensemble of the climatology of planetary-scale Rossby waves is found to be well-simulated, but differences among models are noticed. In the third step, during HW, models have large uncertainty in the skewness of PDFs of energy anomalies. Thus, the increase in tails is not clearly identified in CMIP5 models compared to ERA5 and other reanalyses. The comparisons of historical (coupled) and "atmosphere-only" (uncoupled) simulations reveal that uncoupled simulations represent the mean circulation, while coupled can simulate the Rossby-wave patterns but not the intensity. Further work is needed to study the underlying reasons.

## B.1 INTRODUCTION

Record-breaking Eurasian heat waves in recent years have led to devastating socioeconomic and ecological impacts. In the future, they are expected to increase in duration, magnitude and frequency (Seneviratne et al., 2021) as a consequence of projected global mean temperature increase due to rising greenhouse gas concentrations (e.g. Meehl and Tebaldi, 2004; Fischer and Knutti, 2015), the so-called "thermodynamical" driver. The influence of the "dynamical" factor for future heat waves has been studied less due to large uncertainty in regional and global climate models. The climate projections of blocking atmospheric patterns involved in heat wave formation vary among regions and exhibit no trend in the Northern Hemisphere and globally (Gulev et al., 2021; Doblas-Reyes et al., 2021). This can

be partly attributed to reported biases in the mean flow (Berckmans et al., 2013), coarse resolution (Schiemann et al., 2017), parameterisations of orographic drag and convection (e.g. Jung et al., 2010; Pithan et al., 2016). Davini and d’Andrea (2020) noted improvement in the blocking frequency from CMIP5 to CMIP6 by increasing resolution and better physics in a newer model generation. However, blocking over the Euro-Atlantic region is still underrepresented in frequency and persistence (Fabiano et al., 2020). Despite existing biases, the link between atmospheric blocking and heat waves is well-presented in the large-ensemble CMIP5 (e.g. Schaller et al., 2018; Brunner et al., 2018; Jeong et al., 2022), as it also has been shown for the European heat wave in 2018 (Li et al., 2020) and in the regional study over China (Wang et al., 2019). Given that the link is well-represented, it seems puzzling why models still have large uncertainty in projecting circulation changes while the global mean surface temperature trends are likely certain (Lee et al., 2021). Moreover, no study has been attempted to evaluate how well the global Rossby-wave circulation and its statistics are simulated during Eurasian HWs in CMIP5 models. Here, we apply the methodology developed by Strigunova et al. (2022) to assess it.

There are multiple studies (e.g. Thorarinsdottir et al., 2020; Wehner et al., 2020) investigated heat waves metrics in CMIP5 and CMIP6 models and pointed out that there is an improvement in heat wave duration and cumulative heat, however, the magnitude is still overestimated. Sillmann et al. (2013) explored CMIP5 models by comparing the extreme indices with those from observations and reanalyses. They found no substantial differences among models; however, warm biases exist in hot extremes. Daily temperature anomalies are still overestimated in CMIP6, according to Di Luca et al. (2020). Absolute errors of another extreme index, warm spell duration, are reduced in CMIP6 to compared to CMIP5 (Kim et al., 2020), but regional differences remain in CMIP6 (Fan et al., 2020). Moreover, Wang et al. (2023) showed that CMIP6 models do not capture the June 2021 Pacific Northwest heatwave.

Plavcova and Kyselý (2016) showed that a mismatch in heat wave duration is connected with the misrepresentation in blocking duration (or persistence). The model’s median spread for blocking frequency is decreased twice from CMIP5 to CMIP6, but this does not hold for blocking persistence. The models still suffer from substantial biases representing blocking duration (Schiemann et al., 2020). Several studies (e.g. Anstey et al., 2013) identified that biases in the sea surface temperature (SST) are possible sources of misrepresentation. Masato et al. (2013) found that blocking over oceans is overestimated, whereas Castanheira and Marques (2022) showed that the variability of barotropic modes is overestimated in the North Pacific but underestimated in the North Atlantic. Chen et al. (2021) identify this connection in the ensemble mean of CMIP5, however, with large spread among models. Davini and D’Andrea (2016) showed the minor importance of SSTs in blocking process formation in western Russia. Therefore, the problem of accu-

rate representation of atmospheric blocking cannot be solved only by improving one factor but rather the combination of different factors (Woollings et al., 2018).

Better representation in models and, therefore, future changes in blocking are associated with biases and changes in large-scale Rossby circulation, usually referred to as its stationary component (e.g. Wills et al., 2019). Several studies (e.g. Screen and Simmonds, 2014; Fragkoulidis et al., 2018) demonstrated stationary Rossby waves' role in the formation of heat waves throughout blocking formation. Nie et al. (2019) discussed the climatology of the Rossby wave sources (RWS) during the winter and summer seasons and how it is reproduced in the ensemble mean of the CMIP5 models. They found that large-scale RWS is reproduced well; however, most models overestimate RWS in subtropics but underestimate in the midlatitudes. East Asia and western North America are regions of the largest differences among models. The biases in this region can be associated with smoothed topography and overall parameterisations of convection and microphysics. Sandu et al. (2019) showed that atmospheric circulation representation might be topographic processes are parametrised.

From another perspective, Lee et al. (2019) found that biases in Arctic moisture flux are connected with tropical upper troposphere temperatures. Moreover, by analysing future projections with RCP8.5, they identified identical biases as in historical simulations. It highlights that future projections must be analysed cautiously, and the ensemble mean, used as a proxy for "truth", does not always represent the picture realistically.

It has also been shown that small biases in upper-troposphere circulation have a large impact on surface fields in the midlatitudes (Luo et al., 2022). The biases are estimated via wave amplitudes comparison within zonal wave numbers 1-10 obtained by the Fast Fourier Transform of meridional wind at 250 hPa on weekly scales with experiments of atmospheric circulation and soil moisture. It has been shown that CMIP5 models are able to reproduce the summertime Rossby wave climatology with small biases but it leads to significant underestimation on surface.

Here we present another view on global circulation via normal modes in the context of the connection between heat waves over Eurasia and the global balanced circulation via three-dimensional diagnostic across different spatio-temporal scales (MODES). Previous studies show that MODES can be applicable to a wide range of research questions, including diagnostics components of circulation during extreme events Strigunova et al. (2022). Therefore, here we use the same method to assess whether CMIP5 models are able to reproduce the troposphere–barotropic planetary Rossby circulation during Eurasian HWs in the present climate. To answer this, the following questions are addressed:

- Do statistics of HW events in CMIP5 in agreement with ERA5's?
- Do the climatology of planetary Rossby-wave circulation in CMIP5 in agreement with climatology from reanalysis datasets?

- Do HWs have the same signatures in reanalyses and CMIP5 models on planetary scales?

## B.2 DATA AND METHODS

Single ensemble members of historical (coupled) and "atmosphere-only" simulations (uncoupled) from four CMIP5 models (CNRM-CM5, GFDL-CM3, MIROC5, MPI-ESM-LR) are analysed in this study. To identify heat waves, we use 2 m temperature (T2m) over Eurasia, limited by the Ural mountains. Zonal and meridional wind components and geopotential height fields at model levels are employed to project model outputs into the normal-mode functions. The climatology is obtained for the 27-year period (1979-2005) for the months May-September.

### B.2.1 *Heat Waves*

To identify HWs, we applied the same algorithm to reanalysis datasets as in Strigunova et al. (2022). Briefly, daily T2m temperatures are averaged over Eurasia for every model. Their 95th percentiles are subtracted to remove the annual cycle, and only positive anomalies are considered. HW is identified when positive values repeat more than three-time steps (days). Obtained results show a mismatch in the dates of identified events. Therefore, the list created on results from reanalyses cannot be compared with the models' results.

### B.2.2 *CMIP5: climatology of Rossby-wave circulation*

CMIP5 models are decomposed in terms of the waves associated with two main dynamical regimes: Rossby waves (balanced regime) and inertia-gravity waves (unbalanced regime) using MODES (Žagar et al., 2015). The outputs of decomposition are the daily Hough complex coefficients, where each coefficient is a function of the zonal wavenumber  $k$ , the meridional index,  $n$ , and the vertical-mode index,  $m$ . Their total numbers ( $K$ ,  $M$ ,  $N$ ) are truncations of the projection, which depend on the model's vertical and horizontal resolutions listed in Table B.1. Based on each truncation, the number of troposphere-barotropic modes is defined separately for each model. The details of the procedure can be found in Strigunova et al. (2022). For GFDL-CM3 and MPI-ESM-LR, the number of troposphere-barotropic modes is  $m = 1 - 5$ , whereas for CNRM-CM5 and MIROC5, only the first two vertical modes ( $m = 1 - 2$ ). In MODES, the first balanced mode is the mixed Rossby-gravity mode, which has maximum in the tropics. Therefore, we consider all other meridional modes except the first one. In this study, only planetary-scale ( $k = 1 - 3$ ) Rossby waves are discussed.

Table B.1: CMIP5 model parameters and their truncations in MODES (HIST is short for historical simulation, and AMIP stands for "atmosphere-only" simulations)

Model	HIST	AMIP	Horizontal resolution
CNRM-CM5	+	+	N64
GFDL-CM3	+	+	N36
MIROC5	+	+	N64
MPI-ESM-LR	-	+	N48
Model	N. of vertical levels	Top level (in hPa)	Truncation ( $K \times M \times N$ )
CNRM-CM5	28	10	$64 \times 64 \times 20$
GFDL-CM3	45	0.01	$72 \times 36 \times 33$
MIROC5	37	3.5	$80 \times 64 \times 25$
MPI-ESM-LR	44	0.01	$60 \times 48 \times 32$

### B.3 RESULTS

Before proceeding to the discussion of models' ability to reproduce signatures of Eurasian heat waves in the troposphere–barotropic Rossby circulation, we start with discussing how HWs represented in models in comparison with ERA5.

#### B.3.1 Metrics of HWs in CMIP5 models

Before discussing the Rossby circulation during HWs, we are interested in distributions of daily 2 m temperature (T2m) averaged over the Eurasian region limited by Ural mountains (or  $[35^\circ\text{N} - 65^\circ\text{N}, 10^\circ\text{W} - 60^\circ\text{E}]$  in a latitude-longitude domain). Figure B.1 shows box plots of temperatures in ERA5 and individual models from CMIP5. Interquartile ranges (IQRs) are displayed as whiskers with boxes framed with vertical lines (25th and 75th percentiles) along with lines approximately in the middle (50th percentile or median). It is seen that all CMIP5 IQRs overlap with ERA5's IQR; it implies that distributions are similar. However, we see differences in the tails of some distributions, such as GFDL-CM3 (only coupled), with shifts towards lower temperatures. The same model with an uncoupled (AMIP) run demonstrates IQR, which is closer to ERA5's, and it has fewer outliers. Another two models, MIROC5 and CNRM-CM5 (both coupled and uncoupled), demonstrate distribution shifted towards higher temperatures. Positive biases (in median of all CMIP5 models according to Flato et al. (2013)) in these models are shown to be larger than in other models.

The next step is to discuss how anomalies (only positive) from the 95th percentile of T2m differ among models in comparison with ERA5.

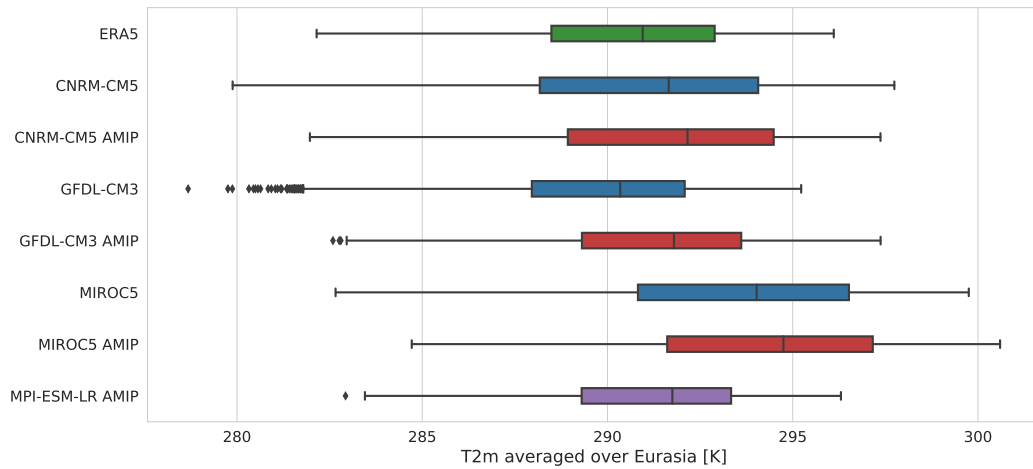


Figure B.1: Box plots of daily 2 m temperature (T2m) averaged over Eurasia. ERA5 is shown as a green boxplot. CMIP5 coupled simulations are displayed as blue box plots, the uncoupled as red box plots. MPI-ESM-LR temperature time series is displayed as a purple boxplot. Interquartile ranges (IQRs) are displayed as whiskers with boxes framed with vertical lines (25th and 75th percentiles).

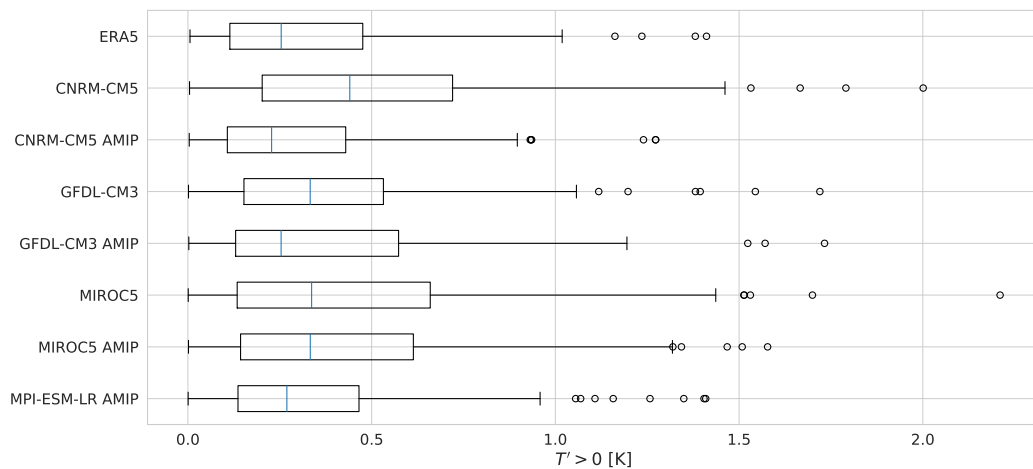


Figure B.2: The same as in Fig. B.1 but only positive deviations from 95th percentile identified for every dataset separately.

Fig. B.2 shows box plots only for positive temperature anomalies from the 95th percentile (the value is computed for every dataset separately). First, all models are within ERA5's IQR, demonstrating that distributions are similar. In detail, the median in CNRM-CM5 is also shifted to the larger anomalies compared to ERA5's median. Moreover, it has one of the largest IQR along with MIROC5, with the

maximum value (more than 2 K) among all datasets. There is no decrease in IQRs among coupled and uncoupled simulations. Still, there is a decrease in the number of outliers suggesting that SST biases are likely to lead to larger overestimation. On another side, there is a clear improvement in CNRM-CM5 when SST is fixed. In contrast, for MIROC5, there is a small decrease in IQR, and, moreover, in GFDL-CM3 uncoupled simulations, IQR is larger than coupled. Therefore, the effect of SSTs is only seen via the number of outliers. However, outliers are sensitive to the number of samples. With sample sizes of around 100, it is likely that these results are non-robust. Therefore, the only robust feature is that datasets have similar distributions of positive temperature anomalies to ERA5, implying that the statistics on HWs are expected to be similar as well.

As a next step, we want to estimate how similar HWs represented among models and how they are comparable to ERA5. As estimates, the following metrics have been used: the number of HW days, the number of HW events, average event duration, and maximum event duration (Perkins-Kirkpatrick and Gibson, 2017). All these metrics based on T2m time series averaged over Eurasia are used to see a more detailed picture of how models perform. According to Table B.2, models show similar results in all metrics and are comparably close to ERA5 results. There are also no systematic differences between coupled and uncoupled (shown in parentheses) simulations.

Overall, we conclude that near-surface temperatures and HWs in CMIP5 models are similar to ERA5.

Table B.2: HW metrics (Perkins-Kirkpatrick and Gibson, 2017). Uncoupled simulations are shown in parentheses.

	N. of HW days	N. of HW events
ERA5	107	23
CNRM-CM5	132 (102)	27 (22)
GFDL-CM3	111 (109)	19 (19)
MIROC5	132 (135)	24 (26)
MPI-ESM-LR	138	21
	average event duration (in days)	max event duration (in days)
ERA5	4.6	12
CNRM-CM5	4.9 (4.6)	14 (12)
GFDL-CM3	5.8 (5.7)	12 (15)
MIROC5	5.5 (5.2)	13 (11)
MPI-ESM-LR	6.6	15



### B.3.2 *Present-day climatology of the troposphere–barotropic planetary-scale Rossby waves in CMIP5 models*

Here, we discuss how the climatology of the troposphere–barotropic planetary-scale Rossby waves is presented among CMIP5 models throughout the mean circulation in grid space and the normalised energy anomalies PDFs in modal space. The mean circulation allows us to estimate the similarity of patterns of planetary Rossby waves averaged in time. The comparison is shown only with ERA5, as other reanalyses demonstrate similar results. The PDFs of normalised energy anomalies describe the variability of daily energy in the Rossby wave in each time step. We can estimate similarity by the quantile-quantile plots. The results are shown only for every model with ERA5 comparison. We also compare the model ensemble (all models) with the reanalyses ensemble (all reanalysis datasets) to evaluate ensemble performance.

Figure B.3a shows the climatology of planetary Rossby waves in ERA5 (the same as in Fig. 7a from Strigunova et al. (2022)) and how it deviates in CMIP5 models (Fig. B.3b-h). Fewer differences are observed in uncoupled simulations compared to coupled. The exception is MIROC5 (Fig. B.3g, h). In AMIP, more differences compared to coupled are seen over northern America, while, in other regions, there is an improvement. Still, this model has the largest discrepancies. Mainly, it is due to positive geopotential height anomalies over northern America where the Rockies are located (effect of orography?) and too strong geopotential height anomalies over the northern Atlantic. There are also larger anomalies over the region of blocking (northern Europe), which are appeared in CNRM-CM5 (only in coupled) as well. To conclude, most of the models show small differences with ERA5 planetary Rossby-wave climatology, except MIROC5, where anomalies in the geopotential height field are larger than in ERA5.

The mean state of troposphere–barotropic planetary Rossby-wave circulation is shown to be represented quite well, with an exception of MIROC5. The next step is to estimate how the variability is simulated in models. For this purpose, we make use of distributions of normalised energy anomalies, metrics used to identify changes during Eurasian HWs. We first compare the energy anomalies distribution consisting of all reanalyses datasets used in the previous study (ERA5, ERA-Interim, JRA55, MERRA) and with distribution with all CMIP5 models used in this study to evaluate the performance of the entire ensemble. To illustrate it, we show quantile-quantile (Q-Q) plots (Fig. B.4a). Overall, models in both runs show a good agreement with reanalyses, which can be seen as overlaps with blue and green dashed lines used as a "perfect" fit reference. Nevertheless, higher quantiles in models are overestimated (the top dot is shifted to the right compared to the dashed line). A similar pattern is observed when we compare individual models (GFDL-CM3 and MPI-ESM-LR) with ERA5 in Fig. B.4c, e. CNRM-CM5 (Fig. B.4b) and MIROC5 (Fig. B.4d) demonstrate a good fit to ERA5, but the quantiles are smaller in range.

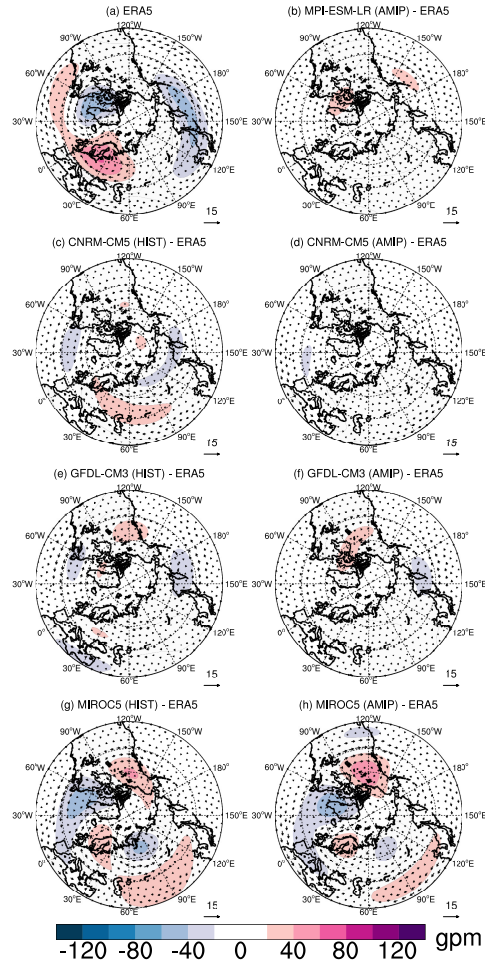


Figure B.3: Climatological Rossby wave circulation for extended boreal summer (MJJAS) at the  $\sigma$  level close to 500 hPa in the midlatitudes in ERA5 (a) and difference in CMIP5 models (c), (e), (g) in coupled and (b), (d), (f), (g) in uncoupled. Only zonal wavenumbers  $k = 1 - 3$ , all meridional modes  $n$  and vertical modes  $m = 1 - 5$  ( $m = 1 - 2$  for CNRM-CM5 and MIROC5) are included.

We also compare skewness and excess kurtosis of the above-mentioned distributions by applying bootstrapping procedure on these two parameters for ERA5 and each model to estimate whether their inter-quantile ranges match each other. For skewness (for excess kurtosis, results are similar) show that only CNRM-CM5 and MIROC5 are within CIs identified from the ERA5 distribution, whereas GFDL-CM3 and MPI-ESM-LR are outside due to larger positive energy anomalies. Therefore, only CNRM-CM5 demonstrates similar climatology (mean and variability) of planetary Rossby waves, whereas MIROC5 has the largest deviations in the mean state. In contrast, GFDL-CM3 and MPI-ESM-LR demonstrate good agreement on the mean state with ERA5, but energy anomaly distributions is statistically different from ERA5.

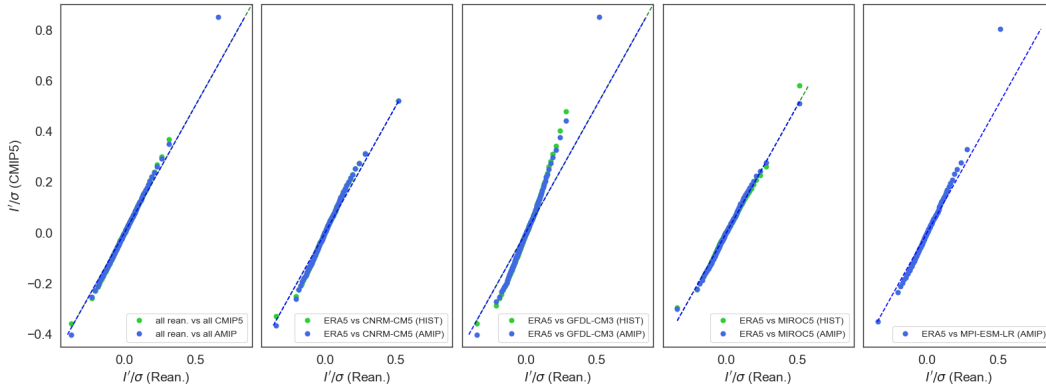


Figure B.4: Quantile-quantile (Q-Q) plots of the normalised energy anomalies in the global balanced (Rossby mode) planetary circulation ( $k = 1 - 3$ ). (a) all reanalyses (x-axis) compared with all CMIP5 models (y-axis). CMIP5 HIST (coupled) are displayed as green dots and AMIP (uncoupled) as blue dots. (b) the same as (a), but only one reanalysis (ERA5) and one model (CNRM-CM3) are displayed. The same is for GFDL-CM3 in (c), MIROC5 in (d) and MPI-ESM-LR in (e). Note that the last model is presented only with an AMIP run. Dashed lines are a "perfect" fit for each comparison.

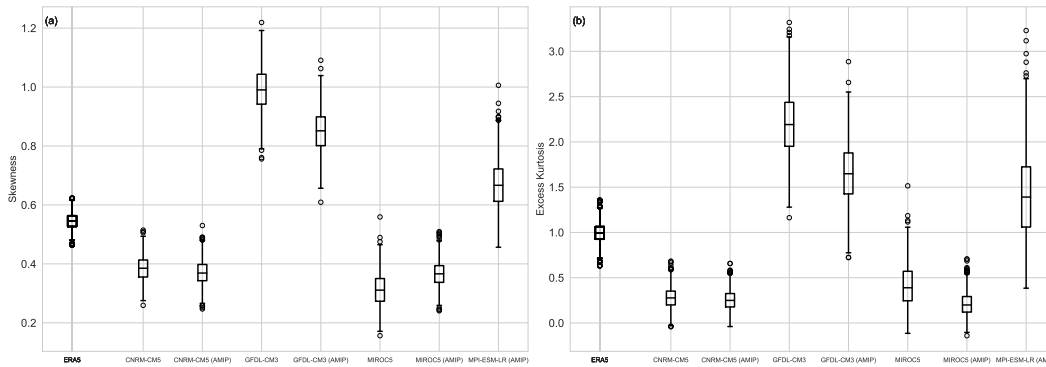


Figure B.5: Box plots for the skewness of the PDFs of normalised energy anomalies for planetary-scale Rossby waves ( $k = 1 - 3$ ) from ERA5 and each CMIP5 model.

We would like to note that there are no distinct differences in PDFs between coupled and uncoupled simulations, implying that models contain biases origin not only from SSTs but other sources of uncertainty such as physical parameterisations, horizontal and vertical resolution atmosphere and ocean, numerical schemes (Woollings et al., 2018).

In total, our findings suggest that the ensemble of models represents well the climatology of planetary Rossby waves (only the troposphere–barotropic part) but individual models have discrepancies in the mean state and in the distributions of energy anomalies.

### B.3.3 Do HWs in reanalyses and CMIP5 models have the same signatures on planetary scales?

Strigunova et al. (2022) revealed an increase in the skewness of PDFs of normalised energy anomalies of planetary-scale Rossby waves. It is also shown as an increase in the probability of larger positive anomalies in energy (Fig. B.6a), and larger anomalies of geopotential height as the mean circulation showed (Fig. B.7a-c).

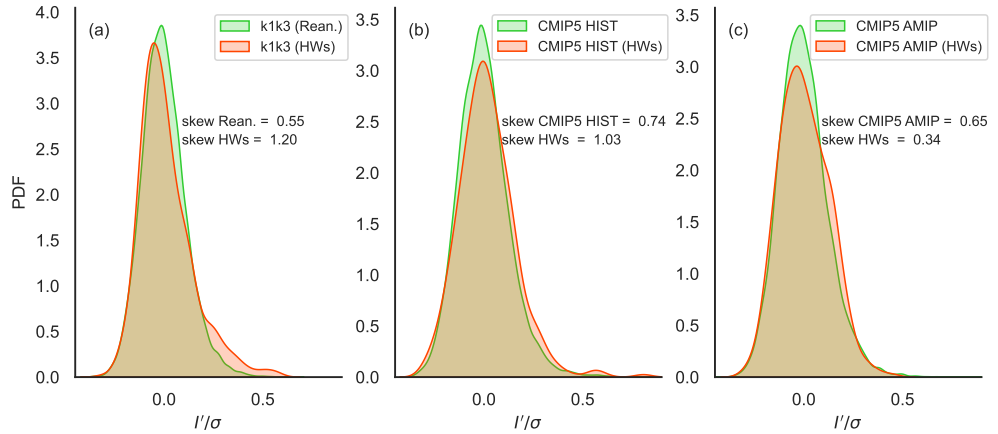


Figure B.6: PDFs of the normalised energy anomalies in the global balanced (Rossby mode) planetary circulation ( $k = 1 - 3$ ). (a) the same as Fig. 6c in Strigunova et al. (2022). Model ensembles with coupled and uncoupled simulations are shown in (b) and (c), respectively. Red curves with shading are energy anomalies only during Eurasian HWs. Note that the identification algorithm is applied for each model and simulation separately.

Here, we evaluate how the change in PDF of planetary Rossby waves is represented in the model ensemble of CMIP5 models with separation on coupled (Fig. B.6b) and uncoupled (Fig. B.6c) runs. There is a common feature of distributions during HWs: they all exhibit an increase in probabilities but for different ranges of energy anomalies. In the historical run, models show a peak at very large energy anomalies, but it is only exhibited in one model (GFDL-CM3). In the AMIP run, there is no increase in probabilities of tails on the right but an increase for intermediate energy anomalies. The change in tails reflects the change in skewness. However, the latter is insignificant for both runs according to bootstrapping procedure. Thus, we presume all changes in PDFs of CMIP5 models are not robust.

Despite large uncertainty in distributions, we find that the CMIP5 model's composite of Rossby-wave patterns is similar to ERA5's. The examples of one model (GFDL-CM3) composites are presented in Fig. B.7d-f. Over the region of occurred HWs, lesser geopotential height anomalies are identified in coupled run compared to ERA5 (Fig. B.7e, e). Figures B.8e, f demonstrate it clearly as GFDL-CM3 fields during HWs were subtracted from respective fields in ERA5. In contrast, the com-

posite of mean circulation (Fig. B.7g-i) in uncoupled (AMIP) simulations revealed larger positive anomalies in the geopotential height field during HWs over this region. However, Fig. B.8h, i show that the location of maximum is shifted to the south (negative values on the north and positive on the south). Figures B.8f, i also reveal that changes in circulation look similar to those depicted as the mean composite during HWs (Fig. B.8e, h). It also revealed that the Rossby-wave pattern in GFDL-CM3 is different compared to ERA5's in other locations, especially in regions over the Pacific. Therefore, we show that one model (for other models, results are similar) can reproduce planetary Rossby-wave circulation during HWs. However, in coupled simulations, anomalies are weaker, and in uncoupled, the core of large positive anomalies is shifted to the south.

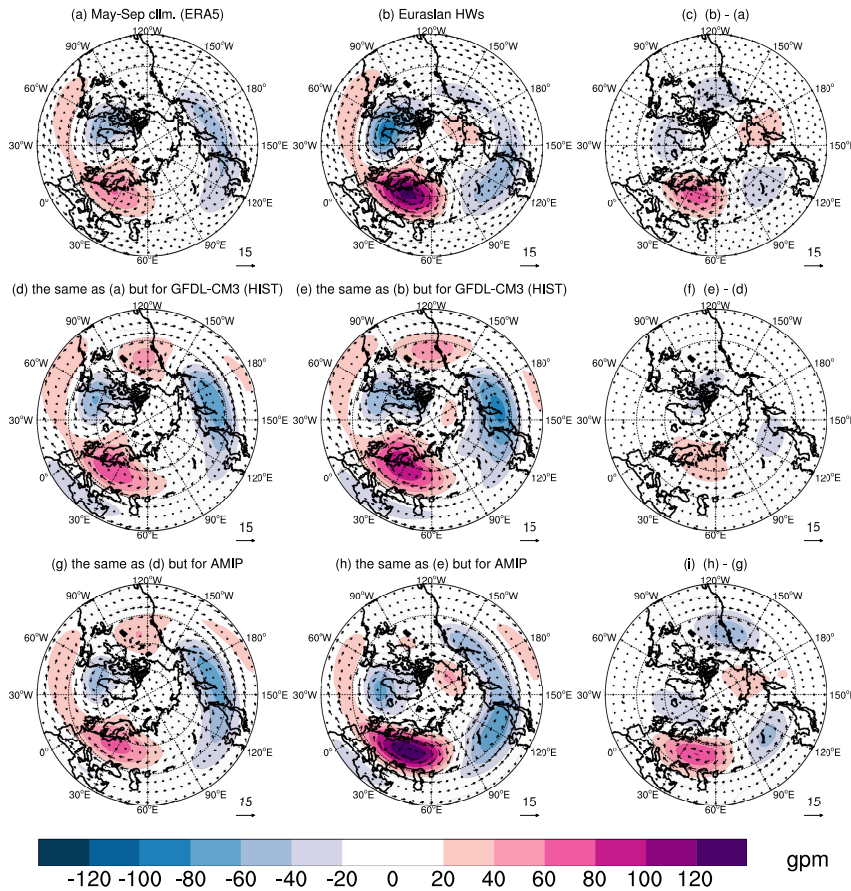


Figure B.7: Planetary-scale, troposphere-barotropic Rossby waves ( $k = 1 - 3$ ,  $m = 1 - 5$ , all  $n$ ) at the  $\sigma$  level close to 500 hPa in ERA5. (a) Mean circulation in May-September in 1980-2019, (b) composite of 28 Eurasian Heat Waves (HWs), (c) difference between (b) and (a). Coloured contours are geopotential height anomalies, every 20 gpm. The wind speed is shown by the arrow length. (d) The same as (a), but GFDL-CM3 (coupled) is displayed (only 1979-2005). (e) the same as (b) but a composite of 23 Eurasian Heat Waves (HWs), (f) the same as (c). Similarly, GFDL-CM3 AMIP is shown in (g)-(i).

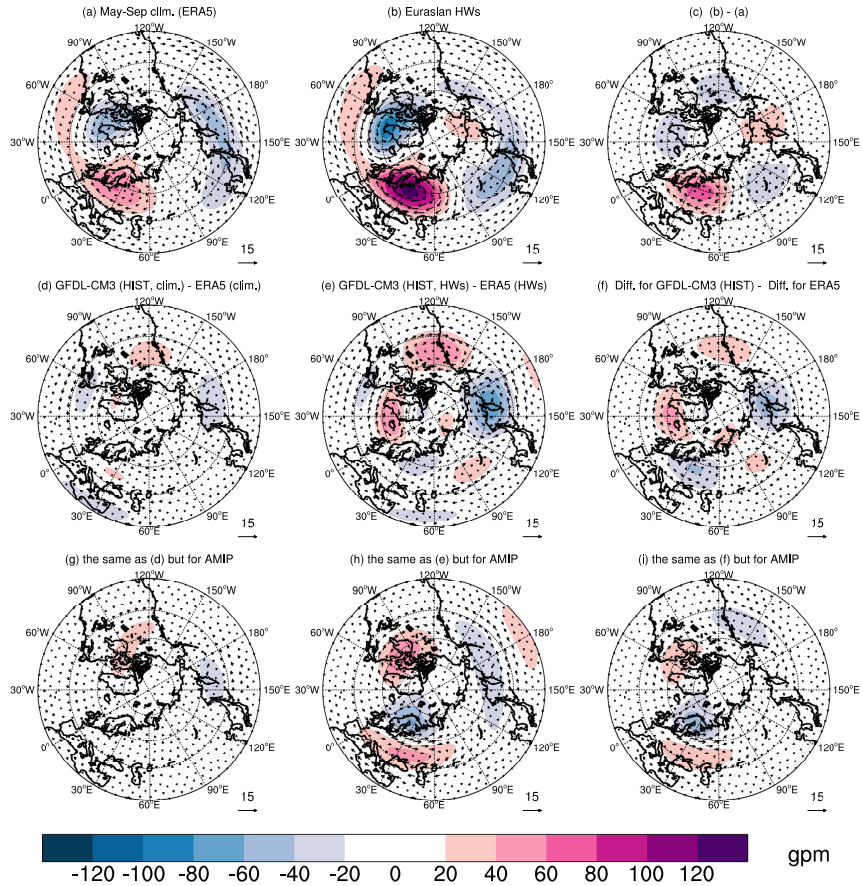


Figure B.8: The same as in Fig. B.7 but ERA5 fields are subtracted from GFDL-CM3's accordingly.

#### B.4 CONCLUSIONS

To diagnose Rossby planetary circulation during HWs, we first compared distributions of T2m and its anomalies for each model with ERA5 used as a reference dataset. The findings show that the distributions are within ERA5's CIs (IQRs). The same holds when considering only deviations from the 95th percentile identified for each model and compared with ERA5 statistics. Moreover, the HW metrics match as well, meaning that CMIP5 models have a good agreement with ERA5.

Second, we discussed how the climatology of Rossby circulation is presented among models. We find that the mean circulation at 500 hPa for every model is similar, except for MIROC5. Nevertheless, when the distributions of normalised energy anomalies of all models are considered together as time series and compared with all reanalyses, there is almost no difference. Nevertheless, the analysis of individual models with only one dataset (ERA5) revealed that the distributions of two models (GFDL-CM3 and MPI-ESM-LR) are more skewed compared to ERA5 and

the difference is statistically significant. Therefore, models show some differences with ERA5, even in climatology.

During HWs, the planetary Rossby waves' variability (normalised energy anomaly distributions) is not reproduced due to the small sample size and inconsistent changes among models in both simulations. The further comparison in time-averaged circulation (only one model is shown) revealed that, in coupled simulations, the anomalies are weaker, and, in uncoupled, they have similar values with ERA5, but the location of the maximum is shifted southward. Discrepancies in other regions are also identified. We speculate that, according to these results, HWs have different realisations in simulations.

## B.5 DISCUSSION

This study illustrated several discrepancies in CMIP5 compared to ERA5, while the 2 m temperature and related metrics used for HW identification seem well-simulated. The mismatch in dates of events can be attributed to the sensitivity of the threshold and, thus, the HWs' identification to internal variability simulated by each model. However, the overall statistics are shown to be similar. Therefore, the role of internal variability remains to be explored.

Composite maps of wind and geopotential fields at 500 hPa representing the climatology of planetary-scale Rossby waves are well-simulated, except for MIROC5. Meanwhile, the PDFs of normalised energy anomalies demonstrate that the two models with the highest vertical resolution significantly differ from ERA5's PDF. According to Table B.1, MPI-ESM-LR and GFDL-CM3 have 47 and 45 vertical levels, respectively, with top-level  $\approx 0.01$  hPa. ERA5 has a similar vertical resolution; however, its horizontal resolution is much higher. Therefore, some model biases in upper levels can be transmitted to the troposphere, resulting in much larger energy anomalies than the reanalysis shows. The preliminary results revealed no significant differences in longitude-vertical cross-sections averaged in the midlatitudes and over the northern hemisphere. Therefore, it might be attributed to biases in other regions. Due to the global domain, the explanation of the different behaviour of PDFs of GFDL-CM3 and MPI-ESM-LR is hard to tackle; therefore, it remains an open question.

The most puzzling is why uncoupled simulations can simulate mean circulation during HWs, whereas coupled are not. Several hypotheses have been proposed.

According to Suarez-Gutierrez et al. (2018), it has been shown that Max-Planck Grand Ensemble (MPI-GE) can reproduce the circulation during European HW 2003. It can be explained that MPI-GE is based on 100 simulations of MPI-ESM-LR with different initial conditions but the same model physics and external forcing. Therefore, among 100 members, there are some realisations which realistically represent the state of atmospheric circulation. Thus, future studies with the same diagnostics and larger ensemble sizes might give a different conclusion than the one given in the present study. Nevertheless, we see that models represent the

same dynamics but with less intensity meaning that it is likely a different cause than some completely different initial conditions.

In Strigunova et al. (2022), it has been demonstrated that during HWs, there is a weakening of the zonal-mean maximum at 45°N with a shift slightly northward along with a strengthening of the zonal-mean wind at centred at 75°N. We find that CMIP5 models' uncoupled simulations are good enough to reproduce this, but coupled simulations are not. It hints that the underlying dynamics of HWs are different and coupled and uncoupled runs. Following Rousi et al. (2022a), a double-jet structure is likely to occur due to the thermal contrast between land and ocean in the Arctic. While land being rapidly warmed for several decades, most likely due to anthropogenic forcing (e.g. Connolly et al., 2019), the ocean warming trend is slower. Therefore, the cause for biases in coupled simulations can be originated from high latitudes (for example, SSTs are larger in simulations and, therefore, the less contrast leads to no double-jet).

These results might also stem from biases identified in models. Liu et al. (2022) also noted an underestimation of blocking intensity in GFDL models in CMIP5 and CMIP6. For boreal summer, they found close alignment in location but not intensity for several models. They also pointed out that biases in zonal eddies contribute to blocking, but the effect appeared to be small. Nevertheless, recent studies mentioned that these small biases might be transmitted to the zonal-mean state through zonal-mean-eddy feedback.

Quasi-stationary planetary-scale Rossby waves are forced not only from land-sea contrast but also from orography, which is poorly represented in models (Pithan et al., 2016). Their transient parts are forced by tropical heating, which is connected to convection in the tropics, another struggle of modern general circulation models (e.g. Nie et al., 2019).



## BIBLIOGRAPHY

---

- Ali, S. M., O. Martius, and M. Röthlisberger (2021). "Recurrent Rossby wave packets modulate the persistence of dry and wet spells across the globe." In: *Geophys. Res. Lett.* 48.5, e2020GL091452. DOI: [10.1029/2020GL091452](https://doi.org/10.1029/2020GL091452).
- Amazirh, A., S. Er-Raki, A. Chehbouni, V. Rivalland, A. Diarra, S. Khabba, J. Ez-zahar, and O. Merlin (2017). "Modified Penman–Monteith equation for monitoring evapotranspiration of wheat crop: Relationship between the surface resistance and remotely sensed stress index." In: *Biosyst. Eng.* 164, pp. 68–84. DOI: [10.1016/j.biosystemseng.2017.09.015](https://doi.org/10.1016/j.biosystemseng.2017.09.015).
- Anstey, J. A., P. Davini, L. J. Gray, T. J. Woollings, N. Butchart, C. Cagnazzo, B. Christiansen, S. C. Hardiman, S. M. Osprey, and S. Yang (2013). "Multi-model analysis of Northern Hemisphere winter blocking: Model biases and the role of resolution." In: *J. Geophys. Res. Atmos.* 118.10, pp. 3956–3971. DOI: [10.1002/jgrd.50231](https://doi.org/10.1002/jgrd.50231).
- Bader, J. and M. Latif (2005). "North Atlantic Oscillation response to anomalous Indian Ocean SST in a coupled GCM." In: *J. Clim.* 18.24, pp. 5382–5389. DOI: [10.1175/JCLI3577.1](https://doi.org/10.1175/JCLI3577.1).
- Barnes, E. A. and L. Polvani (2013). "Response of the midlatitude jets, and of their variability, to increased greenhouse gases in the CMIP5 models." In: *J. Clim.* 26.18, pp. 7117–7135. DOI: [10.1175/JCLI-D-12-00536.1](https://doi.org/10.1175/JCLI-D-12-00536.1).
- Barriopedro, D., E. M. Fischer, J. Luterbacher, R. M. Trigo, and R. García-Herrera (2011). "The Hot Summer of 2010: Redrawing the Temperature Record Map of Europe." In: *Science* 332.6026, pp. 220–224. DOI: [10.1126/science.1201224](https://doi.org/10.1126/science.1201224).
- Behera, S. K., J. V. Ratnam, Y. Masumoto, and T. Yamagata (2012). "Origin of extreme summers in Europe: the Indo-Pacific connection." In: *Clim. Dyn.* 41, pp. 663–676. DOI: [10.1007/s00382-012-1524-8](https://doi.org/10.1007/s00382-012-1524-8).
- Berckmans, J., T. Woollings, M.-E. Demory, P.-L. Vidale, and M. Roberts (2013). "Atmospheric blocking in a high resolution climate model: influences of mean state, orography and eddy forcing." In: *Atmos. Sci. Lett.* 14.1, pp. 34–40. DOI: [10.1002/asl2.412](https://doi.org/10.1002/asl2.412).
- Blackport, R. and J. A. Screen (2020). "Insignificant effect of Arctic amplification on the amplitude of midlatitude atmospheric waves." In: *Sci. Adv.* 6.8, eaay2880. DOI: [10.1126/sciadv.aay2880](https://doi.org/10.1126/sciadv.aay2880).
- Brunner, L., N. Schaller, J. Anstey, J. Sillmann, and A. K. Steiner (2018). "Dependence of present and future European temperature extremes on the location of atmospheric blocking." In: *Geophys. Res. Lett.* 45.12, pp. 6311–6320. DOI: [10.1029/2018GL077837](https://doi.org/10.1029/2018GL077837).
- Carvalho, D., S. Cardoso Pereira, and A. Rocha (2021). "Future surface temperatures over Europe according to CMIP6 climate projections: an analysis with

- original and bias-corrected data." In: *Clim. Change* 167.1, pp. 1–17. DOI: [10.1007/s10584-021-03159-0](https://doi.org/10.1007/s10584-021-03159-0).
- Castanheira, J. M. and C. A. F. Marques (2022). "Biases of the barotropic atmospheric circulation variability in CMIP6 models." In: *J. Clim.*, pp. 1–40. DOI: [10.1175/JCLI-D-21-0581.1](https://doi.org/10.1175/JCLI-D-21-0581.1).
- Cattiaux, J., H. Douville, and Y. Peings (2013). "European temperatures in CMIP5: origins of present-day biases and future uncertainties." In: *Clim. Dyn.* 41.11, pp. 2889–2907. DOI: [10.1007/s00382-013-1731-y](https://doi.org/10.1007/s00382-013-1731-y).
- Chang, E. K. M. (2001). "The structure of baroclinic wave packets." In: *J. Atmos. Sci.* 58.13, pp. 1694–1713.
- Chang, E. K. M., C.-G. Ma, C. Zheng, and A. M. W. Yau (2016). "Observed and projected decrease in Northern Hemisphere extratropical cyclone activity in summer and its impacts on maximum temperature." In: *Geophys. Res. Lett.* 43.5, pp. 2200–2208. DOI: [10.1002/2016GL068172](https://doi.org/10.1002/2016GL068172).
- Chen, D. et al. (2021). "Framing, Context and Methods." In: *Climate Change 2021: The Physical Science Basis. Contribution of Working Group I to the Sixth Assessment Report of the Intergovernmental Panel on Climate Change*. Cambridge, United Kingdom and New York, NY, USA: Cambridge University Press, pp. 147–286. DOI: [10.1017/9781009157896.003](https://doi.org/10.1017/9781009157896.003).
- Connolly, R., M. Connolly, W. Soon, D. R. Legates, R. G. Cionco, and Víctor M. Velasco H. (2019). "Northern hemisphere snow-cover trends (1967–2018): a comparison between climate models and observations." In: *Geosciences* 9.3, p. 135. DOI: [doi.org/10.3390/geosciences9030135](https://doi.org/10.3390/geosciences9030135).
- Coumou, D., G. Di Capua, S. Vavrus, L. Wang, and S. Wang (2018). "The influence of Arctic amplification on mid-latitude summer circulation." In: *Nat. Commun.* 9.1, pp. 1–12. DOI: [10.1038/s41467-018-05256-8](https://doi.org/10.1038/s41467-018-05256-8).
- Coumou, D., J. Lehmann, and J. Beckmann (Mar. 2015). "Climate change. The weakening summer circulation in the Northern Hemisphere mid-latitudes." In: *Science (New York, N.Y.)* 348. DOI: [10.1126/science.1261768](https://doi.org/10.1126/science.1261768).
- Coumou, D., V. Petoukhov, S. Rahmstorf, S. Petri, and H. J. Schellnhuber (2014). "Quasi-resonant circulation regimes and hemispheric synchronization of extreme weather in boreal summer." In: *Proc. Natl. Acad. Sci. U.S.A.* 111.34, pp. 12331–12336. DOI: [10.1073/pnas.1412797111](https://doi.org/10.1073/pnas.1412797111).
- Davini, P. and F. D'Andrea (2016). "Northern Hemisphere atmospheric blocking representation in global climate models: twenty years of improvements?" In: *J. Clim.* 29.24, pp. 8823–8840. DOI: [10.1175/JCLI-D-16-0242.1](https://doi.org/10.1175/JCLI-D-16-0242.1).
- Davini, P. and F. d'Andrea (2020). "From CMIP3 to CMIP6: Northern Hemisphere atmospheric blocking simulation in present and future climate." In: *J. Clim.* 33.23, pp. 10021–10038. DOI: [10.1175/jcli-d-19-0862.1](https://doi.org/10.1175/jcli-d-19-0862.1).
- Dee, D. P. et al. (2011). "The ERA-Interim reanalysis: configuration and performance of the data assimilation system." In: *Q. J. R. Meteorol. Soc.* 137.656, pp. 553–597. DOI: [10.1002/qj.828](https://doi.org/10.1002/qj.828).

- Della-Marta, P. M., J. Luterbacher, H. von Weissenfluh, E. Xoplaki, M. Brunet, and H. Wanner (2007). "Summer heat waves over western Europe 1880–2003, their relationship to large-scale forcings and predictability." In: *Clim. Dyn.* 29.2, pp. 251–275. DOI: [10.1007/s00382-007-0233-1](https://doi.org/10.1007/s00382-007-0233-1).
- Deng, K., S. Yang, M. Ting, A. Lin, and Z. Wang (2018). "An intensified mode of variability modulating the summer heat waves in eastern Europe and northern China." In: *Geophys. Res. Lett.* 45.20, pp. 11–361. DOI: [10.1029/2018GL079836](https://doi.org/10.1029/2018GL079836).
- Di Capua, G., J. Runge, R. V. Donner, B. van den Hurk, A. G. Turner, R. Vellore, R. Krishnan, and D. Coumou (2020). "Dominant patterns of interaction between the tropics and mid-latitudes in boreal summer: causal relationships and the role of timescales." In: *Weather Clim. Dynam.* 1.2, pp. 519–539. DOI: [10.5194/wcd-1-519-2020](https://doi.org/10.5194/wcd-1-519-2020).
- Di Luca, A., A. J. Pitman, and R. de Elía (2020). "Decomposing temperature extremes errors in CMIP5 and CMIP6 models." In: *Geophys. Res. Lett.* 47.14, e2020GL088031. DOI: [10.1029/2020GL088031](https://doi.org/10.1029/2020GL088031).
- Ding, Q. and B. Wang (2005). "Circumglobal teleconnection in the Northern Hemisphere summer." In: *J. Clim.* 18.17, pp. 3483–3505. DOI: [10.1175/JCLI3473.1](https://doi.org/10.1175/JCLI3473.1).
- Doblas-Reyes, F.J. et al. (2021). "Linking Global to Regional Climate Change." In: *Climate Change 2021: The Physical Science Basis. Contribution of Working Group I to the Sixth Assessment Report of the Intergovernmental Panel on Climate Change*. Cambridge, United Kingdom and New York, NY, USA: Cambridge University Press, 1363–1512. DOI: [10.1017/9781009157896.012](https://doi.org/10.1017/9781009157896.012).
- Domeisen, D. I. V., E. A. B. Eltahir, E. M. Fischer, R. Knutti, S. E. Perkins-Kirkpatrick, C. Schär, S. I. Seneviratne, A. Weisheimer, and H. Wernli (2022). "Prediction and projection of heatwaves." In: *Nat. Rev. Earth Environ.*, pp. 1–15. DOI: [10.1038/s43017-022-00371-z](https://doi.org/10.1038/s43017-022-00371-z).
- Drouard, M. and T. Woollings (2018). "Contrasting mechanisms of summer blocking over western Eurasia." In: *Geophys. Res. Lett.* 45.21, pp. 12–040. DOI: [10.1029/2018GL079894](https://doi.org/10.1029/2018GL079894).
- Emerton, R., C. Brimicombe, L. Magnusson, C. Roberts, C. Di Napoli, H. L. Cloke, and F. Pappenberger (2022). "Predicting the unprecedented: forecasting the June 2021 Pacific Northwest heatwave." In: *Weather* n/a.n/a. DOI: <https://doi.org/10.1002/wea.4257>.
- Eyring, V., P. M. Cox, G. M. Flato, P. J. Gleckler, G. Abramowitz, P. Caldwell, W. D. Collins, B. K. Gier, A. D. Hall, F. M. Hoffman, et al. (2019). "Taking climate model evaluation to the next level." In: *Nat. Clim. Change* 9.2, pp. 102–110. DOI: [10.1038/s41558-018-0355-y](https://doi.org/10.1038/s41558-018-0355-y).
- Eyring, V. et al. (2021). "Human Influence on the Climate System." In: *Climate Change 2021: The Physical Science Basis. Contribution of Working Group I to the Sixth Assessment Report of the Intergovernmental Panel on Climate Change*. Cambridge, United Kingdom and New York, NY, USA: Cambridge University Press, 423–552. DOI: [10.1017/9781009157896.005](https://doi.org/10.1017/9781009157896.005).

- Eyster, H. N. and B. Beckage (2022). "Conifers May Ameliorate Urban Heat Waves Better Than Broadleaf Trees: Evidence from Vancouver, Canada." In: *Atmosphere* 13.5, p. 830. DOI: [10.3390/atmos13050830](https://doi.org/10.3390/atmos13050830).
- Fabiano, F., H. M. Christensen, K. Strommen, P. Athanasiadis, A. Baker, R. Schiemann, and S. Corti (2020). "Euro-Atlantic weather Regimes in the PRIMAVERA coupled climate simulations: impact of resolution and mean state biases on model performance." In: *Clim. Dyn.* 54.11, pp. 5031–5048. DOI: [10.1007/s00382-020-05271-w](https://doi.org/10.1007/s00382-020-05271-w).
- Fan, X., C. Miao, Q. Duan, C. Shen, and Y. Wu (2020). "The performance of CMIP6 versus CMIP5 in simulating temperature extremes over the global land surface." In: *J. Geophys. Res. Atmos.* 125.18, e2020JD033031. DOI: [10.1029/2020JD033031](https://doi.org/10.1029/2020JD033031).
- Feudale, L. and J. Shukla (2011). "Influence of sea surface temperature on the European heat wave of 2003 summer. Part I: an observational study." In: *Clim. Dyn.* 36.9, pp. 1691–1703. DOI: [10.1007/s00382-010-0788-0](https://doi.org/10.1007/s00382-010-0788-0).
- Fischer, E. M. and R. Knutti (2015). "Anthropogenic contribution to global occurrence of heavy-precipitation and high-temperature extremes." In: *Nat. Clim. Change* 5.6, pp. 560–564. DOI: [10.1038/nclimate2617](https://doi.org/10.1038/nclimate2617).
- Fischer, E. M., S. I. Seneviratne, P. L. Vidale, D. Lüthi, and C. Schär (2007). "Soil moisture–atmosphere interactions during the 2003 European summer heat wave." In: *J. Clim.* 20.20, pp. 5081–5099. DOI: [doi.org/10.1175/JCLI4288.1](https://doi.org/10.1175/JCLI4288.1).
- Flato, G. et al. (2013). "Evaluation of Climate Models." In: *Climate Change 2013: The Physical Science Basis. Contribution of Working Group I to the Fifth Assessment Report of the Intergovernmental Panel on Climate Change*. Cambridge, United Kingdom and New York, NY, USA: Cambridge University Press, 741–866. DOI: [10.1017/CB09781107415324.020](https://doi.org/10.1017/CB09781107415324.020).
- Folland, C. K., J. Knight, H. W. Linderholm, D. Fereday, S. Ineson, and J. W. Hurrell (2009). "The summer North Atlantic Oscillation: past, present, and future." In: *J. Clim.* 22.5, pp. 1082–1103. DOI: [10.1175/2008JCLI2459.1](https://doi.org/10.1175/2008JCLI2459.1).
- Fragkoulidis, G., V. Wirth, P. Bossmann, and A. H. Fink (2018). "Linking Northern Hemisphere temperature extremes to Rossby wave packets." In: *Q. J. R. Meteorol. Soc.* 144.711, pp. 553–566. DOI: [10.1002/qj.3228](https://doi.org/10.1002/qj.3228).
- Fuentes-Franco, R., T. Koenigk, D. Docquier, F. Graef, and K. Wyser (2022). "Exploring the influence of the North Pacific Rossby wave sources on the variability of summer atmospheric circulation and precipitation over the Northern Hemisphere." In: *Clim. Dyn.*, pp. 1–15. DOI: [10.1007/s00382-022-06194-4](https://doi.org/10.1007/s00382-022-06194-4).
- Galfi, V. M. and V. Lucarini (June 2021). "Fingerprinting Heatwaves and Cold Spells and Assessing Their Response to Climate Change Using Large Deviation Theory." In: *Phys. Rev. Lett.* 127 (5), p. 058701. DOI: [10.1103/PhysRevLett.127.058701](https://doi.org/10.1103/PhysRevLett.127.058701).
- Gleick, James (1997). *Chaos: Making a new science*. Penguin.
- Gulev, S.K. et al. (2021). "Changing State of the Climate System." In: *Climate Change 2021: The Physical Science Basis. Contribution of Working Group I to the Sixth Assess-*

- ment Report of the Intergovernmental Panel on Climate Change. Cambridge, United Kingdom and New York, NY, USA: Cambridge University Press, 287–422. DOI: [10.1017/9781009157896.004](https://doi.org/10.1017/9781009157896.004).
- Hersbach, H., B. Bell, P. Berrisford, S. Hirahara, A. Horányi, J. Muñoz-Sabater, J. Nicolas, C. Peubey, R. Radu, D. Schepers, et al. (2020). “The ERA5 global reanalysis.” In: *Q. J. R. Meteorol. Soc.* 146.730, pp. 1999–2049. DOI: [doi.org/10.1002/qj.3803](https://doi.org/10.1002/qj.3803).
- Hirsch, A. L., N. N. Ridder, S. E. Perkins-Kirkpatrick, and A. Ukkola (2021). “CMIP6 MultiModel Evaluation of Present-Day Heatwave Attributes.” In: *Geophys. Res. Lett.* 48.22, e2021GL095161. DOI: [10.1029/2021GL095161](https://doi.org/10.1029/2021GL095161).
- Horton, R. M., J. S. Mankin, C. Lesk, E. Coffel, and C. Raymond (2016). “A review of recent advances in research on extreme heat events.” In: *Curr. Clim. Change Rep.* 2.4, pp. 242–259. DOI: [10.1007/s40641-016-0042-x](https://doi.org/10.1007/s40641-016-0042-x).
- Hsu, P.-C., Y. Qian, Y. Liu, H. Murakami, and Y. Gao (2020). “Role of abnormally enhanced MJO over the Western Pacific in the formation and subseasonal predictability of the record-breaking Northeast Asian heatwave in the summer of 2018.” In: *J. C.* 33.8, pp. 3333–3349. DOI: [10.1175/JCLI-D-19-0337.1](https://doi.org/10.1175/JCLI-D-19-0337.1).
- Jeong, D. II, A. J. Cannon, and B. Yu (2022). “Influences of atmospheric blocking on North American summer heatwaves in a changing climate: a comparison of two Canadian Earth system model large ensembles.” In: *Clim. Change* 172.1, pp. 1–21. DOI: [10.1007/s10584-022-03358-3](https://doi.org/10.1007/s10584-022-03358-3).
- Jung, T., G. Balsamo, P. Bechtold, ACM Beljaars, M. Koehler, M.J. Miller, J.-J. Morcrette, A. Orr, M.J. Rodwell, and A. M. Tompkins (2010). “The ECMWF model climate: recent progress through improved physical parametrizations.” In: *Q. J. R. Meteorol. Soc.* 136.650, pp. 1145–1160. DOI: [10.1002/qj.634](https://doi.org/10.1002/qj.634).
- Kasahara, A. and K. Puri (1981). “Spectral representation of three-dimensional global data by expansion in normal mode functions.” In: *Mon. Wea. Rev.* 109, pp. 37–51.
- Kautz, L.-A., O. Martius, S. Pfahl, J G Pinto, A M Ramos, P M Sousa, and T. Woollings (2022). “Atmospheric blocking and weather extremes over the Euro-Atlantic sector—a review.” In: *Weather Clim. Dynam.* 3.1, pp. 305–336. DOI: [10.5194/wcd-3-305-2022](https://doi.org/10.5194/wcd-3-305-2022).
- Kenney, W. L., D. H. Craighead, and L. M. Alexander (2014). “Heat waves, aging, and human cardiovascular health.” In: *Med Sci Sports Exerc* 46.10, p. 1891. DOI: [10.1249/MSS.0000000000000325](https://doi.org/10.1249/MSS.0000000000000325).
- Kim, Y.-H., S.-K. Min, X. Zhang, J. Sillmann, and M. Sandstad (2020). “Evaluation of the CMIP6 multi-model ensemble for climate extreme indices.” In: *Weather Clim. Extremes* 29, p. 100269. DOI: [10.1016/j.wace.2020.100269](https://doi.org/10.1016/j.wace.2020.100269).
- Kobayashi, S. et al. (2015). “The JRA-55 reanalysis: General specifications and basic characteristics.” In: *J. Meteorol. Soc. Jpn. Ser. II* 93.1, pp. 5–48. DOI: [10.2151/jmsj.2015-001](https://doi.org/10.2151/jmsj.2015-001).
- Kornhuber, K., D. Coumou, E. Vogel, C. Lesk, J F Donges, J. Lehmann, and R M Horton (2020). “Amplified Rossby waves enhance risk of concurrent heatwaves

- in major breadbasket regions." In: *Nat. Clim. Change* 10.1, pp. 48–53. DOI: [10.1038/s41558-019-0637-z](https://doi.org/10.1038/s41558-019-0637-z).
- Kornhuber, K., S. Osprey, D. Coumou, S. Petri, P. Vladimir, and Gray L. Stefan R. and (Apr. 2019). "Extreme weather events in early summer 2018 connected by a recurrent hemispheric wave-7 pattern." In: *Environ. Res. Lett.* 14.5, p. 054002. DOI: [10.1088/1748-9326/ab13bf](https://doi.org/10.1088/1748-9326/ab13bf).
- Kornhuber, K., V. Petoukhov, S. Petri, S. Rahmstorf, and D. Coumou (2017). "Evidence for wave resonance as a key mechanism for generating high-amplitude quasi-stationary waves in boreal summer." In: *Clim. Dyn.* 49.5, pp. 1961–1979. DOI: [10.1007/s00382-016-3399-6](https://doi.org/10.1007/s00382-016-3399-6).
- Kueh, M.-T. and C.-Y. Lin (2020). "The 2018 summer heatwaves over northwestern Europe and its extended-range prediction." In: *Sci. Rep.* 10.1, pp. 1–18. DOI: [10.1038/s41598-020-76181-4](https://doi.org/10.1038/s41598-020-76181-4).
- Lau, W. KM and Kyu-Myong Kim (2012). "The 2010 Pakistan flood and Russian heat wave: Teleconnection of hydrometeorological extremes." In: *J Hydrometeorol.* 13.1, pp. 392–403. DOI: [10.1175/JHM-D-11-016.1](https://doi.org/10.1175/JHM-D-11-016.1).
- Lee, J.-Y. et al. (2021). "Future Global Climate: Scenario-Based Projections and Near-Term Information." In: *Climate Change 2021: The Physical Science Basis. Contribution of Working Group I to the Sixth Assessment Report of the Intergovernmental Panel on Climate Change*. Cambridge, United Kingdom and New York, NY, USA: Cambridge University Press, 553–672. DOI: [10.1017/9781009157896.006](https://doi.org/10.1017/9781009157896.006).
- Lee, M.-H., S. Lee, H.-J. Song, and C.-H. Ho (2017). "The recent increase in the occurrence of a boreal summer teleconnection and its relationship with temperature extremes." In: *J. Clim.* 30.18, pp. 7493–7504. DOI: [10.1175/JCLI-D-16-0094.1](https://doi.org/10.1175/JCLI-D-16-0094.1).
- Lee, S., C. Woods, and R. Caballero (2019). "Relation between Arctic moisture flux and tropical temperature biases in CMIP5 simulations and its fingerprint in RCP8.5 projections." In: *Geophys. Res. Lett.* 46.2, pp. 1088–1096. DOI: [doi.org/10.1029/2018GL080562](https://doi.org/10.1029/2018GL080562).
- Lee, Y.-Y. and R. Grotjahn (2019). "Evidence of specific MJO phase occurrence with summertime California Central Valley extreme hot weather." In: *Adv. Atmos. Sci.* 36.6, pp. 589–602. DOI: [10.1007/s00376-019-8167-1](https://doi.org/10.1007/s00376-019-8167-1).
- Li, M., Y. Yao, I. Simmonds, D. Luo, L. Zhong, and X. Chen (2020). "Collaborative impact of the NAO and atmospheric blocking on European heatwaves, with a focus on the hot summer of 2018." In: *Environ. Res. Lett.* 15.11, p. 114003. DOI: [10.1088/1748-9326/aba6ad](https://doi.org/10.1088/1748-9326/aba6ad).
- Liu, P., K. A. Reed, S. T. Garner, M. Zhao, and Y. Zhu (2022). "Blocking Simulations in GFDL GCMs for CMIP5 and CMIP6." In: *J. Clim.*, pp. 1–53. DOI: [10.1175/JCLI-D-21-0456.1](https://doi.org/10.1175/JCLI-D-21-0456.1).
- Lobell, D. B., C. J. Bonfils, L. M. Kueppers, and M. A. Snyder (2008). "Irrigation cooling effect on temperature and heat index extremes." In: *Geophys. Res. Lett.* 35.9. DOI: [10.1029/2008GL034145](https://doi.org/10.1029/2008GL034145).

- Lucarini, V. and A. Gritsun (2020a). “A new mathematical framework for atmospheric blocking events.” In: *Clim. Dyn.* 54.1, pp. 575–598. DOI: [10.1007/s00382-019-05018-2](https://doi.org/10.1007/s00382-019-05018-2).
- (2020b). “A new mathematical framework for atmospheric blocking events.” In: *Clim. Dyn.* 54.1, pp. 575–598. DOI: [10.1007/s00382-019-05018-2](https://doi.org/10.1007/s00382-019-05018-2).
- Luo, F., F. Selten, K. Wehrli, K. Kornhuber, P. Le Sager, W. May, T. Reerink, S. I. Seneviratne, H. Shiogama, D. Tokuda, et al. (2022). “Summertime Rossby waves in climate models: Substantial biases in surface imprint associated with small biases in upper-level circulation.” In: *Weather and Clim. Dyn.* 3.3, pp. 905–935. DOI: [10.5194/wcd-3-905-2022](https://doi.org/10.5194/wcd-3-905-2022).
- Ma, Q. and C. L. E. Franzke (2021). “The role of transient eddies and diabatic heating in the maintenance of European heat waves: a nonlinear quasi-stationary wave perspective.” In: *Clim. Dyn.* 56, pp. 2983–3002. DOI: [10.1007/s00382-021-05628-9](https://doi.org/10.1007/s00382-021-05628-9).
- Masato, G., B. J. Hoskins, and T. Woollings (2013). “Winter and summer Northern Hemisphere blocking in CMIP5 models.” In: *J. Clim.* 26.18, pp. 7044–7059. DOI: [10.1175/JCLI-D-12-00466.1](https://doi.org/10.1175/JCLI-D-12-00466.1).
- McKinnon, K. A., A. Rhines, M. P. Tingley, and P. Huybers (2016). “Long-lead predictions of eastern United States hot days from Pacific sea surface temperatures.” In: *Nat. Geosci.* 9.5, pp. 389–394. DOI: [10.1038/ngeo2687](https://doi.org/10.1038/ngeo2687).
- Meehl, G. A. and C. Tebaldi (2004). “More intense, more frequent, and longer lasting heat waves in the 21st century.” In: *Science* 305.5686, pp. 994–997. DOI: [10.1126/science.1098704](https://doi.org/10.1126/science.1098704).
- Miralles, D. G., A. J. Teuling, C. C. Van Heerwaarden, and J. Vilà-Guerau de Arellano (2014). “Mega-heatwave temperatures due to combined soil desiccation and atmospheric heat accumulation.” In: *Nat. Geosci.* 7.5, pp. 345–349. DOI: [10.1038/ngeo2141](https://doi.org/10.1038/ngeo2141).
- Moreno-Chamarro, E., L.-P. Caron, S. Loosveldt T., J. Vegas-Regidor, O. Gutjahr, M.-P. Moine, D. Putrasahan, C. D. Roberts, M. J. Roberts, R. Senan, et al. (2022). “Impact of increased resolution on long-standing biases in HighResMIP-PRIMAVERA climate models.” In: *Geosci. Model Dev.* 15.1, pp. 269–289. DOI: [10.5194/gmd-15-269-2022](https://doi.org/10.5194/gmd-15-269-2022).
- Nabizadeh, E., S. W. Lubis, and P. Hassanzadeh (2021). “The 3D structure of Northern Hemisphere blocking events: Climatology, role of moisture, and response to climate change.” In: *J. Clim.* 34.24, pp. 9837–9860. DOI: [10.1175/JCLI-D-21-0141.1](https://doi.org/10.1175/JCLI-D-21-0141.1).
- Nakamura, N. and C SY Huang (2018). “Atmospheric blocking as a traffic jam in the jet stream.” In: *Science* 361.6397, pp. 42–47. DOI: [10.1126/science.aat0721](https://doi.org/10.1126/science.aat0721).
- Nie, Y., Y. Zhang, X.-Q. Yang, and H.-L. Ren (2019). “Winter and summer Rossby wave sources in the CMIP5 models.” In: *Earth Space Sci.* 6.10, pp. 1831–1846.
- Ogi, M., K. Yamazaki, and Y. Tachibana (2005). “The summer northern annular mode and abnormal summer weather in 2003.” In: *Geophys. Res. Lett.* 32.4. DOI: [10.1029/2004GL021528](https://doi.org/10.1029/2004GL021528).

- Park, C., S.-K. Min, D. Lee, D.-H. Cha, M.-S. Suh, H.-S. Kang, S.-Y. Hong, D.-K. Lee, H.-J. Baek, and K.-O. Boo (2016). "Evaluation of multiple regional climate models for summer climate extremes over East Asia." In: *Clim. Dyn.* 46.7, pp. 2469–2486. DOI: [10.1007/s00382-015-2713-z](https://doi.org/10.1007/s00382-015-2713-z).
- Park, M. and S. Lee (2019). "Relationship between tropical and extratropical diabatic heating and their impact on stationary–transient wave interference." In: *J Atmos Sci* 76.9, pp. 2617–2633. DOI: [10.1175/JAS-D-18-0371.1](https://doi.org/10.1175/JAS-D-18-0371.1).
- Perkins-Kirkpatrick, S. E. and P. B. Gibson (2017). "Changes in regional heatwave characteristics as a function of increasing global temperature." In: *Sci. Rep.* 7.1, pp. 1–12. DOI: [10.1038/s41598-017-12520-2](https://doi.org/10.1038/s41598-017-12520-2).
- Perkins, S. E. (2015). "A review on the scientific understanding of heatwaves—Their measurement, driving mechanisms, and changes at the global scale." In: *Atmos. Res.* 164, pp. 242–267. DOI: [10.1016/j.atmosres.2015.05.014](https://doi.org/10.1016/j.atmosres.2015.05.014).
- Perron, M. and P. Sura (2013). "Climatology of non-Gaussian atmospheric statistics." In: *J. Clim.* 26.3, pp. 1063–1083. DOI: [10.1175/JCLI-D-11-00504.1](https://doi.org/10.1175/JCLI-D-11-00504.1).
- Petoukhov, V., S. Rahmstorf, S. Petri, and H. J. Schellnhuber (2013). "Quasiresonant amplification of planetary waves and recent Northern Hemisphere weather extremes." In: *Proc. Natl. Acad. Sci. U.S.A.* 110.14, pp. 5336–5341. DOI: [10.1073/pnas.1222000110](https://doi.org/10.1073/pnas.1222000110).
- Pfahl, S., C. Schwierz, M. Croci-Maspoli, C. M. Grams, and H. Wernli (2015). "Importance of latent heat release in ascending air streams for atmospheric blocking." In: *Nat. Geosci.* 8.8, pp. 610–614. DOI: [10.1038/ngeo2487](https://doi.org/10.1038/ngeo2487).
- Pfahl, S. and H. Wernli (2012). "Quantifying the relevance of atmospheric blocking for co-located temperature extremes in the Northern Hemisphere on (sub-) daily time scales." In: *Geophys. Res. Lett.* 39.12. DOI: [10.1029/2012GL052261](https://doi.org/10.1029/2012GL052261).
- Pithan, F., T. G. Shepherd, G. Zappa, and I. Sandu (2016). "Climate model biases in jet streams, blocking and storm tracks resulting from missing orographic drag." In: *Geophys. Res. Lett.* 43.13, pp. 7231–7240. DOI: [10.1002/2016GL069551](https://doi.org/10.1002/2016GL069551).
- Plavcova, E. and J. Kyselý (2016). "Overly persistent circulation in climate models contributes to overestimated frequency and duration of heat waves and cold spells." In: *Clim. Dyn.* 46.9, pp. 2805–2820. DOI: [10.1007/s00382-015-2733-8](https://doi.org/10.1007/s00382-015-2733-8).
- Ragone, F. and F. Bouchet (June 2021). "Rare Event Algorithm Study of Extreme Warm Summers and Heatwaves Over Europe." In: *Geophys. Res. Lett.* 48.12. DOI: [doi.org/10.1029/2020GL091197](https://doi.org/10.1029/2020GL091197).
- Riboldi, J., F. Lott, F. d'Andrea, and G. Rivière (2020). "On the linkage between Rossby wave phase speed, atmospheric blocking, and Arctic amplification." In: *Geophys. Res. Lett.* 47.19, e2020GL087796. DOI: [10.1029/2020GL087796](https://doi.org/10.1029/2020GL087796).
- Rienecker, M. M., M. J. Suarez, R. Gelaro, R. Todling, J. Bacmeister, E. Liu, M. G. Bosilovich, S. D. Schubert, L. Takacs, G.-K. Kim, et al. (2011). "MERRA: NASA's modern-era retrospective analysis for research and applications." In: *J. Clim.* 24.14, pp. 3624–3648. DOI: [10.1175/JCLI-D-11-00015.1](https://doi.org/10.1175/JCLI-D-11-00015.1).



- Rousi, E., K. Kornhuber, G. Beobide-Arsuaga, F. Luo, and D. Coumou (2022a). "Accelerated western European heatwave trends linked to more-persistent double jets over Eurasia." In: *Nat. Commun.* 13, p. 3851. DOI: [10.1038/s41467-022-31432-y](https://doi.org/10.1038/s41467-022-31432-y).
- (2022b). "Accelerated western European heatwave trends linked to more-persistent double jets over Eurasia." In: *Nat Commun* 13, p. 3851. DOI: <https://doi.org/10.1038/s41467-022-31432-y>.
- Russo, S., J. Sillmann, and E. M. Fischer (2015). "Top ten European heatwaves since 1950 and their occurrence in the coming decades." In: *Environ. Res. Lett.* 10.12, p. 124003. DOI: [10.1088/1748-9326/10/12/124003](https://doi.org/10.1088/1748-9326/10/12/124003).
- Sandu, I., A. van Niekerk, T. G. Shepherd, S. B. Vosper, A. Zadra, J. Bacmeister, A. Beljaars, A. R. Brown, A. Dörnbrack, N. McFarlane, et al. (2019). "Impacts of orography on large-scale atmospheric circulation." In: *npj Clim Atmos Sci* 2.1, pp. 1–8. DOI: [10.1038/s41612-019-0065-9](https://doi.org/10.1038/s41612-019-0065-9).
- Scaife, A. A., D. Copsey, C. Gordon, C. Harris, T. Hinton, S. Keeley, A. O'Neill, M. Roberts, and K. Williams (2011). "Improved Atlantic winter blocking in a climate model." In: *Geophys. Res. Lett.* 38.23. DOI: [10.1029/2011GL049573](https://doi.org/10.1029/2011GL049573).
- Schaller, N., J. Sillmann, J. Anstey, E. M. Fischer, C. M. Grams, and S. Russo (2018). "Influence of blocking on Northern European and Western Russian heatwaves in large climate model ensembles." In: *Environ. Res. Lett.* 13.5, p. 054015. DOI: [10.1088/1748-9326/aaba55](https://doi.org/10.1088/1748-9326/aaba55).
- Schiemann, R., P. Athanasiadis, D. Barriopedro, F. Doblas-Reyes, K. Lohmann, M. J. Roberts, D. V. Sein, C. D. Roberts, L. Terray, and P.-L. Vidale (2020). "Northern Hemisphere blocking simulation in current climate models: evaluating progress from the Climate Model Intercomparison Project Phase 5 to 6 and sensitivity to resolution." In: *Weather and Clim. Dynam.* 1.1, pp. 277–292. DOI: [10.5194/wcd-1-277-2020](https://doi.org/10.5194/wcd-1-277-2020).
- Schiemann, R., M.-E. Demory, L. C. Shaffrey, J. Strachan, P.-L. Vidale, M. S. Mizielski, M. J. Roberts, M. Matsueda, M. F. Wehner, and T. Jung (2017). "The resolution sensitivity of Northern Hemisphere blocking in four 25-km atmospheric global circulation models." In: *J. Clim.* 30.1, pp. 337–358. DOI: [10.1175/JCLI-D-16-0100.1](https://doi.org/10.1175/JCLI-D-16-0100.1).
- Schneiderreit, A., S. Schubert, P. Vargin, F. Lunkeit, X. Zhu, D. HW Peters, and K. Fraedrich (2012). "Large-scale flow and the long-lasting blocking high over Russia: Summer 2010." In: *Mon Weather Rev.* 140.9, pp. 2967–2981. DOI: [10.1175/MWR-D-11-00249.1](https://doi.org/10.1175/MWR-D-11-00249.1).
- Schubert, S. D., H. Wang, R. D. Koster, M. J. Suarez, and P. Y. Groisman (2014). "Northern Eurasian heat waves and droughts." In: *J. Clim.* 27.9, pp. 3169–3207. DOI: [10.1175/JCLI-D-13-00360.1](https://doi.org/10.1175/JCLI-D-13-00360.1).
- Schubert, S., H. Wang, and M. Suarez (2011). "Warm season subseasonal variability and climate extremes in the Northern Hemisphere: The role of stationary Rossby waves." In: *J. Clim.* 24.18, pp. 4773–4792. DOI: [10.1175/JCLI-D-10-05035.1](https://doi.org/10.1175/JCLI-D-10-05035.1).

- Schumacher, D. L., J. Keune, C. C. Van Heerwaarden, J. Vilà-Guerau de Arellano, A. J. Teuling, and D. G. Miralles (2019). "Amplification of mega-heatwaves through heat torrents fuelled by upwind drought." In: *Nat. Geosci.* 12.9, pp. 712–717. DOI: [10.1038/s41561-019-0431-6](https://doi.org/10.1038/s41561-019-0431-6).
- Schwaab, J., E. L. Davin, P. Bebi, A. Duguay-Tetzlaff, L. T. Waser, M. Haeni, and R. Meier (2020). "Increasing the broad-leaved tree fraction in European forests mitigates hot temperature extremes." In: *Sci. Rep.* 10.1, pp. 1–9. DOI: [10.1038/s41598-020-71055-1](https://doi.org/10.1038/s41598-020-71055-1).
- Screen, J. A. and I. Simmonds (2013). "Exploring links between Arctic amplification and mid-latitude weather." In: *Geophys. Res. Lett.* 40.5, pp. 959–964. DOI: [10.1002/grl.50174](https://doi.org/10.1002/grl.50174).
- Screen, J. A. and I. Simmonds (Aug. 2014). "Amplified mid-latitude planetary waves favour particular regional weather extremes." In: *Nat. Clim. Change* 4.8, pp. 704–709. DOI: [10.1038/nclimate2271](https://doi.org/10.1038/nclimate2271).
- Seneviratne, S. I., T. Corti, E. L. Davin, M. Hirschi, E. B. Jaeger, I. Lehner, B. Orlovsky, and A. J. Teuling (2010). "Investigating soil moisture–climate interactions in a changing climate: A review." In: *Earth Sci Rev* 99.3-4, pp. 125–161. DOI: [10.1016/j.earscirev.2010.02.004](https://doi.org/10.1016/j.earscirev.2010.02.004).
- Seneviratne, S.I. et al. (2021). "Weather and Climate Extreme Events in a Changing Climate." In: *Climate Change 2021: The Physical Science Basis. Contribution of Working Group I to the Sixth Assessment Report of the Intergovernmental Panel on Climate Change*. Cambridge, United Kingdom and New York, NY, USA: Cambridge University Press, 1513–1766. DOI: [10.1017/9781009157896.013](https://doi.org/10.1017/9781009157896.013).
- Shepherd, T. G. (2014). "Atmospheric circulation as a source of uncertainty in climate change projections." In: *Nat. Geosci.* 7.10, pp. 703–708. DOI: [10.1038/ngeo2253](https://doi.org/10.1038/ngeo2253).
- Shutts, GJ (1983). "The propagation of eddies in diffluent jetstreams: Eddy vorticity forcing of 'blocking' flow fields." In: *Q. J. R. Meteorol. Soc.* 109.462, pp. 737–761. DOI: [10.1002/qj.49710946204](https://doi.org/10.1002/qj.49710946204).
- Sillmann, J., V. V. Kharin, X. Zhang, F. W. Zwiers, and D. Bronaugh (2013). "Climate extremes indices in the CMIP5 multimodel ensemble: Part 1. Model evaluation in the present climate." In: *J. Geophys. Res. Atmos.* 118.4, pp. 1716–1733. DOI: [10.1002/jgrd.50203](https://doi.org/10.1002/jgrd.50203).
- Sousa, P. M., R. M. Trigo, D. Barriopedro, P. M. M. Soares, and J. A. Santos (2018). "European temperature responses to blocking and ridge regional patterns." In: *Clim. Dyn.* 50.1, pp. 457–477. DOI: [10.1007/s00382-017-3620-2](https://doi.org/10.1007/s00382-017-3620-2).
- Stefanon, M., F. D'Andrea, and P. Drobinski (Feb. 2012). "Heatwave classification over Europe and the Mediterranean region." In: *Environ. Res. Lett.* 7.1, p. 014023. DOI: [10.1088/1748-9326/7/1/014023](https://doi.org/10.1088/1748-9326/7/1/014023).
- Stéfanon, M., P. Drobinski, F. D'Andrea, C. Lebeaupin-Brossier, and S. Bastin (2014). "Soil moisture-temperature feedbacks at meso-scale during summer heat waves over Western Europe." In: *Clim. Dyn.* 42.5, pp. 1309–1324. DOI: [10.1007/s00382-013-1794-9](https://doi.org/10.1007/s00382-013-1794-9).

- Stillman, J. H. (2019). "Heat waves, the new normal: summertime temperature extremes will impact animals, ecosystems, and human communities." In: *Physiol.* 34.2, pp. 86–100. DOI: [10.1152/physiol.00040.2018](https://doi.org/10.1152/physiol.00040.2018).
- Strigunova, I., R. Blender, F. Lunkeit, and N. Žagar (2022). "Signatures of Eurasian heat waves in global Rossby wave spectra." In: *Weather Clim. Dynam.* 3.4, pp. 1399–1414. DOI: [10.5194/wcd-3-1399-2022](https://doi.org/10.5194/wcd-3-1399-2022).
- Suarez-Gutierrez, L., C. Li, W. A. Müller, and J. Marotzke (2018). "Internal variability in European summer temperatures at 1.5 C and 2 C of global warming." In: *Environ. Res. Lett.* 13.6, p. 064026. DOI: [10.1088/1748-9326/aaba58](https://doi.org/10.1088/1748-9326/aaba58).
- Suarez-Gutierrez, L., W. A. Müller, C. Li, and J. Marotzke (2020). "Dynamical and thermodynamical drivers of variability in European summer heat extremes." In: *Clim. Dyn.* 54.9, pp. 4351–4366. DOI: [10.1007/s00382-020-05233-2](https://doi.org/10.1007/s00382-020-05233-2).
- Sura, P., M. Newman, Cé. Penland, and P. Sardeshmukh (2005). "Multiplicative noise and non-Gaussianity: A paradigm for atmospheric regimes?" In: *J. Atmos. Sci.* 62.5, pp. 1391–1409. DOI: [10.1175/JAS3408.1](https://doi.org/10.1175/JAS3408.1).
- Tachibana, Y., T. Nakamura, H. Komiya, and M. Takahashi (2010). "Abrupt evolution of the summer Northern Hemisphere annular mode and its association with blocking." In: *J. Geophys. Res. Atmos.* 115.D12. DOI: [10.1029/2009JD012894](https://doi.org/10.1029/2009JD012894).
- Taylor, K. E., R. J. Stouffer, and G. A. Meehl (2012). "An overview of CMIP5 and the experiment design." In: *Bull. Am. Meteorol. Soc.* 93.4, pp. 485–498. DOI: [10.1175/BAMS-D-11-00094.1](https://doi.org/10.1175/BAMS-D-11-00094.1).
- Teng, H. and G. Branstator (2012). "A zonal wavenumber 3 pattern of Northern Hemisphere wintertime planetary wave variability at high latitudes." In: *J. Clim.* 25.19, pp. 6756–6769. DOI: [10.1175/JCLI-D-11-00664.1](https://doi.org/10.1175/JCLI-D-11-00664.1).
- (2019). "Amplification of Waveguide Teleconnections in the Boreal Summer." In: *Curr. Climate Change Rep.* 5, pp. 421–432. DOI: [10.1007/s40641-019-00150-x](https://doi.org/10.1007/s40641-019-00150-x).
- Teng, H., G. Branstator, H. Wang, G. A. Meehl, and W. M. Washington (2013). "Probability of US heat waves affected by a subseasonal planetary wave pattern." In: *Nat. Geosci.* 6.12, pp. 1056–1061. DOI: [10.1038/ngeo1988](https://doi.org/10.1038/ngeo1988).
- Terray, L. (2021). "A dynamical adjustment perspective on extreme event attribution." In: *Weather Clim. Dynam.* 2.4, pp. 971–989. DOI: [10.5194/wcd-2-971-2021](https://doi.org/10.5194/wcd-2-971-2021).
- Thomas, N. P., M. G. Bosilovich, A. B. Marquardt Collow, R. D. Koster, S. D. Schubert, A. Dezfuli, and S. P. Mahanama (2020). "Mechanisms associated with daytime and nighttime heat waves over the contiguous United States." In: *J. Appl. Meteorol. Climatol.* 59.11, pp. 1865–1882. DOI: [10.1175/JAMC-D-20-0053.1](https://doi.org/10.1175/JAMC-D-20-0053.1).
- Thorarinsdottir, T. L., J. Sillmann, M. Haugen, N. Gissibl, and M. Sandstad (2020). "Evaluation of CMIP5 and CMIP6 simulations of historical surface air temperature extremes using proper evaluation methods." In: *Environ. Res. Lett.* 15.12, p. 124041. DOI: [10.1088/1748-9326/abc778](https://doi.org/10.1088/1748-9326/abc778).
- Trenberth, K. E and J. T Fasullo (2012). "Climate extremes and climate change: The Russian heat wave and other climate extremes of 2010." In: *J. Geophys. Res. Atmos.* 117.D17. DOI: [10.1029/2012JD018020](https://doi.org/10.1029/2012JD018020).

- Turner, J., H. Lu, J. C. King, S. Carpentier, M. Lazzara, T. Phillips, and J. Wille (2022). "An extreme high temperature event in coastal East Antarctica associated with an atmospheric river and record summer downslope winds." In: *Geophys. Res. Lett.* 49.4, e2021GL097108. DOI: [10.1029/2021GL097108](https://doi.org/10.1029/2021GL097108).
- Van Oldenborgh, G. J., M. F. Wehner, R. Vautard, F. E. L. Otto, S. I. Seneviratne, P. A. Stott, G. C. Hegerl, S. Y. Philip, and S. F. Kew (2022). "Attributing and projecting heatwaves is hard: we can do better." In: *Earth's Future* 10.6, e2021EF002271. DOI: [10.1029/2021EF002271](https://doi.org/10.1029/2021EF002271).
- Vijverberg, S. and D. Coumou (2022). "The role of the Pacific Decadal Oscillation and ocean-atmosphere interactions in driving US temperature predictability." In: *npj Clim. Atmos. Sci.* 5.1, pp. 1–11. DOI: [10.1038/s41612-022-00237-7](https://doi.org/10.1038/s41612-022-00237-7).
- Wang, C., J. Zheng, W. Lin, and Y. Wang (2023). "Unprecedented Heatwave in Western North America during Late June of 2021: Roles of Atmospheric Circulation and Global Warming." In: *Adv Atmos Sci* 40.1, pp. 14–28. DOI: [10.1007/s00376-022-2078-2](https://doi.org/10.1007/s00376-022-2078-2).
- Wang, P., P. Hui, D. Xue, and J. Tang (2019). "Future projection of heat waves over China under global warming within the CORDEX-EA-II project." In: *Clim. Dyn.* 53.1, pp. 957–973. DOI: [10.1007/s00382-019-04621-7](https://doi.org/10.1007/s00382-019-04621-7).
- Wehner, M., P. Gleckler, and J. Lee (2020). "Characterization of long period return values of extreme daily temperature and precipitation in the CMIP6 models: Part 1, model evaluation." In: *Weather and Climate Extremes* 30, p. 100283. DOI: [10.1016/j.wace.2020.100283](https://doi.org/10.1016/j.wace.2020.100283).
- Wehrli, K., B. P. Guillod, M. Hauser, M. Leclair, and S. I. Seneviratne (2019). "Identifying key driving processes of major recent heat waves." In: *J. Geophys. Res. Atmos.* 124.22, pp. 11746–11765. DOI: [10.1029/2019JD030635](https://doi.org/10.1029/2019JD030635).
- Wei, N., L. Zhou, and Y. Dai (2017). "Evaluation of simulated climatological diurnal temperature range in CMIP5 models from the perspective of planetary boundary layer turbulent mixing." In: *Clim. Dyn.* 49.1, pp. 1–22. DOI: [10.1007/s00382-016-3323-0](https://doi.org/10.1007/s00382-016-3323-0).
- Whan, K., J. Zscheischler, R. Orth, M. Shongwe, M. Rahimi, E. O. Asare, and S. I. Seneviratne (2015). "Impact of soil moisture on extreme maximum temperatures in Europe." In: *Weather Clim. Extrem.* 9, pp. 57–67. DOI: [10.1016/j.wace.2015.05.001](https://doi.org/10.1016/j.wace.2015.05.001).
- White, R. H., K. Kornhuber, O. Martius, and V. Wirth (2022). "From Atmospheric Waves to Heatwaves: A Waveguide Perspective for Understanding and Predicting Concurrent, Persistent, and Extreme Extratropical Weather." In: *Bull. Am. Meteorol. Soc.* 103.3, E923–E935. DOI: [10.1175/BAMS-D-21-0170.1](https://doi.org/10.1175/BAMS-D-21-0170.1).
- Wiedenmann, J. M, A. R Lupo, I. I Mokhov, and E. A Tikhonova (2002). "The climatology of blocking anticyclones for the Northern and Southern Hemispheres: Block intensity as a diagnostic." In: *J. Clim.* 15.23, pp. 3459–3473. DOI: [10.1175/1520-0442\(2002\)015<3459:TCOBAF>2.0.CO;2](https://doi.org/10.1175/1520-0442(2002)015<3459:TCOBAF>2.0.CO;2).

- Wilks, Daniel S. (2011). *Statistical methods in the atmospheric sciences*. Third. Vol. 100. International Geophysics. Academic Press. URL: <http://www.sciencedirect.com/science/bookseries/00746142/100/supp/C>.
- Wills, R., R. H. White, and X. J. Levine (2019). "Northern Hemisphere stationary waves in a changing climate." In: *Curr. Clim. Change Rep.* 5.4, pp. 372–389. DOI: [10.1007/s40641-019-00147-6](https://doi.org/10.1007/s40641-019-00147-6).
- Wirth, V. and C. Polster (2021). "The problem of diagnosing jet waveguidability in the presence of large-amplitude eddies." In: *J. Atmos. Sci.* 78.10, pp. 3137–3151. DOI: [10.1175/JAS-D-20-0292.1](https://doi.org/10.1175/JAS-D-20-0292.1).
- Wong, T. S. T. (2015). "Statistical analysis of heat waves in the state of Victoria in Australia." In: *Aust N Z J Stat* 57.4, pp. 463–480. DOI: [10.1111/anzs.12137](https://doi.org/10.1111/anzs.12137).
- Woollings, T., D. Barriopedro, J. Methven, S.-W. Son, O. Martius, B. Harvey, J. Sillmann, A. R Lupo, and S. Seneviratne (2018). "Blocking and its response to climate change." In: *Curr. Clim. Change Rep.* 4.3, pp. 287–300. DOI: [10.1007/s40641-018-0108-z](https://doi.org/10.1007/s40641-018-0108-z).
- Wu, L., F. He, Z. Liu, and C. Li (2007). "Atmospheric teleconnections of tropical Atlantic variability: Interhemispheric, tropical–extratropical, and cross-basin interactions." In: *J. Clim.* 20.5, pp. 856–870. DOI: [10.1175/JCLI4019.1](https://doi.org/10.1175/JCLI4019.1).
- Xu, P., L. Wang, Y. Liu, W. Chen, and P. Huang (2020). "The record-breaking heat wave of June 2019 in Central Europe." In: *Atmos. Sci. Lett.* 21.4, e964. DOI: [10.1002/asl.964](https://doi.org/10.1002/asl.964).
- Yamazaki, A. and H. Itoh (2013). "Vortex–vortex interactions for the maintenance of blocking. Part I: The selective absorption mechanism and a case study." In: *J. Atmos. Sci.* 70.3, pp. 725–742. DOI: [10.1175/JAS-D-11-0295.1](https://doi.org/10.1175/JAS-D-11-0295.1).
- Yao, Y., Y. Luo, J. Huang, and Z. Zhao (2013). "Comparison of monthly temperature extremes simulated by CMIP3 and CMIP5 models." In: *J. Clim.* 26.19, pp. 7692–7707. DOI: [10.1175/JCLI-D-12-00560.1](https://doi.org/10.1175/JCLI-D-12-00560.1).
- Yu, S., S. F. B. Tett, N. Freychet, and Z. Yan (2021). "Changes in regional wet heatwave in Eurasia during summer (1979–2017)." In: *Environ. Res. Lett.* 16.6, p. 064094. DOI: [10.1088/1748-9326/ac0745](https://doi.org/10.1088/1748-9326/ac0745).
- Žagar, N. and C. L. E. Franzke (2015). "Systematic decomposition of the Madden-Julian Oscillation into balanced and inertia-gravity components." In: *Geophys. Res. Lett.* 42.16, pp. 6829–6835. DOI: [10.1002/2015GL065130](https://doi.org/10.1002/2015GL065130).
- Žagar, N., D. Jelić, M. Blaauw, and P. Bechtold (2017). "Energy spectra and inertia-gravity waves in global analyses." In: *J. Atmos. Sci.* 74.8, pp. 2447–2466. DOI: [10.1175/JAS-D-16-0341.1](https://doi.org/10.1175/JAS-D-16-0341.1).
- Žagar, N., K. Kosovelj, E. Manzini, M. Horvat, and J. Castanheira (2019). "An assessment of scale-dependent variability and bias in global prediction models." In: *Clim. Dyn.* 54, pp. 287–306. DOI: [10.1007/s00382-019-05001-x](https://doi.org/10.1007/s00382-019-05001-x).
- Žagar, N., Ž. Zaplotnik, and K. Karami (2020). "Atmospheric subseasonal variability and circulation regimes: spectra, trends, and uncertainties." In: *J. Clim.* 33.21, pp. 9375–9390. DOI: [10.1175/JCLI-D-20-0225.1](https://doi.org/10.1175/JCLI-D-20-0225.1).

- Zelinka, M. D., T. A. Myers, D. T. McCoy, S. Po-Chedley, P. M. Caldwell, P. Ceppi, S. A. Klein, and K. E. Taylor (2020). "Causes of higher climate sensitivity in CMIP6 models." In: *Geophys. Res. Lett.* 47.1, e2019GL085782. DOI: [10.1029/2019GL085782](https://doi.org/10.1029/2019GL085782).
- Zhou, Y. and Z. Wu (2016). "Possible impacts of mega-El Niño/Southern Oscillation and Atlantic Multidecadal Oscillation on Eurasian heatwave frequency variability." In: *Q. J. R. Meteorol. Soc.* 142.697, pp. 1647–1661. DOI: [10.1002/qj.2759](https://doi.org/10.1002/qj.2759).
- Zschenderlein, P., A. H. Fink, S. Pfahl, and H. Wernli (2019). "Processes determining heat waves across different European climates." In: *Q. J. R. Meteorol. Soc.* 145.724, pp. 2973–2989. DOI: [10.1002/qj.3599](https://doi.org/10.1002/qj.3599).
- Zuo, J., S. Pullen, J. Palmer, H. Bennetts, N. Chileshe, and T. Ma (2015). "Impacts of heat waves and corresponding measures: a review." In: *J. Clean. Prod.* 92, pp. 1–12. DOI: [10.1016/j.jclepro.2014.12.078](https://doi.org/10.1016/j.jclepro.2014.12.078).
- Žagar, N., A. Kasahara, K. Terasaki, J. Tribbia, and H.L. Tanaka (2015). "Normal-mode function representation of global 3D datasets: open-access software for the atmospheric research community." In: *Geosci. Model Dev.* 8, pp. 1169–1195. DOI: <https://doi.org/10.5194/gmd-8-1169-2015>.
- Žagar, N. and J. Tribbia (2020). *Modal View of Atmospheric Variability: Applications of Normal-Mode Function Decomposition in Weather and Climate Research*. 1st ed. Mathematics of Planet Earth 8. Springer International Publishing;Springer. ISBN: 978-3-030-60962-7,978-3-030-60963-4. DOI: <https://doi.org/10.1007/978-3-030-60963-4>.

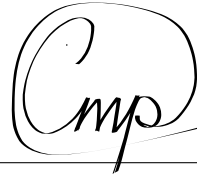
EIDESSTATTLICHE VERSICHERUNG – DECLARATION ON  
OATH

---

Hiermit erkläre ich an Eides statt, dass ich die vorliegende Dissertationsschrift selbst verfasst und keine anderen als die angegebenen Quellen und Hilfsmittel benutzt habe.

I hereby declare upon oath that I have written the present dissertation independently and have not used further resources and aids than those stated.

*Hamburg, January 2023*

A handwritten signature in black ink, consisting of a large, stylized capital 'C' followed by the lowercase letters 'mp' in a cursive script.

---

Iana Strigunova

## Hinweis / Reference

Die gesamten Veröffentlichungen in der Publikationsreihe des MPI-M  
„Berichte zur Erdsystemforschung / Reports on Earth System Science“,  
ISSN 1614-1199

sind über die Internetseiten des Max-Planck-Instituts für Meteorologie erhältlich:  
**<https://mpimet.mpg.de/forschung/publikationen>**

*All the publications in the series of the MPI -M  
„Berichte zur Erdsystemforschung / Reports on Earth System Science“,  
ISSN 1614-1199*

*are available on the website of the Max Planck Institute for Meteorology:  
**<https://mpimet.mpg.de/en/research/publications>***



